Emergent Patterns in Nonlinear Systems and their Applications

A thesis
submitted by

Vivek Kohar

in partial fulfillment of
the requirements for the degree of

Doctor of Philosophy

Indian Institute of Science Education and Research (IISER)
Mohali

July, 2014

Certificate of Examination

This is to certify that the dissertation titled *Emergent Patterns in Nonlinear Systems and their Applications* submitted by **Mr. Vivek Kohar** (Reg. No. Ph10074) for the partial fulfillment of Doctor of Philosophy programme of the Institute, has been examined by the thesis committee duly appointed by the Institute. The committee finds the work done by the candidate satisfactory and recommends that the report be accepted.

Dr. Rajeev Kapri Dr. K. P. Singh Prof. Sudeshna Sinha

(Supervisor)

Declaration

The work presented in this dissertation has been carried out by me under the guidance of Professor Sudeshna Sinha at the Indian Institute of Science Education and Research Mohali.

This work has not been submitted in part or in full for a degree, a diploma, or a fellowship to any other university or institute. Whenever contributions of others are involved, every effort is made to indicate this clearly, with due acknowledgement of collaborative research and discussions. This thesis is a bonafide record of original work done by me and all sources listed within have been detailed in the bibliography.

Vivek Kohar

(Candidate)

17 July 2014

In my capacity as the supervisor of the candidates doctoral thesis, I certify that the above statements by the candidate are true to the best of my knowledge.

Prof. Sudeshna Sinha

(Supervisor)

Acknowledgements

It is a great pleasure to express my sincere thanks with deep gratitude to my thesis supervisor, Prof. Sudeshna Sinha, for her guidance during my study and research at Indian Institute of Science Education and Research, Mohali. She has been my "Guru" for all academic and non academic discussions during my stay at IISER. Her patience, flexibility, warm encouragement, and thoughtful guidance alongwith genuine caring and concern has been motivating and enlightening. Her perpetual energy and enthusiasm in life has motivated me and will continue to do so for rest of my life. For this, I cannot thank her enough. I am forever grateful.

I am thankful to my doctoral committee members Dr. K. P. Singh and Dr. R. Kapri. Their academic support and input and personal cheering are greatly appreciated. My sincere thanks goes to Prof. Cristina Masoller and Prof. Jüergen Kurths for offering me internship opportunities in their groups giving me opportunities to work on diverse exciting projects. I thank Sandro, Peng, Deniz, Paul and Bedartha for their friendship, help and cooperation during these visits. I am grateful to Dr. K. P. Yogendran, Dr. Sanjeev Kumar, Dr. Yogesh Singh, Dr. H. K. Jassal, Dr. Abhishek Chaudhuri, Dr. R S Johal, Dr. Ananth Venkatesan, Prof. Arvind and Prof. Jasjeet Bagla for their valuable help and suggestions at various stages. I convey my thanks to Dr. K. Murali for many scientific discussions and his encouragement, insightful comments and hard questions.

I am also thankful to various funding agencies and institutes for providing the financial support and research facilities. Support from the Council of Scientific and Industrial Research (CSIR), India, the German Academic Exchange Service (DAAD), Germany, Potsdam Institute for Climate Impact Research (PIK), Potsdam, the International Centre for Theoretical Physics (ICTP), Trieste, Universitat Politècnica de Catalunya BarcelonaTech (UPC) and Department of Science and Technology (DST), India is duly acknowledged.

A good support system is important for surviving and staying sane during a PhD programme. Over the years it has been my good fortune to encounter many people who have given me more of their time, companionship and personal help. I am very much thankful to my colleagues Anshul, Kanika, Preety, Ankit, George, Jebaratnam, Sandeep, Girish, Amit for their help and nice association during the long hours in the scholar room which made it a convivial place to work. I am also thankful to Shishram, Gopal, Preetinder, Shruti, Harpreet, Pramod, Ritabarta, Debmalya, Bhupesh, Neeraj, Aman and Animesh for their friendship. At this occasion, I will not miss the opportunity to thank many MS students whose company made me feel young and energetic.

Of course, no acknowledgments would be complete without thanking my parents, sister, brother in laws and Navdeep and her parents for their unconditional love and care. My mother, especially, has been a great role model of resilience and strength and Navdeep's companionship ensured that this arduous journey was completed with ease.

Synopsis

Nonlinear dynamical systems exhibit many counterintuitive phenomenon and exotic spatiotemporal patterns. On one hand, phenomenon like chaos and stochastic resonance in individual nonlinear dynamical units challenge our everyday intuitions, on the other, complex systems consisting of interacting nonlinear dynamical units provide us a framework to model many physical, biological, social and engineering systems thereby enabling us to get deeper insights into wide ranging complex phenomena.

The work in this thesis is divided into two broad categories. First, we explore the *application of nonlinear systems in the design of computing devices*. Second, we attempt to broaden our understanding of nonlinear systems in general by investigating the *emergence of spatiotemporal patterns in complex networks with time-varying connections*.

Specifically in the first part, we study the possibility of utilizing the phenomenon of stochastic resonance in bistable or multi-stable nonlinear dynamical systems to implement memory and logic function. This phenomenon has commonly been referred to as "Logical Stochastic Resonance (LSR)". We demonstrate how noise enables a bistable system to behave as a memory device, as well as a logic gate for sub−threshold input signals. It is shown how this system can implement memory using noise constructively to store information. Namely, in some optimal range of noise, the system can operate flexibly, both as a AND/OR gate and a Set−Reset latch, on variation of an asymmetrizing bias.

Then we examine the intriguing possibility of obtaining dynamical behavior equivalent to LSR in a noise-free bistable system, subjected only to periodic forcing, such as a sinusoidal driving or rectangular pulse trains. We find that such a system, despite having no stochastic influence, also yields phenomenon analogous to LSR, in an appropriate window of frequency and amplitude of the periodic forcing. The results are corroborated by electronic circuit experiments.

Next we demonstrate how width of the optimal noise window can be increased by utilizing the constructive interplay of noise and periodic forcing, namely, noise in conjunction with a periodic drive enables the system to yield consistent logic outputs for all noise strengths below a certain threshold. Thus we establish that in scenarios where noise level is below the minimum threshold required for LSR (or stochastic resonance in general), we can add a periodic forcing to obtain the desired effects. We have also

shown that the periodic forcing results in lower latency effects and reduces the switching time, leading to faster operation of the devices. Further, if a LSR element is coupled to another LSR element with a lower potential barrier, then it is able to adapt to varying noise intensity, so that its operation remains robust even under high noise conditions.

Lastly, we test these concepts in vertical-cavity surface-emitting lasers (VCSELs) which are widely used for high-bit-rate data transmission because of their various advantages over conventional edge emitting lasers like low threshold current, single-longitudinal-mode operation, higher modulation bandwidth and circular output beam profile. We attempt to enhance the the operational range of VCSEL based stochastic logic gate by adding a periodic signal. The enhancement is observed in form of decrease in the minimum bit time necessary for successful operation or increase of size of the optimal noise window.

In the second part of this thesis, we study the behaviour of nonlinear dynamical elements coupled with each other. Firstly, we study the impact of small heterogeneity in signals applied to globally coupled nonlinear bistable elements. In absence of coupling, the collective response is simply the average of response to all the uncorrelated signals. When the elements are coupled and a bias is applied, we find that even a very small number of heterogeneous inputs are able to drag the collective response towards the stable state of the minority inputs. In our explicit demonstration we have taken Schmitt triggers as the nonlinear bistable elements, and the inputs are encoded as voltages applied to them. The average of the output voltages of all Schmitt triggers corresponds to the output of the system. We also observe that the minimum heterogeneity that can be detected scales with the ratio of threshold voltage to the source voltage of the Schmitt triggers, and can be be brought down to the limit of single bit detection.

In last two works, we focus on changes in emergent phenomenon when the underlying interaction network is dynamic and the connections evolve with time. Such time variations represent the evolution of interactions over time or any discontinuities in interactions, i.e. when the nodes interact only for limited time. These evolving interaction patterns are commonly found in social networks, communication, biological systems, spread of epidemics, computer networks, world wide web etc and have been shown to result in significantly different emergent phenomena in complex systems.

In the first problem, we study the impact of time varying network topology in epidemic spreading. We study a simple model mimicking disease spreading on a network with dynamically varying connections, and investigate the dynamical consequences of

switching links in the network. Our central observation is that the disease cycles get more synchronized, indicating the onset of epidemics, as the underlying network changes more rapidly. This behavior is found for periodically switched links, as well as links that switch stochastically in time. We find that the influence of changing links is more pronounced in networks where the nodes have lower degree, and the disease cycle has a longer infective stage. Further, in periodically switching links, we observe finer dynamical features, such as beating patterns in the emergent oscillations and resonant enhancement of synchronization, arising from the interplay between the time-scales of the connectivity changes and that of the epidemic outbreaks.

In the second problem, we study the stability of the synchronous state in evolving networks. Many earlier studies have analyzed the stability of the synchronous state by linearizing the dynamical equations. But this approach is valid only in case of small perturbations of the synchronous state. In general, the dynamical equations governing the dynamics over the nodes are nonlinear and the higher order terms no longer remain negligible in case of large perturbations. In such cases, the basin stability approach may be used to complement the linear stability analysis. The basin stability paradigm is particularly useful in case of time varying networks as it can be applied to a large class of systems whereas the linear stability analysis can be done only in some specific cases.

In our study, we consider synchronization of chaotic Rössler oscillators over Watts−Strogatz networks. We vary the fraction of random links, p, to cover broad range of networks varying from regular ring topology for $p = 0$ to random networks for $p = 1$. We find that for sufficiently fast re-wirings, the time varying networks can be approximated by static time averaged networks. Using the basin stability framework, we are able to estimate the rewiring frequency at which the network can be approximated by the static time average. Further we are also able to get insight into how the transition from a static to a time averaged case takes place and show how the stability range changes at different rewiring timescales. We find that not only the basin stability of small world networks highest in static cases as reported earlier, but they approach the time averaged coupling case fastest. Further, we find that faster rewiring networks synchronize quickly and the impact of rewiring is maximum when the number of neighbours is less. Lastly, we show that linear stability analysis alone is not sufficient to accurately predict the stability of synchronized states in time varying networks and the basin stability analysis should also be used to complement the analysis.

In the last chapter of the thesis, we conclude our findings and summarize the important results of all the chapters. We also list some possible extensions of the works presented

in this thesis.

List of Publications

1. **Noise- free logical stochastic resonance**
   Animesh Gupta, Aman Sohane, Vivek Kohar, K. Murali, and Sudeshna Sinha
   Phys. Rev. E (Rapid Communications), 84:055201, (2011)

2. **Noise-assisted morphing of memory and logic function**
   Vivek Kohar and Sudeshna Sinha
   Physics Letters A, 376(89):957-962, (2012)

3. **Emergence of epidemics in rapidly varying networks**
   Vivek Kohar and Sudeshna Sinha
   Chaos, Solitons & Fractals, 54:127-134, (2013)

4. **Verification of scalable ultra-sensitive detection of heterogeneity in an electronic circuit**
   Vivek Kohar, Anshul Choudhary, Kamal P Singh, and Sudeshna Sinha
   The European Physical Journal Special Topics, 222(3-4):721-728, (2013).

5. **Realizing logic gates with time-delayed synthetic genetic networks**
   Amit Sharma, Vivek Kohar, Manish Dev Shrimali, and Sudeshna Sinha
   Nonlinear Dynamics, 76:431-439, (2014)

6. **Enhanced logical stochastic resonance under periodic forcing**
   Vivek Kohar, K. Murali, and Sudeshna Sinha
   Communications in Nonlinear Science and Numerical Simulation, 19(8), 2866-2873 (2014).

7. **Taming Explosive Growth through Dynamic Random Links**
   Anshul Choudhary, Vivek Kohar and Sudeshna Sinha
   Scientific Reports 4, 4308 (2014)

8. **Noise enhanced activity in a complex network**
   Anshul Choudhary, Vivek Kohar, Sudeshna Sinha
   arXiv preprint arXiv:1312.6656, (2013) *(to appear in European Physical Journal B)*

9. **Synchronization in time varying complex networks**
   Vivek Kohar, Peng Ji, Anshul Choudhary, Sudeshna Sinha and Jüergen Kurths
   (to appear in Physical Review E)

10. **Performance enhancement of VCSEL based stochastic logic gate**
    Vivek Kohar, Cristina Masoller and Sudeshna Sinha
    (manuscript under preparation)

11. **Logical Stochastic Resonance**
    Vivek Kohar
    http://demonstrations.wolfram.com/LogicalStochasticResonance/
    Wolfram Demonstrations Project, Published: April 28, 2014

Contents

1 Introduction **1**

1.1 Interplay of noise and nonlinearity 2

1.2 Spatiotemporal patterns in Complex Systems 5

I Nonlinear Dynamics in Computing Systems **11**

2 Noise assisted morphing of memory and logic function **13**

2.1 Introduction 13

2.2 General Principle 14

2.3 Explicit Example 16

2.4 Discussions 19

3 Noise free logical stochastic resonance **23**

3.1 Introduction 23

3.2 General Principle 23

3.3 Explicit Example 24

3.4 Results 25

3.5 Conclusion 30

4 Periodic signal enhanced logical stochastic resonance 33

4.1 Introduction . . . 33

4.2 General Principle . . . 34

4.3 Explicit Example . . . 34

4.4 Results . . . 36

4.5 Adaptive Logical Stochastic Resonance . . . 40

4.6 Conclusion . . . 44

5 Performance enhancement of VCSEL based stochastic logic gates 47

5.1 Introduction . . . 47

5.2 Model Equations . . . 48

5.3 Results . . . 49

5.3.1 Optoelectronic Configuration . . . 49

5.3.2 All-optical configuration . . . 52

5.4 Conclusion . . . 53

II Spatiotemporal patterns in Complex Systems 57

6 Verification of scalable ultra-sensitive detection of heterogeneity in an electronic circuit 59

6.1 Introduction . . . 59

6.2 Coupled bistable elements . . . 60

6.3 Collective response in the presence of heterogeneity . . . 61

6.4 Explicit demonstration of ultra-sensitivity . . . 63

6.5 Conclusion 66

7 Emergence of epidemics in rapidly varying networks 69

7.1 Model of infection spreading 71

7.2 Periodically Switched Links 74

7.2.1 Enhancement of Synchronization in rapidly varying networks . . . 74

7.2.2 Interplay of nodal dynamics and network rewiring 76

7.2.3 Influence of neighbours 78

7.2.4 Fine structure in emergent oscillations 80

7.3 Probabilistic Switching of Links 83

7.4 Discussions 85

8 Synchronization in time varying networks 89

8.1 Introduction 89

8.2 Model 91

8.3 Results 92

8.4 Conclusion 99

9 Conclusions and future directions 103

Chapter 1

Introduction

A system that evolves with time is called a dynamical system and such dynamical systems are often modeled by differential equations

$$\dot{X} = F(X) \tag{1.1}$$

where $X(t) = \{x_1(t), x_2(t).....x_n(t)\}$ is a vector of state variables, t is time and $F(X) = \{f_1(X), f_2(X).....f_n(X)\}$ is vector of functions that encode the dynamics[1]. If time is discrete, then the evolution is given by a map

$$X_{n+1} = F(X_n) \tag{1.2}$$

where X is state vector and F is a set of functions determining the flow of the phase point. If F is a nonlinear function in these coupled differential/difference equations then the system is referred to as nonlinear dynamical system.

Such nonlinear dynamical systems are hard to solve analytically, but the rapid rise in computing power has helped us to understand their behavior by employing numerical analysis techniques. Through numerical simulation of the dynamical equations, it has been found that even very simple dynamical systems can exhibit a range of dynamical behaviours from fixed points and limit cycles to very complex and counterintuitive behaviours like chaos and fractals [2].

1.1 Interplay of noise and nonlinearity

An ubiquitous feature of real systems is the presence of noise. Noise has traditionally been considered a nuisance and something which one should get rid off. Lately, noise has been shown to play not only beneficial but crucial role in many biological and engineering systems. The cooperative interplay of noise and nonlinearity in dynamical systems has attracted the attention of researchers from diverse fields ranging from electronic systems to geologists. Phenomenon such as stochastic resonance (SR), that is, the enhancement of response of a nonlinear system to a weak signal with the assistance of noise have been studied extensively [3, 4].

Stochastic resonance has been observed in a large variety of systems, including bistable ring lasers [5], semiconductor devices [6, 7, 8], chemical reactions [9], neuronal ensembles [10], vertical cavity surface emitting lasers [11], delayed feedback systems [12], geomagnetic polarity reversals [13] models of opinion formation [14] and mechano-receptor cells in the tail fan of a crayfish [15]. The phenomenon of stochastic resonance has been utilized in realizing logic gates [16], information transmission and storage [17, 18], harvesting vibrational energy and genetic switches [19]. It has also been observed with different types of noise like colored noise [20, 21, 22, 23], combination of multiplicative and additive noise [24, 25], pinning noise [26] and in periodic potentials [27, 28].

Stochastic Resonance in double-well potential

The standard equation of a double-well potential is:

$$V(x) = -a_1 x^2/2 + a_2 x^4/4 \tag{1.3}$$

where $a_1, a_2 > 0$. The height and width of the energy barrier are $h = a_1^2/4a_2$ and $w = 2\sqrt{a_1/a_2}$ respectively. The force field corresponding to this potential barrier is $F(x) = -dV(x)/dx = a_1 x - a_2 x^3$. If we neglect inertia and consider the overdamped limit, then the stochastic differential equation (SDE) governing the dynamics is

$$\dot{x} = F(x) + Asin(\Omega t) + D\eta(t) \tag{1.4}$$

where $\eta(t)$ is Gaussian noise and $sin(\Omega t)$ is the driving force with amplitude A. In numerical integration schemes, the Gaussian noise is band-limited by the integration

time step dt to a Nyquist frequency $f_{NQ} = 1/(2dt)$. Noise is quantified by its mean squared amplitude or noise power $\sigma^2 = 2Df_{NQ}$ where $2D$ is the height of the one sided noise spectrum. In absence of driving force ($A = 0$), the mean escape time from either potential well is given by:

$$1/\tau_K = r_K = (\omega_b\omega_0/2\pi)exp(-h/D) \tag{1.5}$$

where r_K is the Kramer's rate and $\omega_0^2 = 2a_1$ and $\omega_b^2 + a_1$ represent the angular frequencies at the potential minima and at the top of the barrier.

At very low noise strength, mean escape time τ_K is very large, so the effective frequency $1/2\tau_K << \Omega$ and the periodic part is not detectable. Similarly, for large D, $1/2\tau_K >> \Omega$ and periodic part is not perceptible. SR takes place when both frequencies are close, i.e.

$$T_\Omega \equiv 2\pi/\Omega = 2\tau_K(D) = (2\sqrt{2}\pi/k_1^2)exp(k_1^2/4Dk_2) \tag{1.6}$$

In this case even when $A < h$, the inter-well switching frequency is close to the frequency of the driving force and this resonance of the two frequencies is called as SR. So the output signal-to-noise ratio (SNR) is maximum for some nonzero noise[29].

Stochastic Resonance in computing systems

Noise in physical systems is one of the biggest challenge for people engaged in design and development of computing devices. The rapid shrinking of computing platforms with smaller power supplies has brought with it problems of smaller noise margins and higher error rates. So wide ranging research efforts in recent years have focused on the issue of reliable operations in the presence of a noise floor[18, 30].

In this context, it was shown that a noisy nonlinear system, when driven by two square waves encoding two logical inputs, consistently goes to a state that mirrors a logical combination of the two inputs (such as AND/NAND and OR/NOR logic) in some optimal range of noise. That is, the probability of getting the correct logical response increases to unity with increase in the intensity of noise and then decreases again when noise exceeds the optimal range. Further one can vary the threshold (or bias) and morph the output into different logical functions.

This concept, named "Logical Stochastic Resonance" (LSR) [16, 31], helps one gain understanding of the counter-intuitive interplay between noise and nonlinearity [3, 32, 4].

Further, from the applied viewpoint, this idea can potentially lead to the design of flexible logic gates with enhanced performance in noisy environments. The main feature of LSR is the capability of the nonlinear device to work optimally in a range of environmental noise; hence LSR is a practical and reasonable answer for computational devices wherein the noise-floor cannot be suppressed. The relevance of LSR has been established in physical systems, ranging from electrical [33] and nanomechanical [34] to optical systems [35, 36]. It has also been found to occur in chemical [37] and biological [38, 39] scenarios.

Now we briefly discuss the general principle of LSR. Consider a general nonlinear system,

$$\dot{x} = F(x) + b + I_{in} + D\eta(t) \tag{1.7}$$

where $F(x)$ is a generic nonlinear function obtained via the negative gradient of a potential with two distinct stable wells. I_{in} is the input signal which encodes the logic inputs, b is bias to asymmetrize the two potential wells, and $\eta(t)$ is an additive zero-mean Gaussian noise with unit variance, with D being the amplitude(intensity) of the noise.

A logical input-output can be obtained by driving the system with two trains of aperiodic square pulses: $I_1 + I_2$, encoding the two logic inputs. For logic operations such as OR/NOR and AND/NAND, we consider the inputs to take value I when the logic input is 1, and value $-I$ when the logic input is 0, where input strength I is: $0 < I < 1$. Since, the binary logic inputs can be either 0 or 1, they produce 4 sets of binary input: $(0, 0)$, $(0, 1)$, $(1, 0)$, $(1, 1)$. These four input conditions give rise to three distinct values of I_{in}. Hence, the input signal I_{in} generated, is a 3-level aperiodic wave form.

The state of this system, can be interpreted as logic output 1 when $x > x^*$ and logic output 0 when $x < x^*$, where x^* is roughly given by the position of the barrier between the two wells. Such an interpretation allows one to consistently obtain logical responses, such as OR and AND (see Table 1.1, when noise intensity D is in an optimal band. Complementary gates, NOR and NAND, can also be obtained in a straight-forward manner, by the alternate output determination : $x < x^*$ corresponding to logic output 1, and 0 otherwise.

In the first part of this thesis, we extend the theoretical and applied aspects of LSR and demonstrate how stochastic resonance in bistable or multi-stable nonlinear dynamical systems can be utilized to implement memory and logic function. We show how a general nonlinear dynamical system can operate flexibly, both as a NAND/AND gate and a

Logic inputs	OR	AND	NOR	NAND
0,0	0	0	1	1
0,1	1	0	0	1
1,0	1	0	0	1
1,1	1	1	0	0

Table 1.1: Relationship between the two logic inputs and the output of the fundamental OR, AND, NOR and NAND logic operations. On addition, the four distinct possible input sets $(0,0)$, $(0,1)$, $(1,0)$ and $(1,1)$ reduce to three conditions, as $(0,1)$ and $(1,0)$ are symmetric. Note that *any* logical circuit can be constructed by combining the NOR (or the NAND) gates [40, 41].

SetReset latch, by variation of an asymmetrizing bias. We also examine the possibility of obtaining dynamical behavior equivalent to LSR in a noise-free bistable system, subjected only to periodic forcing, such as sinusoidal driving or rectangular pulse trains.

Then we demonstrate how the width of the optimal noise window can be increased by utilizing the constructive interplay of noise and periodic forcing, namely noise in conjunction with a periodic drive yields consistent logic outputs for all noise strengths below a certain threshold. Thus we establish that in scenarios where noise level is below the minimum threshold required for logical stochastic resonance (or stochastic resonance in general), we can add a periodic forcing to obtain the desired effects.

We also verify our concepts in Vertical-cavity surface-emitting lasers (VCSELs) which are widely used for high-bit-rate data transmission because of their various advantages over conventional edge emitting lasers like low threshold current, single-longitudinal-mode operation, higher modulation bandwidth and circular output beam profile.

1.2 Spatiotemporal patterns in Complex Systems

In the second part of this thesis, we attempt to broaden our understanding of nonlinear dynamical systems in general by investigating the *emergence of spatiotemporal patterns in complex systems*.

Complex interactive systems provide the framework to model a wide class of phenomena and have been widely used to model spatially extended physical, chemical and biological systems, neural networks, social systems, world wide web and Internet etc. We are ourselves, as individuals, the units of a network of social relationships of different kinds and, as biological systems, the delicate result of a network of biochemical reactions

[42].

Developing models that can mimic the structural properties of real networks and understanding how the dynamical units on such complex networks behave collectively are the two major goals in study of complex systems. Since the seminal papers by Watts and Strogatz on small-world networks[43], and that by Barabási and Albert on scale-free networks [44], many unifying principles and statistical properties common to most of the real networks have been identified.

A prototypical dynamical network involves equations describing the time variation of state variables at the nodes or sites, and a set of links capturing the essence of the connection of a node with subsets of nodes in the system. Empirical results from various networks suggest that the degree distribution of a node, that is the distribution of the number of its direct connections to other nodes significantly deviates from the Poisson distribution expected for a random graph and, in many cases, exhibits a power law (scale-free) tail with an exponent taking a value between 2 and 3. They are also characterized by correlations in the node degrees, relatively short paths between any two nodes (small-world property), and by the presence of a large number of short cycles or specific motifs [42].

Small-World Networks

The small-world (SW) concept describes the fact that despite the large size of certain networks, the distance between any two nodes i.e. the number of edges along the shortest path connecting them, can be quite small. A popular manifestation of SW networks is the six degrees of separation concept, uncovered by the social psychologist Stanley Milgram (1967), who concluded that there was a path of acquaintances with a typical length of about six between most pairs of people in the United States [45]. Another common property of complex networks is clustering which is quantified by the clustering coefficient [43, 45]. For a node i with degree k_i, the clustering coefficient is given by:

$$C_i = 2E_i/k_i(k_i - 1) \tag{1.8}$$

where E_i is the number of edges connecting the node k_i with its k nearest neighbours. As this i^{th} node has degree k, the total number of possible edges is $k(k-1)/2$. The clustering coefficient of the whole network is the average of all individual $C_i s$. The SW networks are characterized by small path lengths and large clustering coefficient which is also observed in case of many real networks.

Disorder either in form of static or quenched inhomogeneities, or coherent driving forces, have yielded a host of interesting, often counter-intuitive, behaviours. For instance, stochastic resonance [3] in coupled arrays [46, 47, 48, 49, 50, 51, 52], diversity induced resonant collective behaviour in ensembles of coupled bistable or excitable systems [53],[54] demonstrated how the response to a sub-threshold input signal is optimized. It was recently shown that the collective response of strongly coupled bistable elements can reflect the presence of very few non-identical inputs in a large array of otherwise identical inputs [55].

As the first problem in the second part of the thesis, we verify the finding of [55] in an array of globally coupled Schmitt triggers. Schmitt trigger is a simple electronic system that can be easily made from commonly available electronic elements like an op-amp, and a few resistors and has been widely used to model bistable systems [56, 6]. In our explicit demonstration we have taken Schmitt triggers as the basic nonlinear bistable elements, and the inputs are encoded as voltages applied to them. The average of output voltages of all the Schmitt triggers corresponds to the global output of the system.

Time varying networks

The links in a complex network could be *static* or *dynamic*. Static or annealed links imply that the connectivity is invariant or quenched throughout the evolution of the system [57, 58]. Dynamic links on the other hand imply that the underlying connections may switch around, and so the nodes couple to changing environments. Studying the implications of such dynamic links is relevant, for example, in a socio-economic network, where the connectivity matrix generically changes over time. In the next two problems of this part of the thesis, we explore how changing the underlying web of connections at different rates influences the emergent spatiotemporal patterns in extended interactive systems.

In the first problem, we focus on a problem of considerable relevance, namely, the nature of infection spreading in a population of individuals connected by links that vary over a large range of time scales. At the level of individuals in the population, we consider the class of communicable diseases that progress as follows: at the outset an individual is *susceptible* to infection (a stage denoted by S); on infection through contact with other infected people, the individual moves to the *infectious* stage (I). In this stage of the disease, an individual may infect susceptible members of the population it comes into contact with. The infectious period is followed by a *refractory* stage (denoted by R), where the individual is immune to the disease and also does not infect others. So

the temporal evolution of the stages of the disease at the nodes of the network will be modeled by the well known epidemiological model of disease progression: the SIRS cycle. This model is appropriate for diseases like small pox, tetanus, influenza, typhoid fever and cholera [59]. We incorporate *changes in the underlying connectivity at varying time-scales*, ranging from fast to slow vis-a-vis the nodal disease dynamics. The important consequence of disease spreading on time varying networks that we will demonstrate is the following: *quick changes in the connections enhance synchronization, as compared with slow network changes*. Namely, epidemic outbreaks emerge in rapidly varying networks, while slowly changing links result in a low fluctuating state of endemic infection.

Synchronization of dynamical units at the nodes has attracted researchers from diverse fields like biology, ecology, sociology, power grids, climatology etc. [60, 61, 62, 63, 64]. Most of the earlier approaches have studied the stability of the synchronized state by linearising the dynamical equations [65, 66]. Such approaches have enabled the analysis of stability of large class of synchronized oscillators. However, there have been studies[67] where local stability predictions do not corroborate with the actual dynamical response of the system. Jost et al.[68], have proved that linear stability provides conditions for stability of synchronized solution that are necessary but not sufficient. Detailed studies of these cases reveal that local stability results can only be valid for small perturbations and here "small" could actually be "infinitesimal" in some cases. Thus to correctly predict the dynamical response to any kind of perturbation, one should have a clear idea about complete landscape of the coupled system. By complete landscape we mean that one should know the size of basin of attraction[69, 70] for all local minimas present in the system.

To probe the stability of the synchronized state in case of large perturbations, it was proposed that the basin of attraction of the synchronized state be also estimated [69]. In this regard, Menck et al. [71] propounded the concept of Basin Stability (BS) based on the volume of basin of attraction and showed that the linear stability and BS may be quite different and both approaches should be considered to evaluate the stability of the synchronized state. They argued that the optimization of synchronizability and the simultaneous optimization of BS act as two opposing forces and their contest results in a topological trade-off: small-worldness [43].

In the last work of this thesis, we study the stability of the synchronized state when the underlying connection network evolves in time. The BS paradigm is particularly useful in case of time varying networks as it can be applied to large class of systems, whereas the linear stability analysis can be done exactly only in some specific cases. We

consider Watts-Strogatz (WS) networks and vary the fraction of random links p to cover broad range of networks varying from regular ring topology for $p = 0$ to random networks for $p = 1$. The time varying character is considered by assuming that each link rewires with a rewiring frequency f. Using the BS framework, we estimate the rewiring frequency at which the network can be approximated by the static time average. Further, we show how the stability range changes at different rewiring timescales and also get insights into how the transition from a static to a time averaged case takes place.

Now we start with the first part of thesis where we explore the *application of nonlinear dynamics in the design of computing systems*. In chapter 2 we shall see how LSR elements can be used as memory devices and demonstrate noise-free LSR in chapter 3. In chapters 4 and 5 enhancement of optimal noise window using a periodic forcing is shown.

Part I

Nonlinear Dynamics in Computing Systems

Chapter 2

Noise assisted morphing of memory and logic function

2.1 Introduction

In this chapter we examine the possibility of utilizing a noisy nonlinear system, not just as a logic gate, but also *directly as a memory device*, i.e., we explore if the system can behave as a latch in some optimal range of noise[1].

A latch is a system that has two stable states and can be used to store state information. The system can be made to change state by signals applied to one or more control inputs, as shown in the truth table (Table 2.1). Latches are fundamental building blocks of a computing machine, and is omnipresent in computers and communication systems. So proposals of implementations of a latch, that are more efficient from the point of view of space or operational time, have far-reaching consequences.

Now latches can be built around a pair of cross-coupled inverting elements, such as vacuum tubes, bipolar transistors, field effect transistors, inverters, and inverting logic gates. Specifically, for instance, conventional latches are constructed out of two cross coupled NAND or alternately NOR gates. Here, unlike traditional latches built by concatenating two logic elements, we will use only *one* element to implement the latch truth table. Our proposal does not necessitate cross-coupling the logic gates, nor does it involve many clock cycles. So the direct realization of the latch here has the potential to save

[1]Results have been published in [72]

both space and time costs.

In the next sections, we shall demonstrate how the Set-Reset latch operation can be obtained consistently in an optimal window of noise i.e. when the noisy bistable system is fed with a low amplitude input signal, consisting of two aperiodic pulses encoding two logic inputs, the output consistently mirrors a latch output (as displayed in Table 2.1). We also show how one can use a bias to get different types of responses from the same system, thereby obtaining an element that is easily *reconfigurable* to yield, not only gates, but a memory device as well. That is, in an optimal range of noise, by varying the bias, the *same* system will yield logic functions like AND, OR etc. as well as give latch operations directly.

2.2 General Principle

Consider the general nonlinear system,

$$\dot{x} = F(x) + b + I_{in} + D\eta(t) \tag{2.1}$$

where $F(x)$ is a generic nonlinear function representing the force field of a potential with two distinct stable wells. I_{in} is the input signal which encodes the logic inputs, b is bias to asymmetrize the two potential wells, and $\eta(t)$ is an additive zero-mean Gaussian noise with unit variance, with D being the amplitude(intensity) of the noise.

A logical input-output correspondence is obtained by driving the system with two trains of aperiodic square pulses: $I_1 + I_2$, encoding the two logic inputs. For logic operations such as OR/NOR and AND/NAND, we consider the inputs to take value I when the logic input is 1, and value $-I$ when the logic input is 0, where input strength I is: $0 < I < 1$. Since, the binary logic inputs can be either 0 or 1, they produce 4 sets of binary input: $(0,0)$, $(0,1)$, $(1,0)$, $(1,1)$. These four input conditions give rise to three distinct values of I_{in}. Hence, the input signal I_{in} generated, is a 3-level aperiodic wave form.

The state of this system, is interpreted as logic output 1 when $x > x^*$ and logic output 0 when $x < x^*$, where x^* is roughly given by the position of the barrier between the two wells. Such an interpretation allows one to consistently obtain logical responses, such as OR and AND, when noise intensity D is in an optimal band. Complementary gates,

Set (I_1)	Reset (I_2)	Latch
0	0	No change(maintain the previous state)
0	1	0
1	0	1
1	1	Restricted Set

Table 2.1: Relationship between the two inputs and the output of Set-Reset latch.

I_1	I_2	Latch
0	0	0
0	1	No change(maintain the previous state)
1	0	No change(maintain the previous state)
1	1	1

Table 2.2: Relationship between the two inputs and the output of a Stochastic Resonance latch.

NOR and NAND, can also be obtained in a straight-forward manner, by the alternate output determination : $x < x^*$ corresponding to logic output 1, and 0 otherwise.

Now, to use this element as a Set-Reset latch, we need to modify the encoding of input values, so that we can distinguish between $(0, 1)$ and $(1, 0)$ states, as the latch truth table is *asymmetric* with respect to inputs unlike the usual logic gates. A simple way to accomplish this is to have the following asymmetric input encoding: the first input I_1 takes the value $-I$ when the logic input is 0 and I when the logic input is 1, while the second input I_2 takes the value I when the logic input is 0 and $-I$ when the logic input is 1, where $0 < I < 1$.

Equivalently, instead of the asymmetric input association described above, we can consider symmetric input associations (as in the logic operations), and apply a NOT operation to the second input I_2. This will also yield the same physical input signal I_{in}. Namely, corresponding to the 4 sets of binary inputs (I_1, I_2): $(0, 0)$, $(0, 1)$, $(1, 0)$, $(1, 1)$, the input signal I_{in} takes the values 0, -1, 1, and 0 respectively. Out of these four sets, the input corresponding to $(1, 1)$ is a restricted set and does not occur in the truth table. So we are left with three input sets, each one giving rise to a *distinct* value of I_{in}. Hence the input signal I_{in} generated, is again a 3-level aperiodic wave form. The other way is to implement a latch with different input-output correspondence. The truth table of such a latch is shown in Table 2.2. We call it a *Stochastic Resonance Latch* and this latch can be implemented with same input encoding as for the logic gates.

Logic response from output can be obtained, as in logic operations, by defining a

Operation	Bias
Set-Reset Latch	0
AND/NAND	-0.5
OR/NOR	0.5

Table 2.3: Representative values of the asymmetrizing bias b in Eqn. 2 that yields the Set-Reset latch operation, OR/NOR logic operation and AND/NAND logic operation. Here $I = 0.5$.

threshold value x^*. If $x > x^*$, i.e., when the system is in the potential well x_+, then the logic output is taken to be 1, and 0, if $x < x^*$ and the system is in other well. Thus, the logic output toggles as the state of the system switches from one well to another.

2.3 Explicit Example

We now explicitly demonstrate latch functionality, using a simple nonlinear system:

$$\dot{x} = 2x - 2x^3 + b + I_{in} + D\eta(t) \tag{2.2}$$

where D is amplitude of the Gaussian noise, b is asymmetrizing bias and the potential energy function is bistable (see Fig. 2.1). The input signal, $I_{in} = I_1 + I_2$, where I_1 and I_2 encode the two logic inputs, with the encoding associations for the logic operations and the set-reset latch being different. The bias b, for different operations, is set as displayed in Table 2.3.

Also note that the nonlinear function above, is efficiently realized by a linear resistor, linear capacitor, and a small number of CMOS transistors [33]. Further, it is capable of operating in very high frequency regimes, and such a system may be implemented with integrated circuits and nanoelectronic devices. Other forms of the nonlinear function $F(x)$ in Eqn. 1 may be realized in optical [35, 73, 36], nanomechanical [34], chemical [37] and biological systems [38, 38].

Input pulses are given to the system in such a way that *all* possible combination of transitions are presented to the system, in *random sequence* (see the top 3 panels of Fig.2.2). The threshold for output determination, x^*, is 0 here. So to obtain the desired logic response, we interpret the state $x > 0$ as logic output 1 and $x < 0$ as the logic output 0. It is clearly evident from Fig. 2.2, that for moderate noise the system consistently yields the Set-Reset latch input-output association, while it fails to do so for very small

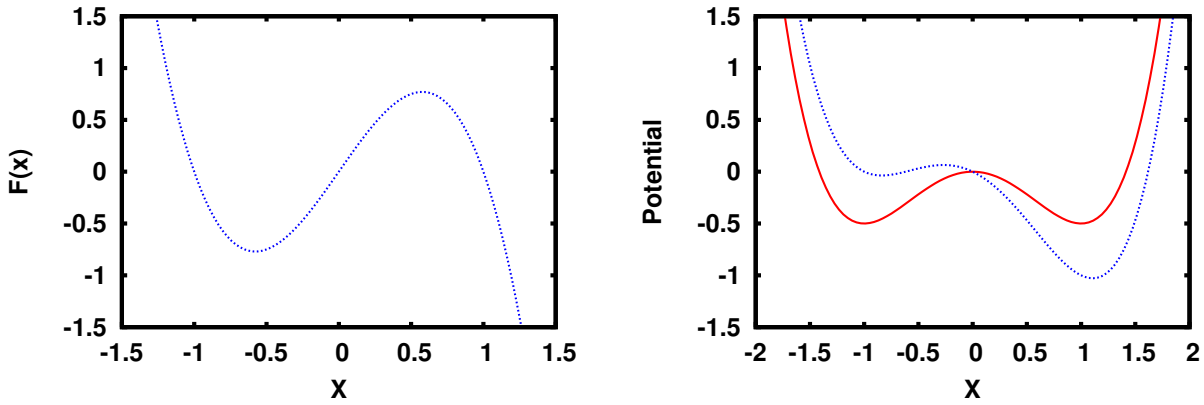

Figure 2.1: For the system described by Eqn.2: (left) the function $F(x) = 2x - 2x^3$ with $b = 0$ and (right) the effective potential obtained by integrating the function $F(x)$ in Eqn.2, with bias $b = 0$ (red solid line) and $b = -0.5$ (dashed blue line).

noise and large noise.

Note that the system holds its output steady, while the input signal is held constant, over long times ($\sim 10^3$ in our simulations). Namely, the system manages to maintain its state, which is in a local equilibrium of the potential, for reasonably small noise intensity D and large barrier height ΔV. This is because the Kramer's rate for escaping from the potential well (i.e., the inverse of the average switching rate induced by noise alone), given by $\sim \exp(-\Delta V/D)$, is very small here. So the system does not switch wells under the influence of noise alone. Rather it needs both signal and noise to effect a change. However, it is evident (for instance from Fig. 2.2) that as noise increases, the probability of random noise-induced well hopping increases, leading to loss of robustness for noise levels beyond the optimal window.

We can quantify the consistency (or reliability) of obtaining a given logic output by calculating the probability of obtaining the desired logic output for different sets of inputs, namely the ratio of successful runs where the desired logic output is obtained (after transience), to the total number of runs.

The system was simulated by keeping the value of one input set constant over 1000 time units, and we simulated the system over a sequence of 500 such sets. Unless otherwise stated, we allow a latency of 100 in the calculation of $P(logic)$. The values of inputs I_1 and I_2 were chosen to be randomly distributed so that $I_{in} = I_1 + I_2$ switched levels in an uncorrelated aperiodic manner. Thus the probability is one only if we get the desired response for all the 500 input sets.

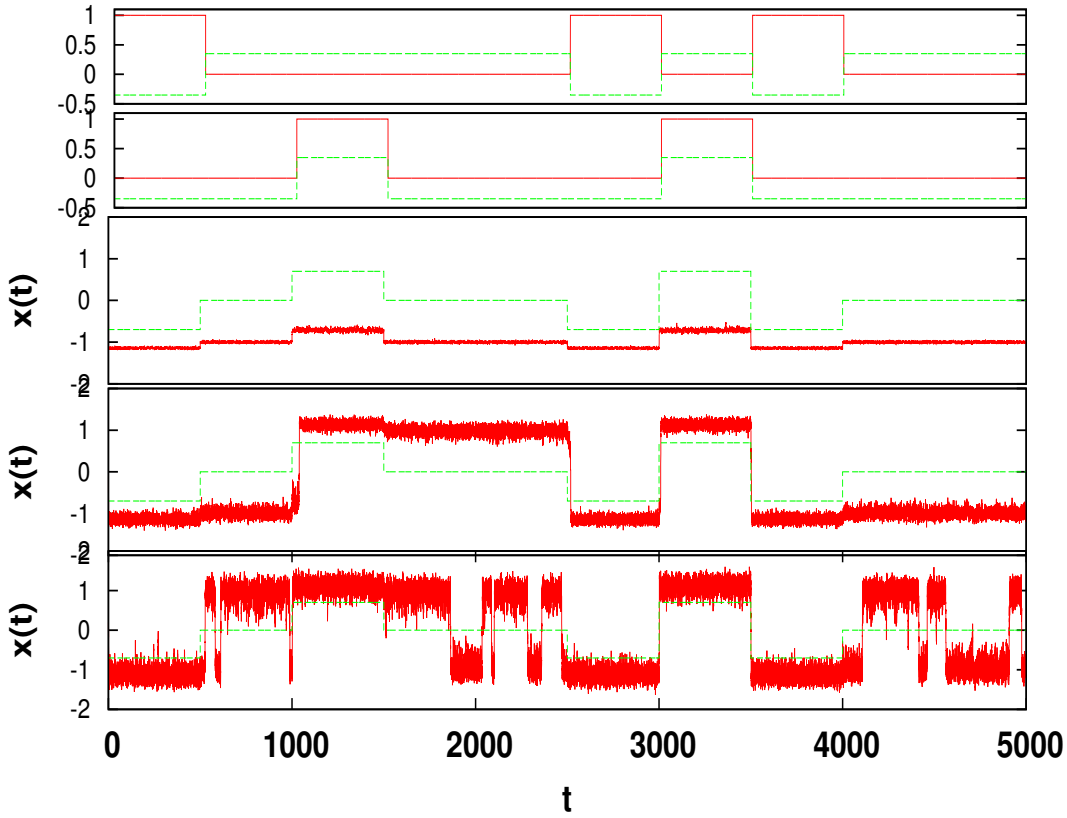

Figure 2.2: Panels 1 and 2 show streams of the two inputs. The input strength is 0.35. The logical value of the input is shown as a solid red line and the actual value as a dashed green line. For I_1 we have -0.35 when logic input is 0 and 0.35 when logic input is 1. For I_2 we have 0.35 when logic input is 0 and -0.35 when logic input is 1. Panels 3-5 show the outputs $x(t)$ corresponding to $D = 0.05$, $D = 0.25$, $D = 0.5$. Here bias $b = 0$, and the input signal $I_{in} = I_1 + I_2$ is indicated by the green line. Clearly, we get the desired output only when noise is within some optimal range (in this case panel 4 i.e. $D = 0.25$)

It is evident from Fig. 2.3 that we obtain consistent memory operation in an optimal window of noise. So the system behaves as a Set-Reset latch even for *sub-threshold input signals*, utilizing noise to store the information. This can lead to development of low power consuming memory devices. Further, one can manipulate the potential function to obtain robust operation in any given noise window (see Fig. 2.4)

We also observed *reduction in latency* with increasing noise. This is evident in Fig. 2.5. Clearly, the system responds faster to inputs when noise intensity is higher. That is, the desired hopping between wells happens more rapidly under the influence of stronger noise. This is yet another feature where noise aids performance (see Fig.2.6).

Further, it is evident from Fig. 2.7 that this system can also yield the logic response

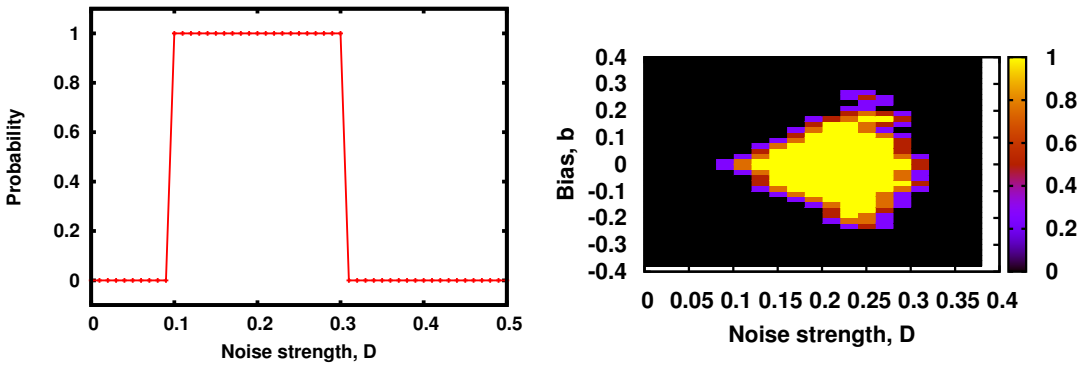

Figure 2.3: Probability for obtaining the Set-Reset latch operation for different values of noise strength, with bias $b = 0$ (left). Right panel shows the region for different bias (y axis) and noise strength (x axis). Evidently we get the Set-Reset latch operation only within an optimal window of noise strength.

of a AND/NAND gate and a OR/NOR gate, by changing the bias b in Eqn. 2. This suggests that within an optimal window of noise strength, we can morph the circuit to act either as a logic gate or as a memory device, by simply adjusting the value of bias, i.e., one can easily switch from Set-Reset latch operation to AND/NAND or OR/NOR logic operation (see Table 2.3). This is made possible by the change in the symmetry and depths of the potential wells with change of bias b.

Note that the noise region of optimal operation depends on the form of the nonlinear function $F(x)$ in Eqn. 1, as well as on the input signal strength, as displayed in Figs. 2.8. In order to obtain an overlapping window of optimal noise strength for the different operations, one can adjust the input strength appropriately or choose a nonlinear function that yields the desired operational window for the given noise floor.

2.4 Discussions

In this work, we have explicitly shown that a nonlinear system functioning in a noisy environment, can produce a completely consistent Set-Reset latch operation on two inputs, streaming in any random sequence. We observed that for very small or very large noise strengths the system does not yield a reliable output. However, in a reasonably wide band of moderate noise strength, the system produces the desired output very consistently. Furthermore, the response of the system could be easily switched from memory to logic operations by varying the bias in the system. Lastly, it was observed that noise reduced latency in the response of the system.

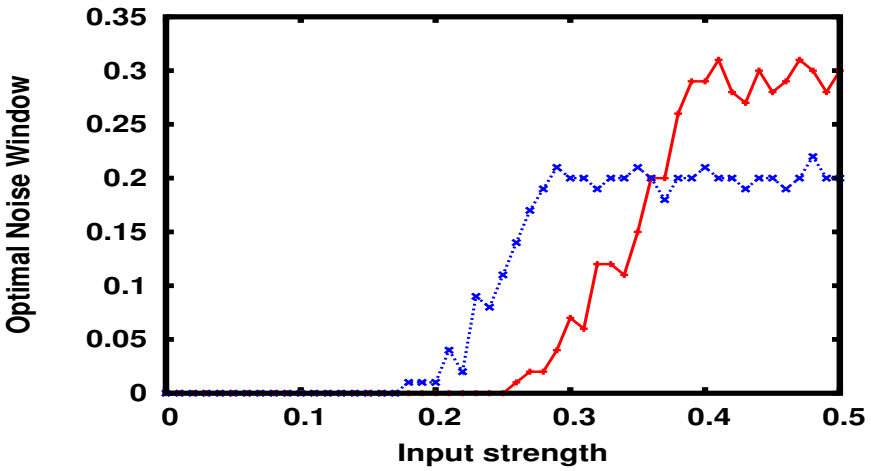

Figure 2.4: Size of the noise window of optimal Set-Reset latch operation for nonlinear function $F(x) = 2x - 2x^3$ (red) and $F(x) = 2x - 4x^3$ (blue), for different values of input signal.

So it is evident that "LSR Elements" can reliably function as memory devices even for sub-threshold signals, thus consuming very low power. Further, the same elements can be used to produce outputs corresponding to, not only latches, but logic gates as well. Thus these "LSR Elements" can potentially act as building blocks of futuristic "Smart Computing Devices".

Potentially, such devices will not only operate robustly in noisy environments, but will also be capable of optimal utilization of their resources by configuring their "LSR Elements" into latches, or any of the logic gates, depending on the requirements of the task being performed. For example, if we are performing tasks requiring more computational power like running a program, then these computing devices will morph most of the LSR elements to logic gates, whereas in case of tasks requiring memory like plotting large values of data, LSR elements will be morphed into memory enabling efficient use of resources. Furthermore, it is conceivable that devices based on such elements can potentially help in reducing boot times thus achieving what is commonly called "instant boot". This can be accomplished by morphing large number of LSR elements into memory at the time of shut down and start up. This significant increase in memory will enable us to keep most of the data required for the applications readily accessible, paving way for faster boot times.

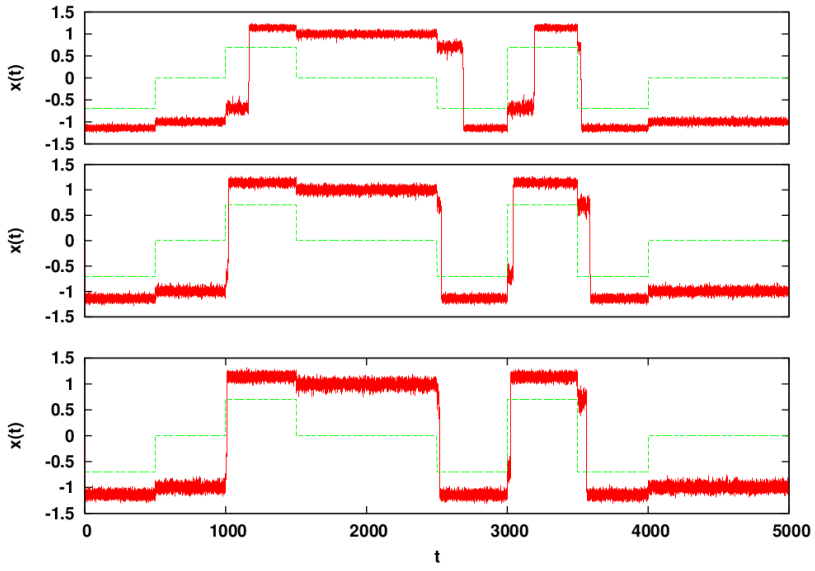

Figure 2.5: Panels 1-3 display the output $x(t)$ corresponding to $D = 0.10$, $D = 0.12$ and $D = 0.15$ (from top to bottom). The stream of inputs $I_{in} = I_1 + I_2$, with $I = 0.35$, is indicated by the green line in the figures. Clearly panel 3 has the shortest transients after input switches.

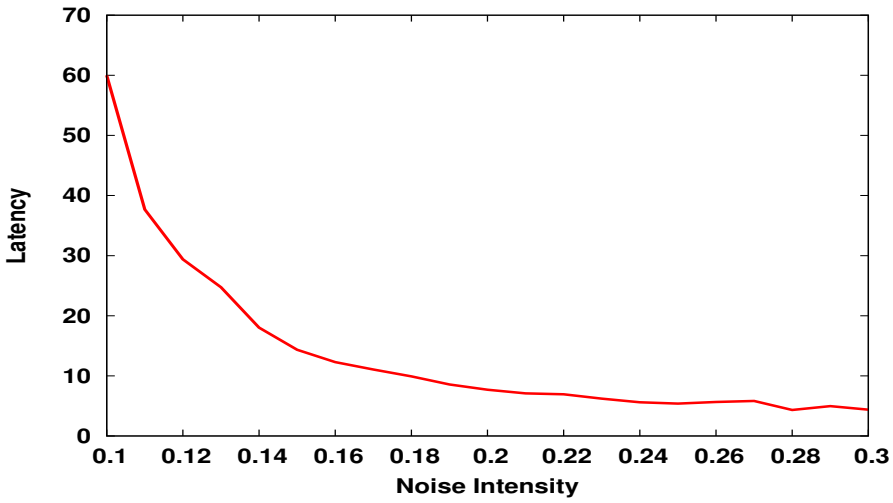

Figure 2.6: Latency (averaged over a random stream of inputs) as a function of noise strength. Here latency has been defined as the time taken to reach the barrier from a well, upon change in the input necessitating a change in the output.

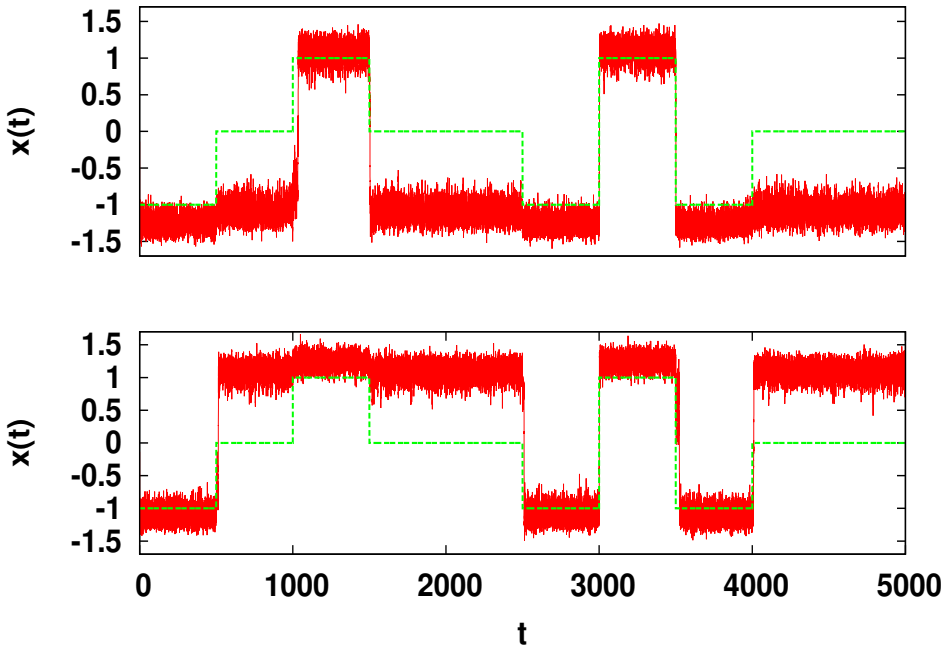

Figure 2.7: Panels showing output $x(t)$ corresponding to bias $b = -0.5$ (top panel) and $b = 0.5$ (bottom panel), with the green line indicating the input signal $I_{in} = I_1 + I_2$. Clearly, by adjusting the bias value we obtain logic output corresponding to AND gate (top) and OR gate (bottom). Here $I = 0.5$ and $D = 0.38$.

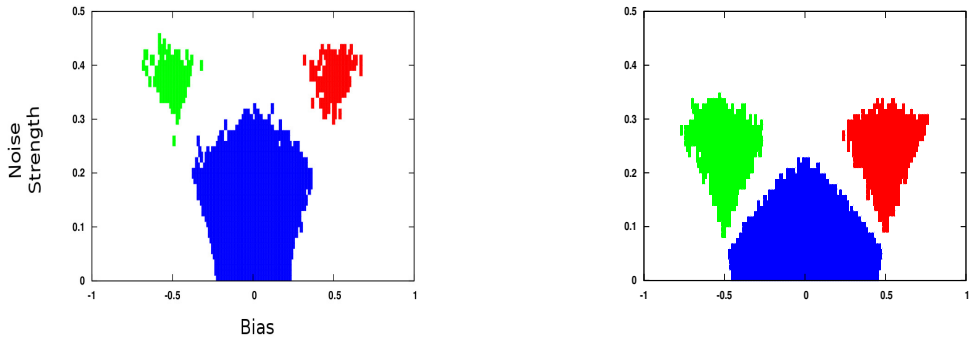

Figure 2.8: Points marking the region where the Set-Reset latch operation (blue), OR/NOR logic (red) and AND/NAND logic (green) are obtained with probability 1, for nonlinear function $F(x) = 2x - 2x^3$ (left) and $F(x) = 2x - 4x^3$ (right), with input signal strength 0.5 (left), and 0.75 (right) for different values of bias (x axis) and noise strength (y axis).

Chapter 3

Noise free logical stochastic resonance

3.1 Introduction

In this chapter we examine the possibility of "noise-free LSR", by driving a two-state system with periodic forcing instead of random noise. The central question is this: if the driving is completely regular, such as sinusoidal forcing, or a periodic train of pulses, would we still observe LSR? Namely, is noise a necessary ingredient of LSR?

Here we will demonstrate how noise-free LSR is indeed possible, i.e. we will show that when a nonlinear bistable system is presented a low amplitude input signal, consisting of (aperiodic) pulses encoding logic inputs, accompanied with periodic forcing, the state of the system accurately and consistently mirrors the output of a logic gate. We also show how one can reconfigure the type of logic response obtained by variation of a readily adjustable bias [1].

3.2 General Principle

First we lay out the general principle. Consider a nonlinear system under periodic forcing:

[1] Results of this chapter have been published in [74]

$$\dot{x} = F(x) + b + I + Df(\omega t) \tag{3.1}$$

where $F(x)$ is a generic nonlinear function obtained via the negative gradient of a potential with two distinct stable energy wells at x_+ and x_-. The bias b has the effect of asymmetrizing the two potential wells. I is the low amplitude input, typically aperiodic, signal. The functional form of the periodic forcing is f, with ω being the frequency and D being the amplitude (intensity) of the forcing.

As before, a logical input-output association (cf. Table 1.1) can be obtained by feeding the system with an input signal $I = I_1 + I_2$, where I_1 and I_2 are two (aperiodic) trains of square pulses encoding the two logic inputs. Without loss of generality, consider the inputs to take value 0.5 when the logic input is 1, and value -0.5 when the logic input is 0. The logic inputs being 0 or 1, produce 4 sets of binary inputs (I_1, I_2): $(0,0)$, $(0,1)$, $(1,0)$, $(1,1)$. These four distinct input conditions give rise to three distinct values of I. Hence, the input signal $I = I_1 + I_2$, is a 3-level aperiodic wave form.

The *logic output* is determined by the state x, and can be defined by a threshold value x^*, obtained from the position of the barrier between the two potential wells. If $x > x^*$, i.e., when the system is around the potential well x_+, then logic output is 1. The logic output is 0 if $x < x^*$, i.e. when the system is in the other well. Thus the output toggles as the state of the system switches between wells.

3.3 Explicit Example

We now explicitly demonstrate noise-free LSR, under sinusoidal forcing, for a system with cubic nonlinearity:

$$\dot{x} = 2x - 4x^3 + b + I_1 + I_2 + r(t) \tag{3.2}$$

where $r(t) = D\sin(\omega t)$.

For this system the threshold value x^*, defining the output, is 0. So, we interpret the state $x > 0$ as logic output 1 and $x < 0$ as the logic output 0. Alternately, complementary gates can be obtained by interpreting the output as 1 when $x < 0$, and as 0 when $x > 0$.

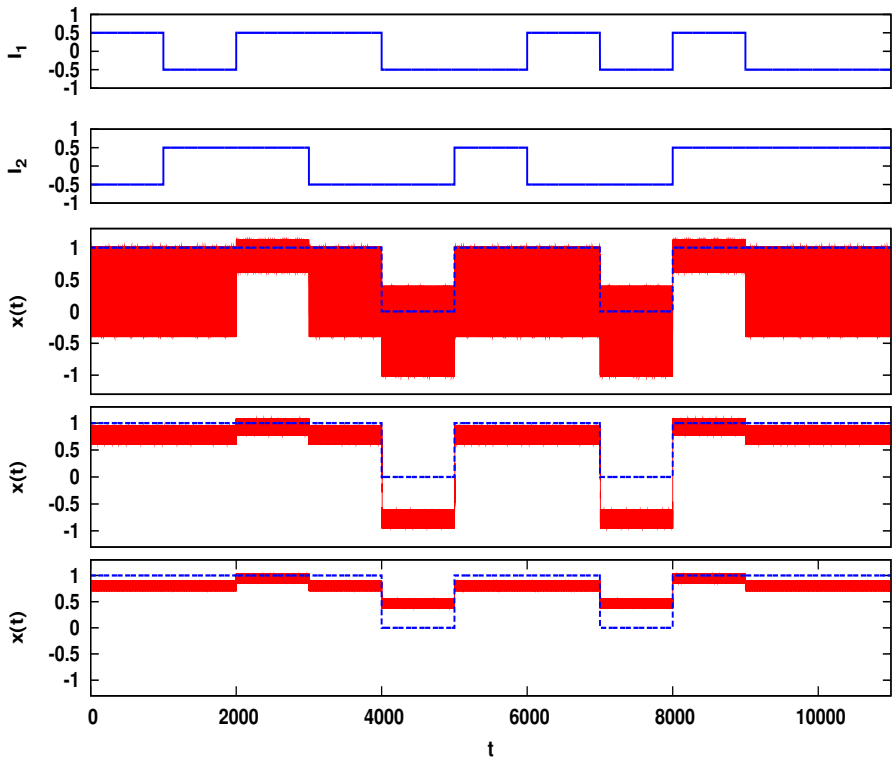

Figure 3.1: (Color online) Panels top to bottom show (a) streams of inputs I_1 and (b) I_2 (which take value -0.5 when logic input is 0 and value 0.5 when logic input is 1), and output $x(t)$ for forcing frequencies (cf. Eq. 3.2): (c) $\omega = 2$, (d) $\omega = 10$ and (e) $\omega = 20$. Here, $b = 0.5$ and $D = 2$. The dashed blue line in panels (c-e) indicates the expected OR logic output (with state $x > 0$ being logic output 1, and $x < 0$ being logic output 0). Clearly, only when $\omega = 10$, we get the desired OR gate consistently.

3.4 Results

The response of the system under different angular frequencies of sinusoidal forcing is displayed in Fig.3.1. Interestingly we observe, that in order to produce a robust logical combination of the inputs, the system requires an appropriate forcing frequency, which is neither too small nor too large. Namely, for a given value of bias b and amplitude of forcing D, we get the desired logical output *only for some suitable range of* ω.

Note that by simply changing the bias we can easily switch to another logic operation. In this case, when bias b is changed from 0.5 to -0.5, we morph from OR logic to AND logic. This is clearly evident from the timing sequences displayed in Fig.3.2. This effect

arises from the change in the symmetry and depths of the potential wells due to changing b. The complementary logic gates, namely NOR and NAND, can be straight-forwardly obtained by the alternate output interpretation.

We can quantify the consistency of obtaining a given logic output as follows: first we calculate the probability of obtaining the desired logic output for different sets of input, i.e. the ratio of the number of successful runs (namely a run where the desired logic output is obtained) to the total number of runs. We then define a very stringent measure P reflecting the reliability of the system as a logic gate: when the probability defined above is ~ 1 (i.e. when the logic operation is correctly obtained for all given input sets) we take P to be 1, and 0 otherwise. Namely, partial success, where certain combinations of inputs fail to give the correct logic output, leads to $P = 0$, since we want the logic response to be obtained for *all* random combinations of inputs. From the point of view of applications, anything less is not useful, and our measure of successful gate operation P reflects this stringent requirement.

Fig.3.3 shows the variation of P for logic operations AND and OR with respect to drive frequency. It is clearly evident that we obtain a window of angular frequency for which our system consistently gives the desired logic response as output, i.e. for $\omega_{low} < \omega < \omega_{high}$ the system yields perfect gate operations. Forcing at angular frequencies lower than ω_{low} acts like a quasi-static "signal", akin to a bias, as the timescale of the drive is too slow and does not vary much vis-a-vis the natural timescale of the system. Frequencies larger than ω_{high} do not achieve the desired response, as the drive then varies so fast that the system effectively responds to an averaged force field. Variation of optimal window of sinusoidal frequency and noise strength for various input strengths is shown in Fig. 3.4. We see that as we increase the input strength, the size of optimal window increases and saturates afterwards. Further, we observe in Fig.3.5 that by increasing the amplitude of sinusoidal forcing (D) the optimal window we get for ω, widens and shifts to the higher end. Namely, the lower and upper thresholds of optimal angular frequency (ω_{low} and ω_{high}) increases for increased value of D.

In order to demonstrate the generality of our results, we now drive the system with a periodic rectangular waveform, and show that this too allows us to obtain a LSR like response. So consider the system in Eq.2 above, now forced with a rectangular wave, where $r(t)$ switches periodically between the values 1 and -1, with time period $T = 2\pi/\omega$, where ω is the angular frequency, D is amplitude of rectangular pulse, and b is the asymmetrizing bias. In this system too, we observe that reliable logic output is obtained for intermediate frequencies.

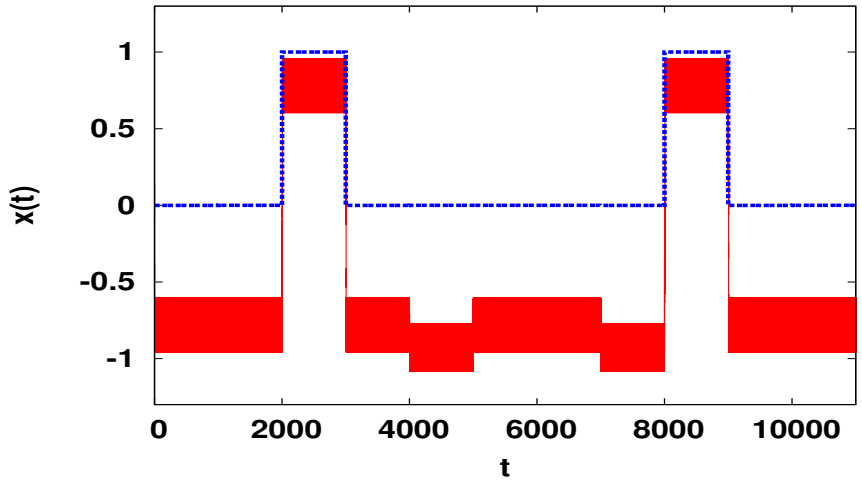

Figure 3.2: Waveform of $x(t)$ (cf. Eq. 3.2) with angular frequency $\omega = 10$, $b = -0.5$ and $D = 2$. The bold blue line indicates the expected AND logic output. By changing bias b from 0.5 to -0.5, we were able to switch from OR (cf. Fig.3.1) to AND gate.

Further it is evident from Fig. 3.5 that driving with rectangular pulses is more efficient, as the system can function as a logic gate for lower amplitudes D, as well as over larger ranges of forcing frequencies for fixed D. We also investigated the logic response under increasingly low input strengths. We found that rectangular forcing allows logic behaviour for lower input strengths than sinusoidal forcing, again demonstrating the efficiency of driving with rectangular waveforms.

In the examples above, we have thus shown that noise is not a necessary condition to obtain a consistent logic response. It is possible to have phenomena completely analogous to LSR, without noise. So the forcing that induces the desired hopping in response to inputs does not have to be random noise, but can be a sine wave or even a cyclic set of pulses. The system needs only appropriate pushes sufficiently often, in order to change its state to the desired well. The timescale of the forcing is crucial, while its form can range from noise to sinusoidal forcing or rectangular pulses.

An explanation for the optimal band of frequencies is obtained by examining the time taken by the system to cross over the barrier from the bottom of the wells under the input signal encoding the logic inputs $(0, 1)$ or $(1, 0)$, which is the most difficult and sensitive case to satisfy consistently. The inverse of this time is analogous to the Kramer's rate representing the characteristic escape rate from a stable state of a potential, and deter-

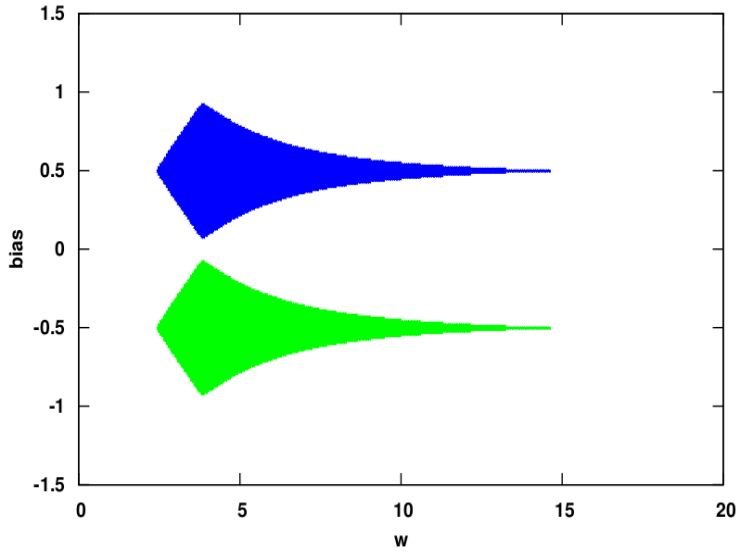

Figure 3.3: The shaded areas indicate where the probability P of obtaining the OR (top blue) and AND (bottom green) logic operation is 1, as functions of angular frequency (x-axis) and bias (y-axis). In both the cases, $D = 2$.

mines the band of forcing frequencies and amplitudes that allow robust logic response. Now, in order to obtain a consistent logic response, the system must simultaneously satisfy certain conditions. First, the driving frequency should be more than the frequency at which the stream of inputs switch. Secondly, for a fixed value of amplitude D, the following has to be ensured: when the input signal encodes the logic input set $(0, 1)$ or $(1, 0)$ (i.e. $I = I_1 + I_2 = 0$), the system should be in the appropriate well. For instance, for OR logic, under net zero input signal the system should be in the higher well. So it should be able to cross the barrier from the lower to the upper side. At the same time, the reverse crossing should not occur. These two conditions set the two limits on forcing frequency (see Fig. 3.6).

Further, the forcing frequency should not be so high that system is unable to respond to it, i.e. the time for which the driving force pushes the system in the requisite direction should be more than the time that the system takes to shift from one well to other. The amount of time taken by the system to cross over to the desired well in response

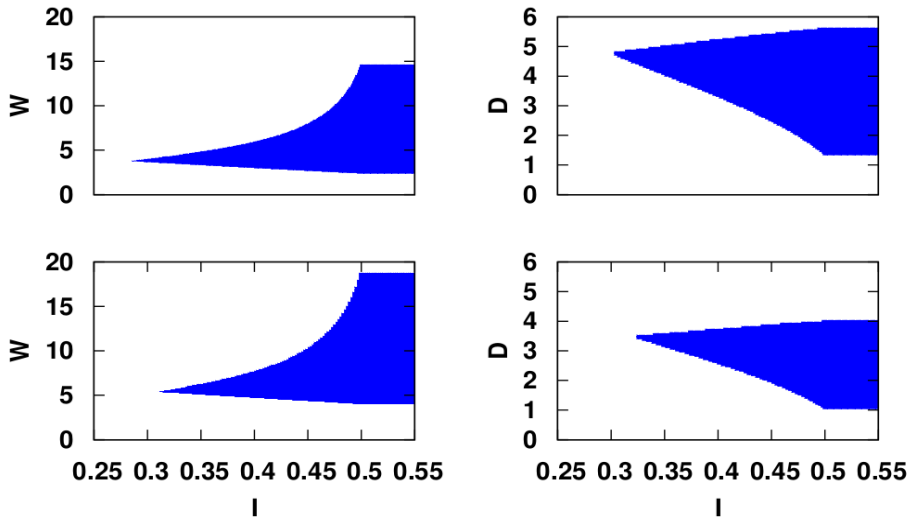

Figure 3.4: The shaded areas indicate where the probability P of obtaining the logic operation is 1, as functions of angular frequency (left) and noise intensity (right) with input strength for fixed noise intensity D (left) and angular frequency ω(right)

to a new input signal, namely the transience (which determines latency), should also be sufficiently high so that system has enough time to make the passage. Further, for very low frequency forcing, the system may have long transience as the transient period must include at least one full cycle of forcing.

Lastly, we present the realization of these results in electronic circuit experiments. In Fig.3.7, the analog simulation circuit for Eq.(2) is depicted. The input sinusoidal signal is denoted as $f(t)$. The amplitude of the sinusoidal signal is fixed at $2V$ and the frequency values range from 500 Hz to 30 KHz. $I(t)$ corresponds to logic input signal $(I_1 + I_2)$, where the logic input signals I_1 and I_2 take value -0.5V when logic input is 0 and value 0.5V when logic input is 1. The bias voltage V_c corresponds to bias b in Eq.(2). We set V_c equal to 0.5V and -0.5V for the different logic operations. The output node voltage (V_O) of operational amplifier OA2 correspond to $x(t)$ of Eq.(2).

Representative results of circuit realizations of sinusoidal forcing are displayed in Fig.3.8. Comparison with Fig.3.1 clearly shows that the same phenomenon is observed in these experiments. Namely, only with sinusoidal forcing with moderate frequency, equal to 10 KHz, do we get the desired logic gate operation reliably.

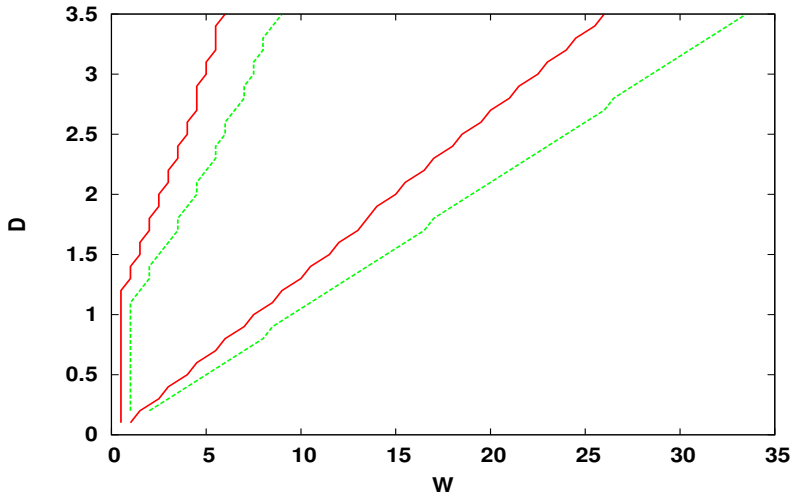

Figure 3.5: The curves indicate the limiting forcing frequencies ω_{low} and ω_{high}, for varying amplitude D, for sinusoidal forcing (red solid line) and rectangular forcing (green dashed line). Here $b = 0.5$ and the probability of obtaining the OR logic operation (leaving small transience after the switching of inputs) is 1 for the values of D and ω lying between the two lines, i.e. the lines mark the highest and lowest forcing frequencies yielding robust logic for different forcing amplitudes (and analogously the highest and lowest driving amplitudes for different frequencies).

3.5 Conclusion

In summary, we have explicitly shown through numerics and circuit experiments, that it is possible to obtain a logic response exactly similar to LSR, without the presence of noise. Using only a periodically driven bistable system, we are able to produce a logical combination of two inputs streaming in any random sequence. For very small or very large forcing frequencies the system does not yield any consistent logic output, but in a wide band of moderate frequencies the system produces the desired logical output very reliably. Furthermore, the logic response of the system can be easily switched from one logic gate to another by varying the bias in the system. Thus it is evident that "Noise Free LSR" indeed exists, and noise is not a necessary ingredient to facilitate changes of state that reliably mirror logical outputs.

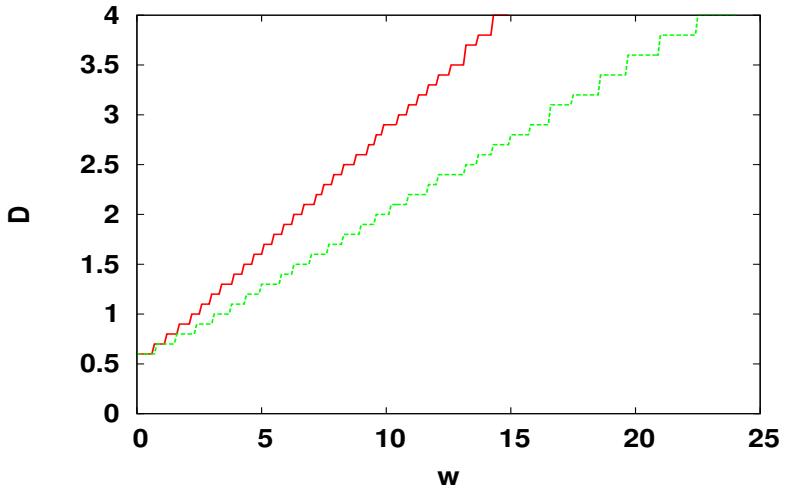

Figure 3.6: Lines indicating the limiting forcing frequencies for which the system crosses the barrier, when driven by a rectangular wave of amplitude D. Specifically for all frequencies ω and amplitudes D above the lines, the system crosses over with probability 1, within 100 time steps, from upper to lower well (solid red line), and from lower well to upper well (dashed green line). Here bias $b = 0.5$ (appropriate for OR logic) and input signal $I = 0$ (namely encoding logic input set $(1, 0)/(0, 1)$). The area inside these curves give the allowed forcing frequency and amplitude band, as it allows the crossing from the lower to the upper well, but not the reverse. These curves mirror the ones displayed in Fig.3.5.

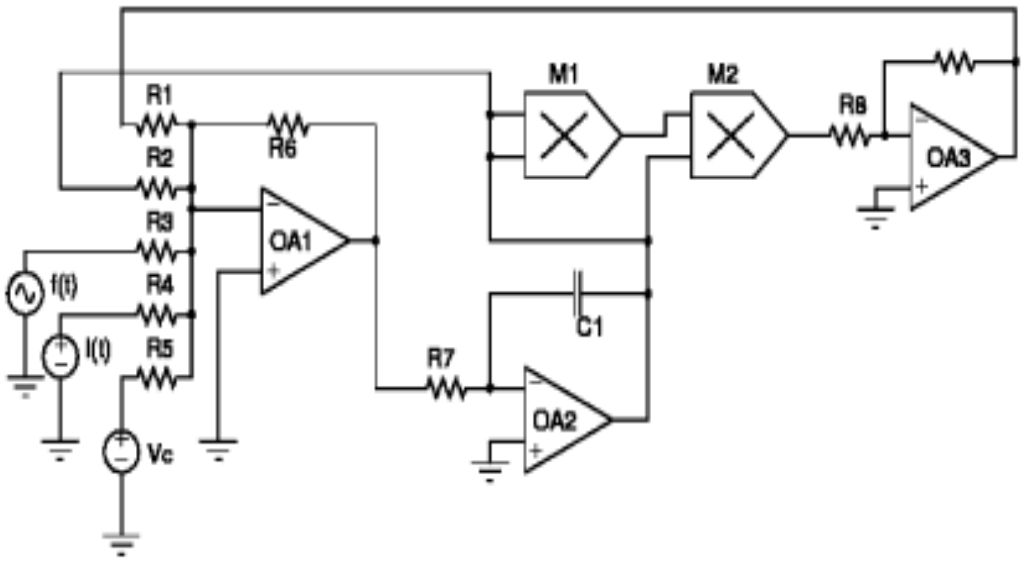

Figure 3.7: Circuit diagram: here OA1, OA2 and OA3 are operational amplifiers (AD712). M1 and M2 are analog multipliers(AD633). The resistor values are fixed as $R1 = R3 = R4 = R5 = R6 = R8 = 100\ k\Omega$. $R2 = 50\ K\Omega$, $R7 = 10\ K\Omega$, $R9 = 400\ k\Omega$. The capacitor value is fixed as $C1 = 0.01\ \mu F$.

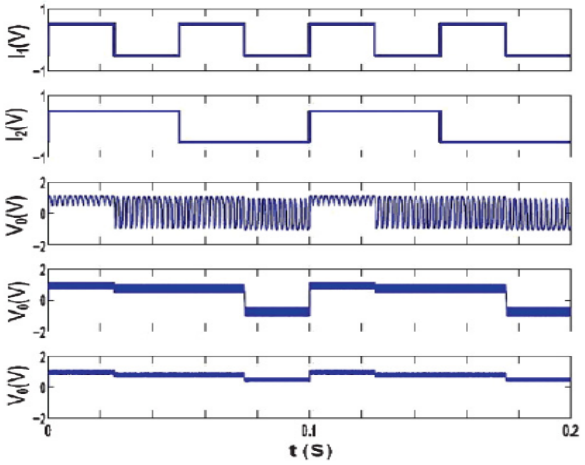

Figure 3.8: From top to bottom: panels a-b show streams of inputs I_1 and I_2, which take value -0.5 when logic input is $0V$ and value $0.5V$ when logic input is 1; panels c-e show the waveforms of the output voltage, with angular frequencies: $\omega = 2$ KHz, $\omega = 10$ KHz and $\omega = 20$ KHz. Here, $b = 0.5V$, $D = 2V$. The bold blue line indicates the expected OR logic output. Clearly, only when $\omega = 10$ KHz, we get the desired OR gate consistently.

Chapter 4

Periodic signal enhanced logical stochastic resonance

4.1 Introduction

In the previous chapters, the phenomena of *logical stochastic resonance* (LSR) was demonstrated: namely, when a bistable system is driven by two inputs it consistently yields a response mirroring a logic function of the two inputs in an optimal window of moderate noise. In chapter 2, it was shown that the same LSR elements can also be morphed into memory devices in a reasonably wide band of noise.

The noise in a system doesn't stay at the same level. Since LSR works in an optimal range, it is possible that the noise in the system is not sufficient to drive the system, i.e. the noise is below the minimum threshold of the optimal noise window. For instance, in case of thermal noise fluctuations in the environment such as ambient temperature, or certain internal processes, such as the work load of the device, may change the level of noise present in the system. So under weak load or in cold environments the system may not operate robustly.

In chapter 3, it was shown that dynamical behavior equivalent to LSR can be obtained in a *noise-free* bistable system, subjected only to periodic forcing, such as sinusoidal driving or rectangular pulse trains. This opens up the possibility of studying the behavior of bistable elements subjected to both a periodic signal, as well as noise. In this chapter, we will demonstrate how periodic forcing and noise interact constructively, thereby allowing us to obtain consistent logic and memory operations over a *much larger noise window.*

Thus, by adding a periodic signal to a noisy nonlinear system we can obtain LSR consistently even if noise level is lower than the minimum threshold required to obtain LSR. Further, we can use two coupled bistable systems in which the output of one bistable system controls the amplitude of the periodic forcing fed into the other system. This suggests a way in which to *adaptively adjust the strength of periodic forcing depending on the noise level present in the system*[1]

4.2 General Principle

Consider the general nonlinear dynamical system,

$$\dot{x} = F(x) + b + I + D\eta(t) + A\ f(\omega t) \tag{4.1}$$

where $F(x)$ is a generic non linear function obtained via the negative gradient of a potential with two distinct stable energy wells. I is the input signal which is the sum of two square pulses encoding the two logic inputs, b is bias to asymmetrize the two potential wells, $\eta(t)$ is an additive zero-mean Gaussian noise with unit variance and D is the amplitude(intensity) of noise. The functional form of the periodic forcing is f, with ω being the frequency and A being the amplitude of the forcing.

A logical input- output correspondence can be obtained by driving the system with two trains of aperiodic square pulses: $I = I_1 + I_2$, where I_1 and I_2 encode the two logic inputs. Logic output can be obtained from the state x by defining a threshold value x^*. If $x > x^*$, then the logic output is interpreted to be 1, and 0 otherwise.

4.3 Explicit Example

We now explicitly demonstrate this phenomena in the system given by:

$$\dot{x} = a_1(x - a_2x^3) + b + I_1 + I_2 + A\sin(\omega t) + D\eta(t) \tag{4.2}$$

where D is the amplitude of noise, b the asymmetrizing bias and the functional form

[1]Results of this chapter have been published in [75]

of periodic forcing is sinusoidal with A being the amplitude of the sinusoidal forcing. The parameters a_1 and a_2 control the height of the potential barrier and the location of potential minima. In absence of other terms, the height of potential barrier is $a_1/4a_2$ and the wells are at $\pm\sqrt{1/a_2}$ as shown in figure 4.1. Here we have taken $a_1 = 4$, and $a_2 = 5$. This function $F(x)$ is reasonably insensitive to noise and its two stable states are close to the encoded values of inputs. This helps to *cascade the gates, and feed the output directly as input, without any scaling factors.*

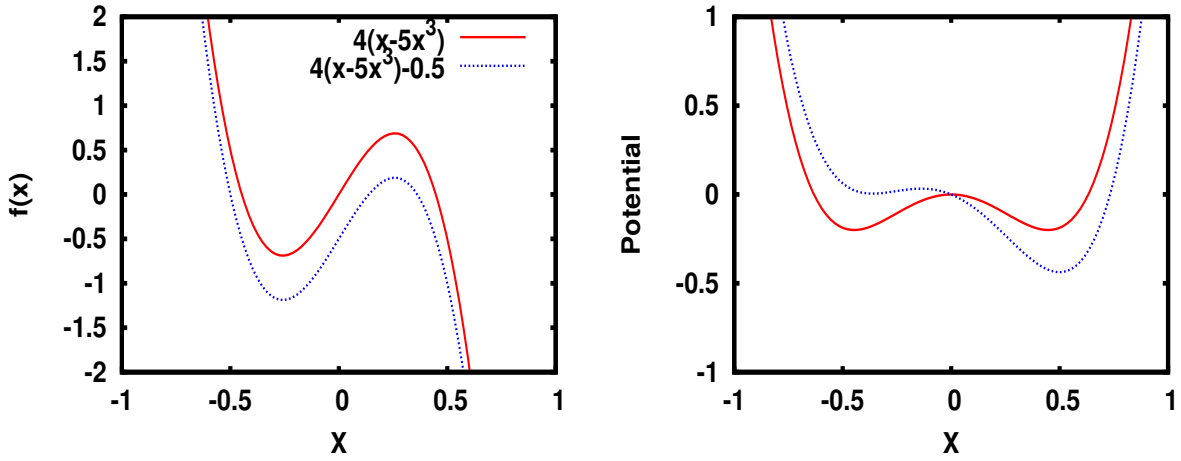

Figure 4.1: For the system (2): (left) the function $F(x)$ and (right) the effective potential obtained by integrating the function $F(x)$, for different bias: (a) $b = 0$ (red solid) and (b) $b = -0.5$ (blue dashed line).

The logic inputs are presented to the system with I_1 and I_2 switching levels in an uncorrelated aperiodic manner. The inputs being 0 or 1, produce 4 sets of binary inputs (I_1, I_2): $(0, 0)$, $(0, 1)$, $(1, 0)$, $(1, 1)$. These four distinct input conditions gives rise to three distinct values of I. Without loss of generality, consider the inputs to take value 0.5 when the logic input is 1, and value -0.5 when the logic input is 0. Hence, the input signal I, generated is a 3-level aperiodic wave form.

We choose 0 as our output determination threshold. If $x > 0$, i.e., when the system is in the positive potential well, then the logic output is interpreted to be 1, and 0 otherwise. Thus the logic output toggles as the system switches wells.

4.4 Results

We simulated the system in equation 4.2 for various possible frequencies and amplitude of the sinusoidal forcing and at various noise strengths. We used $b = -0.5$, so the system is biased to function as AND gate. We know that by changing the bias, we can easily switch to another logic operation. In this case, when bias is changed from -0.5 to 0.5, we obtain the OR gate. When bias is reduced to zero, we get a memory device. This effect arises from change in the symmetry and depths of the potential wells due to changing b. For brevity, we will show the results only for the representative AND gate.

We observe that for low noise strengths the system doesn't give the correct logical response in absence of periodic forcing as expected. However, as we apply some periodic forcing, the system gives the desired response. Notice that this response is obtained through interplay of noise and periodic forcing, as in absence of any one of these the system does not yield the desired response. *Only when both are present simultaneously, do we get the requisite output*, as shown in figure 4.2.

So when the noise level is low, it is not sufficient to induce the desired switch from one well to the other. Similarly, for high frequency or low amplitude, the sinusoidal forcing cannot drive the required hopping. However, when both are present, they aid each other to give the appropriate switching. Thus at low noise, the periodic forcing helps the system to switch wells in the desired fashion, in response to the inputs.

We can quantify the consistency (or reliability) of obtaining a given logic output by calculating the probability of obtaining the desired logic output for different states of input. The probability, here, is the ratio of number of successful runs, i.e. when the desired logic output is obtained, to the total number of runs. In every run, we simulate the system for 7 different possible combinations of I_1 and I_2 such that we get all possible transitions of the inputs. Thus, any run is counted as successful only if the system is in the desired well for all seven possible combinations of the inputs, allowing for a small transience. Here we have chosen the transience time to be equal to 10 percent of the time for which an input is applied. Thus the system must remain in for 90 percent of the input time.

Now we vary the noise strength and amplitude of periodic forcing keeping the frequency of the sinusoidal forcing constant. We observe that when the amplitude of sinusoidal forcing is low, we get the correct logical response only when there is some noise in the system. For very low or very high values of the noise intensity, we get erroneous

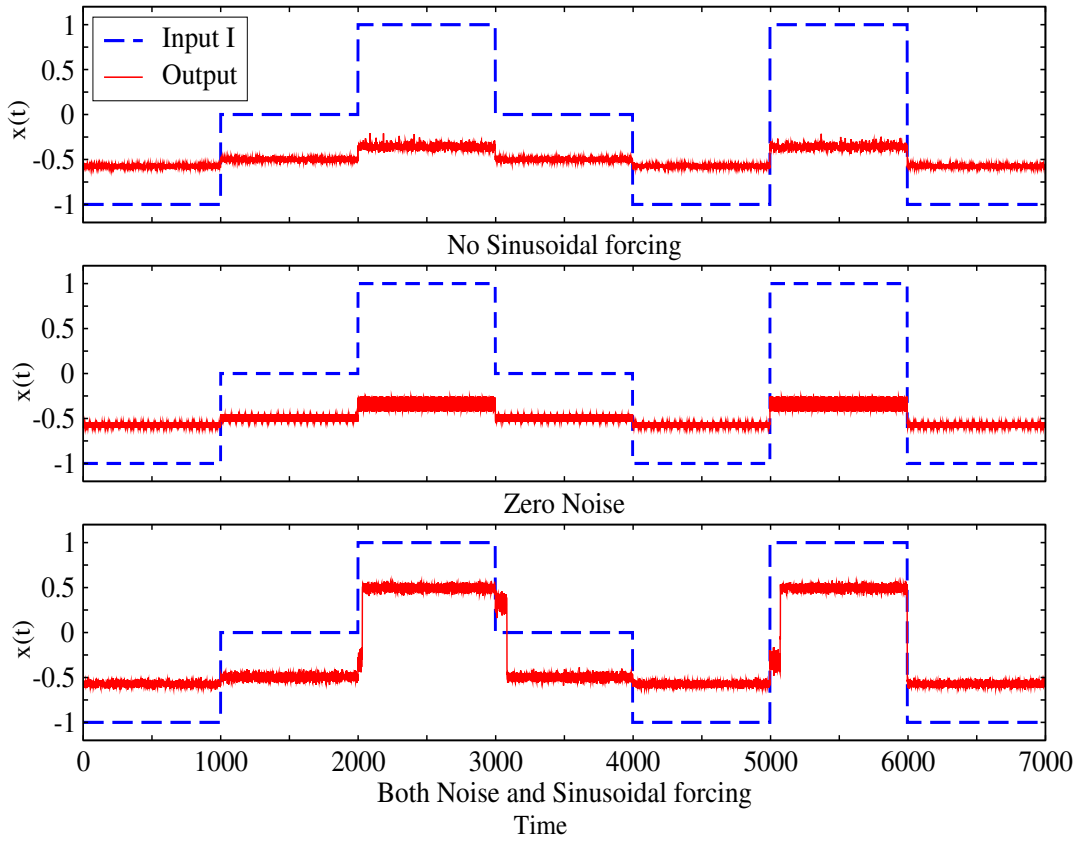

Figure 4.2: The panels show the waveforms of $x(t)$ obtained from simulating the system (2). In the top panel the amplitude of periodic forcing is zero and there is only noise in the system, with the noise intensity being below the minimum threshold required for LSR. In the middle panel the system is driven by periodic forcing only, and its amplitude and frequency are such that it alone can't drive the system to act as a robust logic gate. Only when there are both noise and periodic forcing, we get the desired AND gate (panel 3). The specific values of inputs used are $b = -0.5$, $D = 0.08$, $\omega = 4$ and $A = 0.5$. Dashed blue line shows the input I ($I_1 + I_2$) and red line shows x(t).

results. For higher amplitudes of sinusoidal forcing, periodic forcing alone can drive the system to the desired well, even in absence of noise. Notice that as we keep on increasing the amplitude of sinusoidal forcing, the maximum noise intensity for which we obtain correct logical response decreases slightly. This is expected as the interplay of noise and periodic forcing is likely to worsen the response at higher values of noise strengths, as now the state of the output starts hopping randomly between the two wells as shown in figure 4.3.

Next we keep the amplitude of periodic forcing constant, and vary the frequency of the sine wave. We observe that for low frequencies we obtain the desired response for low noise levels and as the frequency is increased the optimal window reduces and slowly shifts

upwards as seen in figure 4.4. One can rationalize this as follows: when the frequency is higher, the system gets little time to respond to the sinusoidal forcing, thus limiting its effect. This is also evident from the bottom panel of figure 4.4 which clearly shows that if the noise level is constant, then as the frequency of periodic forcing is increased, we need higher and higher values of its amplitude to get the desired response.

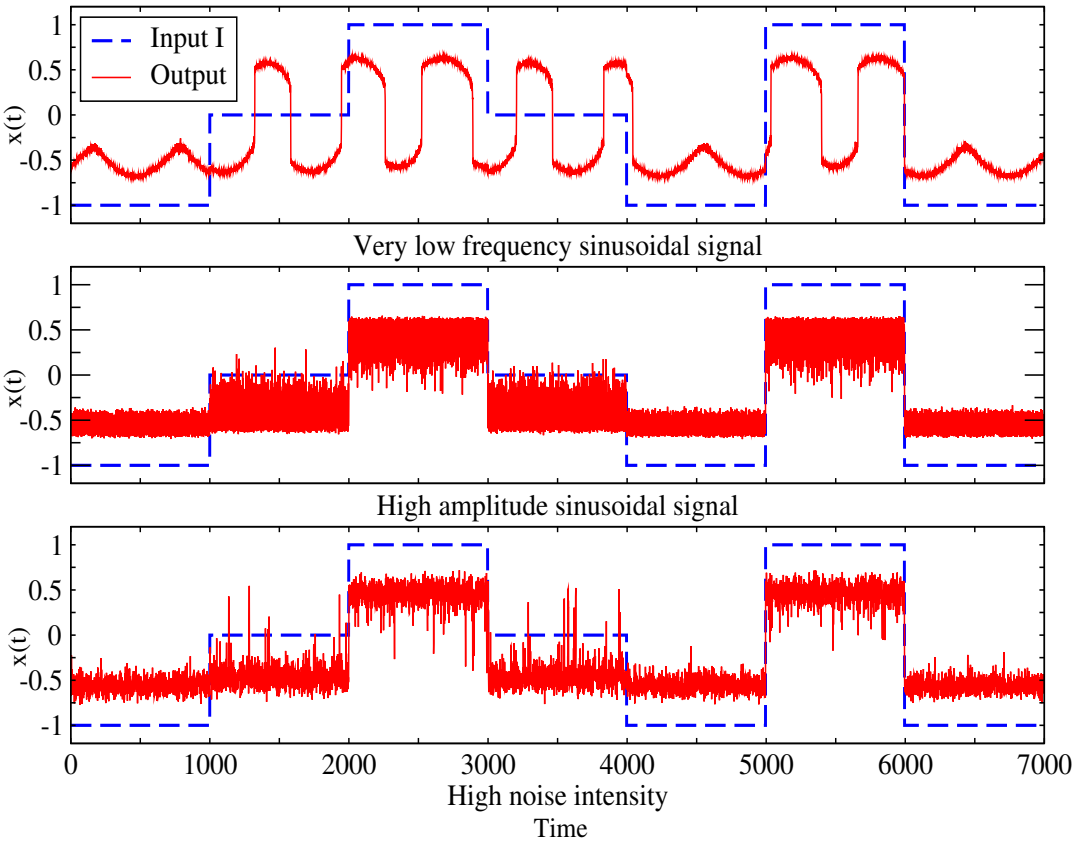

Figure 4.3: This figure shows how decreasing the frequency of periodic forcing to very low value $\omega = .01$ (top panel) or increasing the amplitude of periodic forcing to very high value $A = 2.0$ (middle panel) or very high noise intensity $D = 0.40$ can result in random hopping between the wells, leading to erratic response. Red line is the output of the system and dashed blue line is the sum of the two inputs that was fed into the system as defined in eq. 4.2.

Further, the addition of periodic forcing also results in lower switching times. We calculated the time the output takes to switch from low to high levels, or vice versa, in response to change in the input signal, and averaged it over 1000 such switches. We observed that for low noise intensities there is sharp reduction in the average switching time when a periodic signal is added (see figure 4.5). For faster operation of the logic gate, it is desirable that time of an input or bit time be as low as possible. This can be done by setting the bit time equal to the minimum switching time plus time required

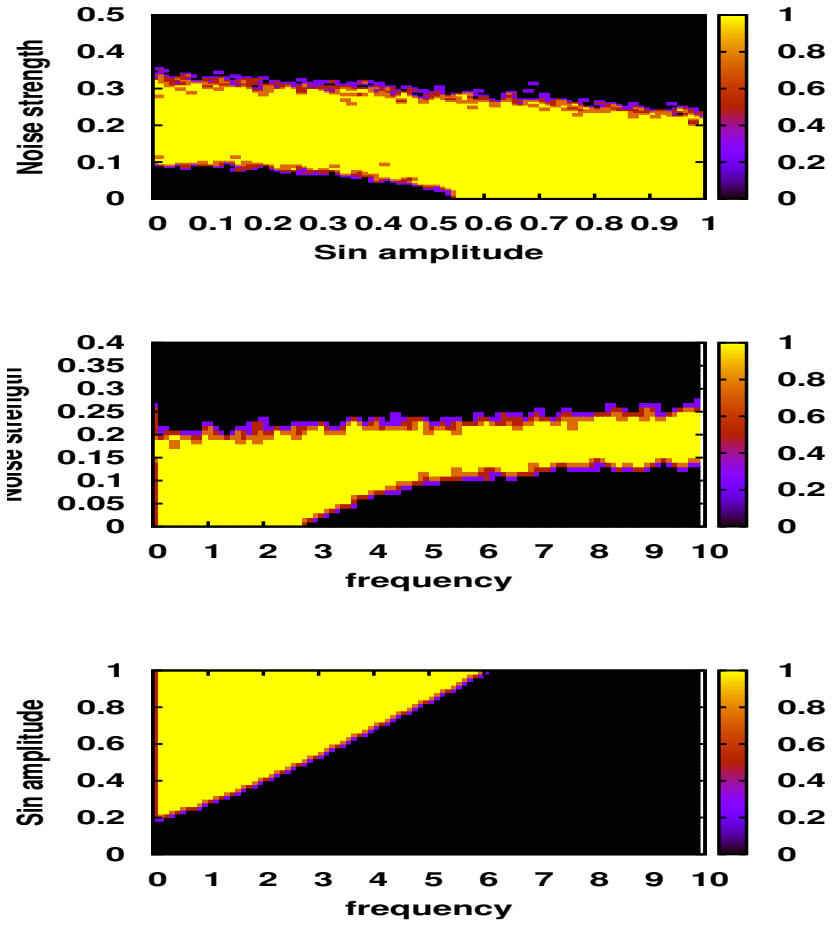

Figure 4.4: Probability of obtaining the AND logic operation with $b = -0.5$. Here $\omega = 4$ for left panel, $A = 0.5$ for middle panel and $D = 0.08$ for right panel. The system was simulated for 100 random combinations of the two inputs. The transience was set at 10 percent of the input timescale.

for reading the state of the output. This gives us the minimum time for which an input should be applied so that we get robust operation of the logic gate. We explored the minimum switching time for various combinations of modulation frequencies, modulation amplitude and noise strengths. We found that systems driven by a periodic forcing of appropriate frequency and amplitude can function robustly for bit times as low as one time unit (e.g by setting $A = 1$ and $\omega = 2.7$).

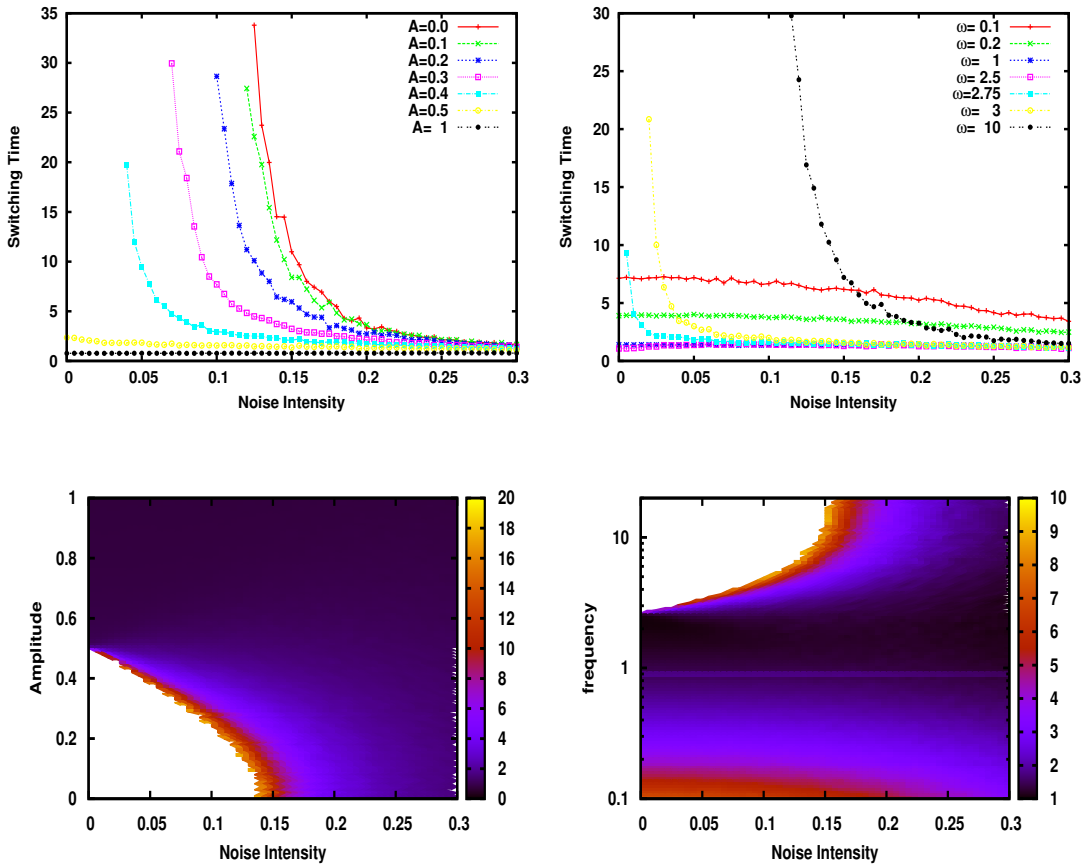

Figure 4.5: Switching time averaged over 1000 switches of output for the AND gate operation, over a range of noise strengths, amplitudes and frequencies. Here $b = -0.5$, $\omega = 2.7$ (left) and $A = 0.5$ (right). Note that for low amplitudes we don't get robust AND operation for low noise intensities. In the density plots, the colors represent the switching time, the white area corresponds to the range where the operation of the logic gate is not robust, and the frequency is plotted on a log scale in the density plot on the right.

4.5 Adaptive Logical Stochastic Resonance

In the above results we have seen that noise and a periodic forcing interfere constructively and aid the switching of the system between the two wells. This on one hand, helps to obtain desired responses at lower noise strengths but at the same time the response deteriorates slightly at higher values of noise intensity. This deterioration is not so significant and is at the higher noise boundary where one typically does not operate. Still, if we want to ensure robust operation even in the higher noise window, one way to accomplish this would be to keep monitoring the noise levels in the system and then adjusting either the frequency or amplitude of periodic forcing, if the noise level crosses some threshold level. That is to say, we switch off the periodic forcing if the noise level is within the

optimal window.

This approach will work fine if the changes in the noise strengths occur only occasionally. On the other hand, if the fluctuations in noise levels are quite frequent, then it will be better if the system could *automatically adapt itself to the changing noise levels for robust operation.*

Now we will show that by coupling two bistable systems we can enable robust operation of LSR elements over large spectrum of noise intensities. Here one of the bistable systems will be used to control the amplitude or frequency of the periodic forcing that is fed to the other system.

Consider the coupled systems:

$$\dot{x} = a_1(x - a_2x^3) + b + I_1 + I_2 + Ay\sin(\omega t) + D\eta(t) \tag{4.3}$$

$$\dot{y} = a_3(y - a_4y^3) + D\eta(t) \tag{4.4}$$

Here the output of second system modulates the sinusoidal forcing applied to the first system. The working principle in this form of coupling is that the second system has a lower potential barrier as compared to the first. When the noise is very low, the output of the second system will stay in the same well. Thus it will act as a constant signal and the sinusoidal forcing will simply be scaled by a factor, and the frequency of periodic forcing fed into first system will be same as that of the sinusoidal signal. This sinusoidal forcing then enables the operation of LSR elements even in low noise conditions, as was shown in chapter 3.

When the noise level increases, y jumps between the two wells according to the Kramer's rate, essentially behaving like a signal of high frequency as shown in figure 4.6 . As the modulating signal has a high frequency, the signal fed into the first system has a frequency much greater than the frequency of the sinusoidal signal. Thus the system doesn't get sufficient time to respond to this signal and hence the sinusoidal forcing doesn't lead to random hops. The minimum frequency that we can choose for the sinusoidal forcing is governed by the transience time in which the system must reach the desired state. This is so because within this time the system should receive at least one full cycle of the periodic forcing. As mentioned earlier, we set the potential barrier for the second system much lower compared to first by selecting appropriate values of a_3 and a_4. Further, the parameters chosen are such that the frequency of sinusoidal forcing is lower than the frequency obtained from Kramer's rate for noise strengths where noise

alone is sufficient for robust operation of the LSR elements.

We simulated the system as given by equations 4.3 and 4.4 for 100 different initial conditions. In particular, we choose $a_1 = 4$, $a_2 = 5$, $a_3 = 2$, $a_4 = 8$, $\omega = 0.05$, $A = 0.6$ and calculate the range of D over which we get the robust logic operation. As before, in each run we took 7 different possible combinations of I_1 and I_2. A run was counted as successful if and only if the time series matched the desired output 100 percent of the time, leaving out a small transient period. Then the ratio of successful runs to the total number of runs was defined as the probability of obtaining the correct logic. As shown in figure 4.7, we find that the probability of correct logic is 1 for much larger noise windows. Specifically, it is one for *all* noise intensities less than the maximum noise intensity for which correct logic was obtained in the absence of periodic forcing. Additionally the lower limit on noise intensity now no longer exists, and we can obtain robust logic operations even in noise-free case.

Moreover, if we use a slightly relaxed criteria for correct logic, that is, if we assume that logic is correct even if time series matches for a little less than 100 percent, then the critical noise intensity upto which correct logic is obtained increases further, as seen in the second and third panel of figure 4.7.

It is evident from figure 4.7 that the noise intensity upto which we get robust operations is slightly lower than that obtained in absence of periodic forcing. This arises from the enhancement of random hopping due to the added effect of periodic drive and noise.

Lastly, we consider adaptively changing the amplitude of sinusoidal forcing instead of the frequency. For this, consider the system given by:

$$\dot{x} = a_1(x - a_2x^3) + b + I_1 + I_2 + A\ \langle y \rangle\ \sin(\omega t) + D\eta(t) \tag{4.5}$$

$$\dot{y} = a_3(y - a_4y^3) + D\eta(t) \tag{4.6}$$

where $\langle y \rangle$ is the average of y over a short interval of time. This kind of coupling is particularly relevant in chemical and biological systems, where the instantaneous state of the system is not easily detectable, but a short-time average is more accessible. Here instead of instantaneous value of y, its average over previous few values is fed back to the coupled system. When the noise in the system is low, the average value of its state will be equal to that of the potential well in which it is lying. When the noise level increases, the system jumps between the two wells according to the Kramer's rate. As the two wells are symmetric about zero, the average value approaches zero as the hopping rate increases,

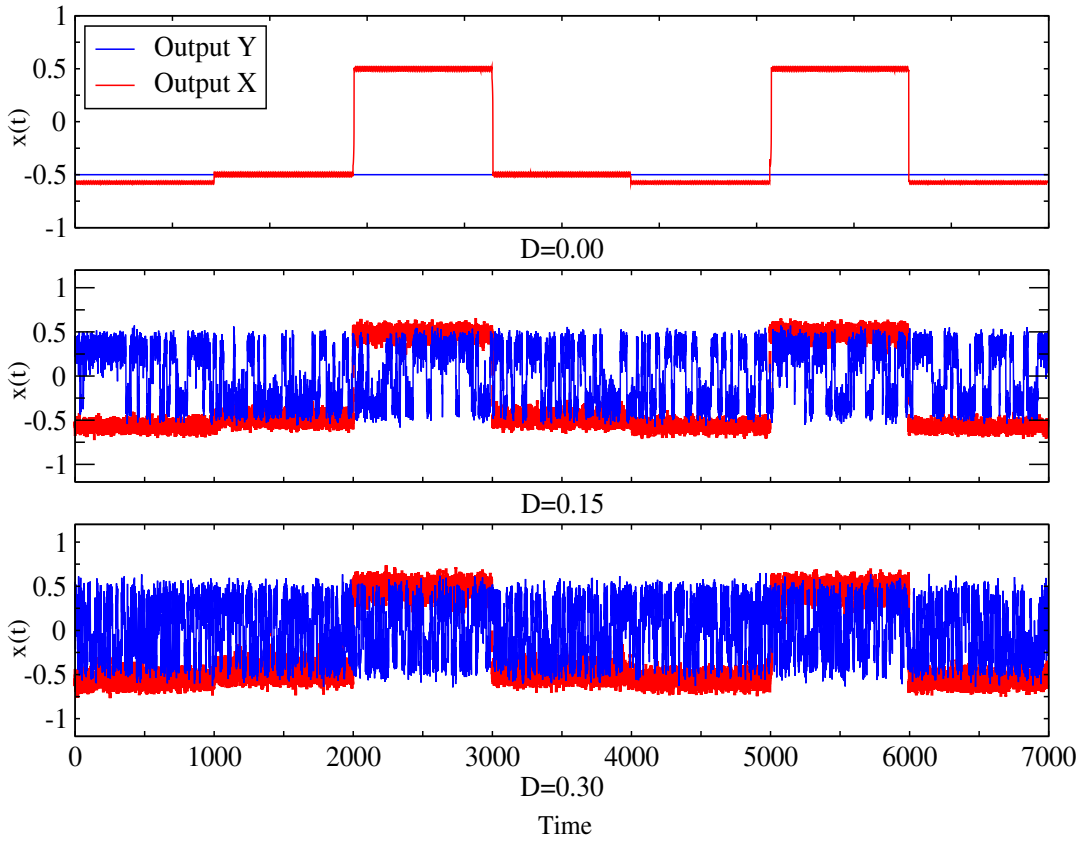

Figure 4.6: Time series for y (blue) and output (red) for the system given by eq. 4.3 and eq. 4.4 for noise intensities $D = 0$ (top), $D = 0.15$ (middle) and $D = 0.3$ (bottom).

as shown in figure 4.8. Thus the amplitude of sinusoidal signal is reduced to zero.

We simulated the coupled systems given by equations 4.5 and 4.6 by averaging the value of y over 100 time units (the time for which an input is applied). Further, when the average is taken over a larger time interval, the response of these coupled systems will be better, provided that this time is smaller than the timescale over which the noise strength itself changes. The results are shown in figures 4.9. We see that in this case, not only does the lower limit on optimal noise window vanish, but for higher noise intensities too the results match with those obtained in absence of a periodic forcing.

The results are qualitatively the same even if there is some delay in propagation of $\langle y \rangle$, provided it not so large that noise intensity itself changes in this time. Additionally, similar results were obtained if we use a moving or running average of y. This is particularly helpful in electronic systems where a running average is far more easy to implement vis-a-vis a normal average which may involve a lot more computations and consequently result in delays.

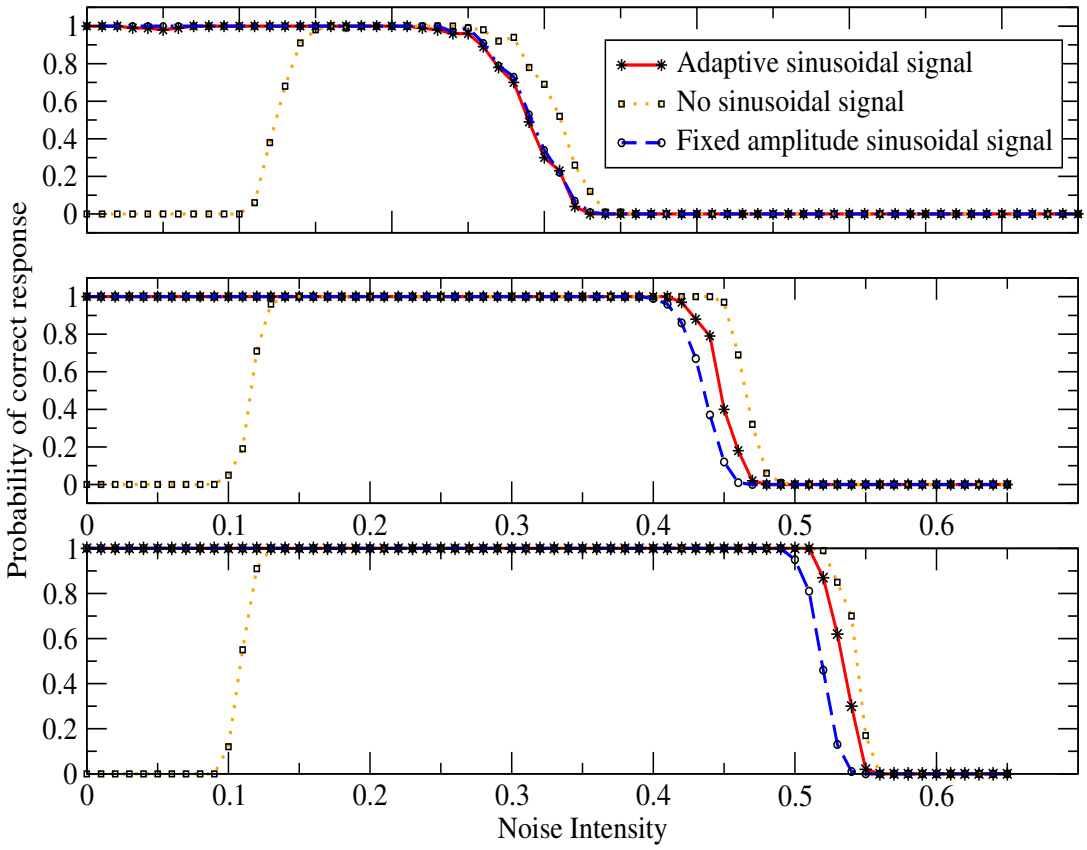

Figure 4.7: Probability of obtaining the AND logic operation with $b = -0.5$ Here $\omega = 0.05$, $A = 0.6$. The red line corresponds to simulations as given by eq. 4.3 and 4.4. Dashed orange and blue lines are obtained taking $A = 0$ and $A = 0.35$ in eq. 4.2. The system was simulated for 100 runs where each run was combination of seven different possible input sets of the two inputs. A run was taken to be successful if the time series matched the expected output 100 percent (top), 98 percent (middle) and 95 percent (bottom) of the time, after leaving out transience.

4.6 Conclusion

In conclusion, we have explicitly shown that by utilizing the constructive interplay of noise and periodic forcing it is possible to obtain a logic response similar to LSR even when the strength of noise is lower then the minimum threshold. This enables us to use the LSR elements in sub-threshold noise conditions. Further, by coupling the LSR element to another LSR element with a lower potential barrier we can make the systems adapt to varying noise intensity, so that its operation is robust even in high noise conditions. The results presented here are quite general, and can potentially be extended to other systems which show enhanced performance in the presence of noise, such as typically observed in generalized stochastic resonance phenomena.

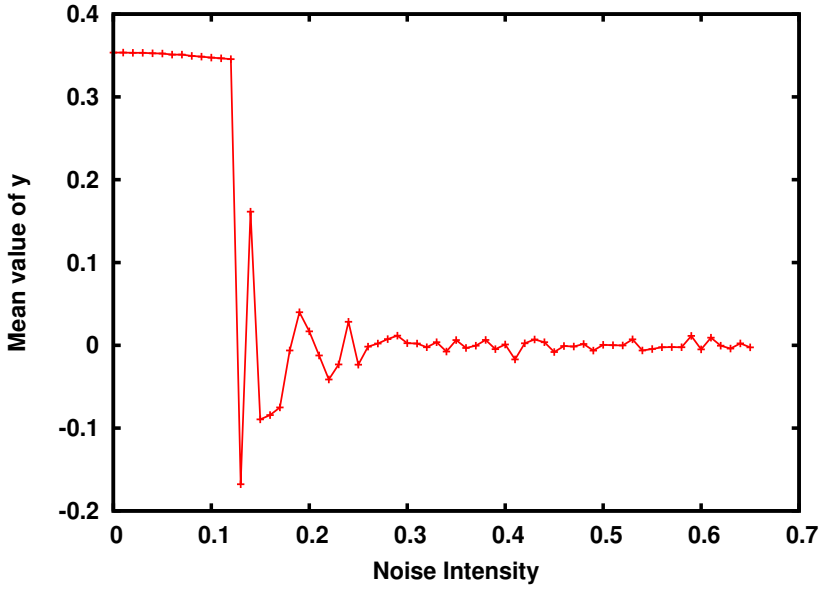

Figure 4.8: Every point represents mean value of y over previous 100 time units for that particular noise intensity, for the system given by eq. 4.6.

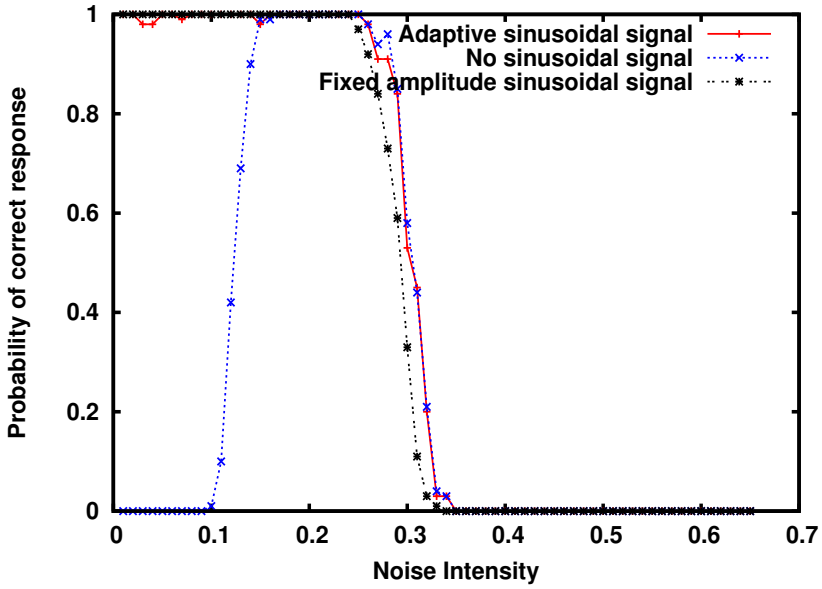

Figure 4.9: Probability of obtaining the AND logic operation, for the system given by eqs. $4.5 - 4.6$. Further we show the case with no sinusoidal forcing and the case where the amplitude of the periodic forcing is constant. The system was simulated for 100 runs where each run was combination of seven different possible input sets of the two inputs. A run was taken to be successful if the time series matched the expected output 100 percent of the time, after transience.

Chapter 5

Performance enhancement of VCSEL based stochastic logic gates

5.1 Introduction

Vertical-cavity surface-emitting lasers (VCSELs) are widely used for high-bit-rate data transmission because of their various advantages over conventional edge emitting lasers like low threshold current, single-longitudinal-mode operation, higher modulation bandwidth and circular output beam profile. They emit linearly polarized light whose direction can change with change in operating conditions like temperature or the injection current [76]. It involves switching between the two orthogonal linearly polarized modes. More dynamical features emerge when there is optical feedback, current modulation or optical injection [77]. This polarization-bistability of VCSELs has been used to build optical buffer memories [78].

Zamora-Munt et al demonstrated the phenomenon of LSR in VCSEL by encoding the logic inputs in an aperiodic signal which directly modulates the laser bias current [35]. The probability of correct response was observed to be ~ 1 in a wide region of noise strengths. They associated LSR with optimal noise-activated polarization switchings (the so-called inter-well dynamics if one considers the VCSEL as a bistable system described by a double-well potential) and optimal sensitivity to spontaneous emission in each polarization (the intra-well dynamics in the double-well potential picture).

In another work [73], by encoding the logic inputs in the strength of the light injected into the suppressed polarization mode of the VCSEL (the so-called orthogonal injection),

and by decoding the output logic response from the polarization state of the emitted light, Perrone et al demonstrated an all-optical stochastic logic gate. It was observed that correct logic output response can be obtained for as short as 5 ns bit times thus lowering the the minimum bit time for successful operation from 30-40 ns observed in the opto-electronic stochastic logic gate [35],[73].

In chapter 3 of this thesis, it was shown that in absence of noise a behaviour similar to LSR can be observed by addition of a periodic forcing (sinusoidal or rectangular). As in case of LSR, robust operation is obtained only when the amplitude and frequency of the periodic forcing is within an optimal range. Further, when noise is also present, this periodic forcing interacts cooperatively and in situations when noise is below the minimum threshold of optimal range, the periodic forcing allows us to operate successfully even under sub threshold noise conditions. At the higher end of optimal noise window, this periodic forcing leads to slight deterioration in performance. We can then couple another bistable system to control the effective amplitude or frequency of the periodic forcing so that we obtain robust operation for all noise intensities below the maximum threshold (see chapter 4).

In this chapter, we explore the possibility of enhancing the operational range of VCSEL based stochastic logic gate by addition of a periodic signal. The enhancement can be either in form of decrease in the minimum bit time necessary for successful operation or in terms of increasing the optimal window of noise in which this logic gate can function robustly. We try this with both opto-electronic as well as the all optical configuration. Specifically, we try by adding periodic forcing as $E_{injection}$ in the opto-electronic configuration. In the all optical configuration, we explore the effect of periodic forcing in two ways: firstly, by modulating the bias current and secondly, by adding it as $E_{injection}$ as in the opto-electronic configuration.

We discuss the model rate equations used to simulate the VCSEL in the next section and report our results in the subsequent section and then discuss the results and the conclusions drawn in the last section.

5.2 Model Equations

We use the spin-flip model [79] to simulate the polarization dynamics of VCSELs. This model is a set of six ordinary differential equations describing the evolution of the real and imaginary parts of two complex optical fields (associated with two orthogonal polar-

izations) as well as two carrier densities with opposite spin. The model has been extended to take into account Y-polarized optical injection. The equations are

$$\begin{aligned}
dE_x/dt &= \kappa(1+i\alpha)[(N-1)E_x + inE_y] - (\gamma_a + i(\gamma_p + \Delta\omega))E_x \\
&\quad + \sqrt{\beta_{sp}\gamma_N N}\xi_x \\
dE_y/dt &= \kappa(1+i\alpha)[(N-1)E_y - inE_x] + (\gamma_a + i(\gamma_p - \Delta\omega))E_y \\
&\quad + \sqrt{\beta_{sp}\gamma_N N}\xi_y + \kappa E_{inj} \\
dN/dt &= \gamma_N[\mu - N(1 + |E_x|^2 + |E_y|^2) - in(E_y E_x^* - E_x E_y^*)] \\
dn/dt &= -\gamma_s n - \gamma_N(n|E_x|^2 + |E_y|^2) + iN(E_y E_x^* - E_x E_y^*)]
\end{aligned}$$

where E_x and E_y are linearly polarized slowly-varying complex amplitudes, N is the total carrier population, and n is the population difference between the carrier densities with positive and negative spin values, k is the field decay rate, γ_N is the decay rate of the total carrier population, γ_s is the spin-flip rate, α the linewidth enhancement factor, γ_a and γ_p are linear anisotropies representing dichroism and birefringence, μ is the injection current parameter normalized such that the threshold in the absence of anisotropies is at $\mu_{th} = 1$, and $\xi_{x,y}$ are uncorrelated Gaussian white noises with zero mean and unit variance[73].

The optical power injected into the Y polarization is represented by $P_{inj} = E_{inj}^2$. The model equations are written in the reference frame of the injected field, and thus the detuning $\Delta\omega$ is the difference between the optical frequency of the injected field and the frequency intermediate between the X and the Y polarization. Without optical injection and with $\gamma_a = 0$, the angular optical frequencies of the X and the Y polarizations are $-\gamma_p$ and γ_p respectively, and therefore, $\Delta\omega = -\gamma_p$ $(+\ \gamma_p)$ means that the injected field is resonant with the X (Y) polarized mode of the solitary VCSEL [73].

5.3 Results

5.3.1 Optoelectronic Configuration

We use the opto-electronic configuration as in [35] for using VCSEL as a stochastic logic gate. In this configuration, the two logic inputs are encoded in a three-level aperiodic

modulation directly applied to the laser pump current. The laser response is determined by the polarization of the emitted light. The parameters are chosen such that the laser emits either the x or the y polarization and the parameter regions where there is anti-correlated polarization coexistence or elliptically polarized light are avoided. The laser response is considered a logical 1 if, for instance, the x polarization is emitted, and a logical 0, if the y polarization is emitted. One can obtain the complementary logic gate by detecting the orthogonal polarization.

In fig 5.1 we plot E_x vs μ for different rates of change of μ.

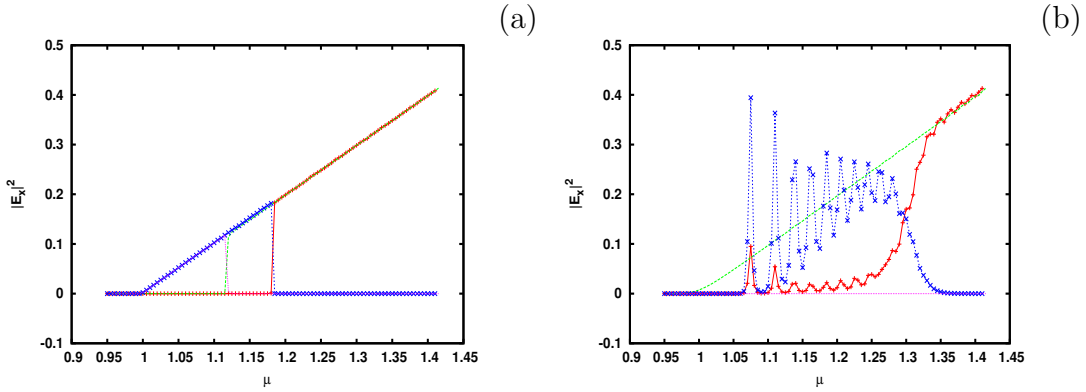

Figure 5.1: Intensities of x and y polarizations when the injection current increases and decreases linearly from $\mu_i = 0.9$ to $\mu_f = 1.4$ slowly (top) and fast (bottom). The parameters are $\kappa = 300ns^{-1}$, $\alpha = 3$, $\gamma_N = 1ns^{-1}$, $\gamma_a = 0.5ns^{-1}$, $\gamma_p = 50radns^{-1}$ and $D = 10^{-6}ns^{-1}$.

We observe hysteresis in both the cases. Further, as μ varies at a fast rate we observe oscillations.

In fig 5.2, we find that this system functions as a stochastic logic gate for optimal values of noise intensity. For low or high noise strengths, the percentage of power emitted in specific polarization doesn't switch with changes in the input signal. When noise intensity is low, polarization switching is delayed whereas a high noise intensity results in emission in both polarization modes.

We calculate the probability of correct logical response by evaluating the response of this gate for large number of input bits. To decide whether the response is right or wrong, we calculate the fraction of power emitted in any one polarization state. If the polarization state corresponds to correct response and percentage of power emitted in this polarization is more than the threshold P_{th}^{max} value, we call it as correct response. Alternately, we also define P_{th}^{min} as the minimum threshold and power emitted should be

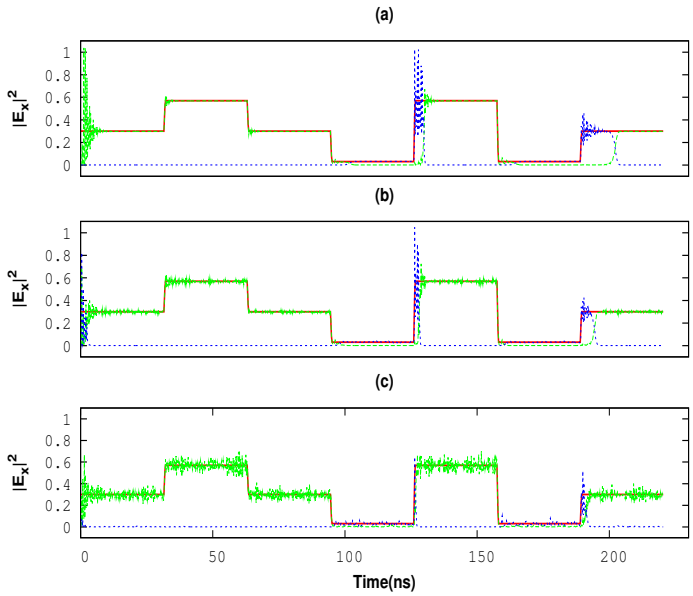

Figure 5.2: Time traces of the x polarization (solid green), y polarization (dotted blue), and the injection current $\mu - 1$ for different noise intensities (a) $D = 5 \times 10^{-7}$ (b) $D = 4 \times 10^{-4}$ and (c) $D = 6 \times 10^{-3}$. The parameters are $T = 31.5ns$, $\mu_0 = 1.3$, $\Delta\mu = 0.27$, $\kappa = 300ns^{-1}$, $\alpha = 3$, $\gamma_N = 1ns^{-1}$, $\gamma_a = 0.5ns^{-1}$ and $\gamma_p = 50radns^{-1}$.

lower than this threshold if this is wrong polarization. In our simulations, we evaluate the responses at three different thresholds, 70%, 80% and 90%. The results are displayed in fig. 5.3. It can be seen that for relaxed criteria i.e. 70%, the probability of correct operation is higher. Further, we get $P = 1$ for intermediate values of noise strength.

Next, we apply a periodic forcing as E_{inj} to the opto-electronic configuration to see if the performance of VCSEL based stochastic logic gate can be improved. As we can see in fig. 5.3, the performance of the stochastic logic gate is enhanced for low noise intensities and decreases for high noise intensities when periodic forcing is added. Again from fig. 5.3, we can see that noise free morphing is also possible.

As we can see that at low noise intensities, orthogonal injection improves the performance of this system. So the next logical question is to see if the logic operations can be realized even in absence of noise and using only the orthogonal injection as shown in fig. 5.4.

Now we study the effect of orthogonal injection on the minimum bit time necessary for successful operation. As can be seen in fig. 5.5, for low noise intensities, there is marked decrease in the minimum bit time necessary for successful operation. At higher noise intensities, the orthogonal injection doesn't affect much.

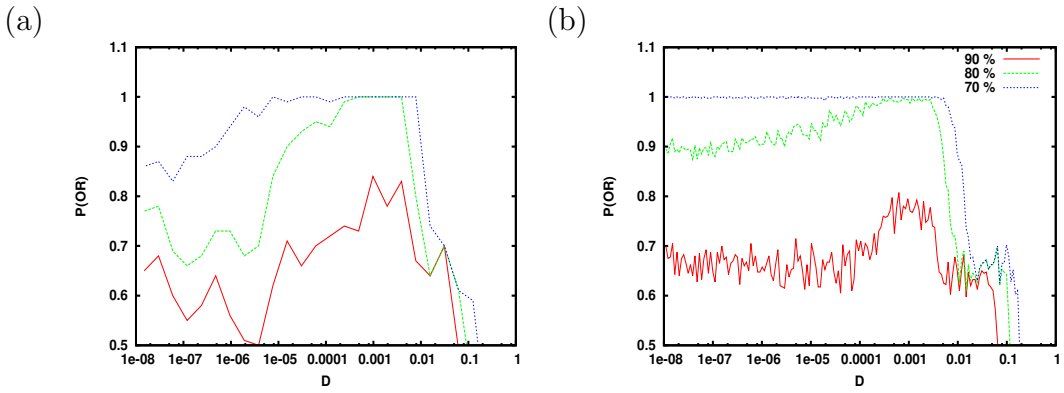

Figure 5.3: The probability of correct operation of stochastic logic gate vs noise intensity in the optoelectronic configuration when periodic forcing is added as E_{inj} in the orthogonal LP mode. Left figure shows the results in absence of periodic forcing. Clearly there is performance enhancement of the gate for low noise intensities. Here $T_{bit} = 31.5ns^{-1}$

These observed behaviours can be explained by considering that just like the noise, periodic forcing also facilitates the switchings between the polarizations and when noise is low or insufficient to result in polarization switching by itself, then periodic frequency aids the polarization switchings in such cases.

5.3.2 All-optical configuration

In this section, we analyze the performance of the stochastic logic gate in the all optical configuration. In this configuration, the logic inputs are encoded in the strength of the light injected into the suppressed polarization mode of the VCSEL and the output logic response is decoded from the polarization state of the emitted light[73]. We consider addition of periodic forcing in two ways: first by small fluctuations in modulation current μ and secondly by adding a small periodic forcing to E_{inj}. We explored the minimum bit times for different values of modulation current and when the modulation current varied between two levels. The results are displayed in fig 5.6. We can see that by adjusting the current modulation, we can obtain robust operations in different noise conditions. The results for injection current modulation are presented next.

First we plot the probability of correct response vs noise intensity (see fig 5.7) and then vs bit time (see fig 5.8) for the all optical configuration. From the figures, it is clear that probability of correct response increases for the 80% threshold criteria. At higher noise intensities, the performance degrades for all the cases. Similarly, the bit times improve for 70% criteria but degrade for 90% threshold criteria. So we can tune

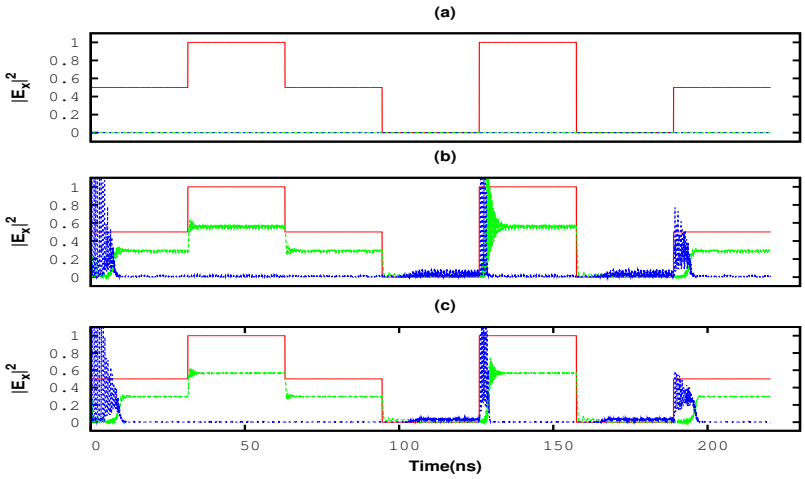

Figure 5.4: Noise Free morphing i.e. when $D = 0$ and (a) No sinusoidal forcing (b) With sinusoidal forcing with $\omega = 0.5$ and $A = 0.02$ and (c) With a sinusoidal forcing of low frequency $\omega = 0.2$ and $A = 0.01$. The sinusoidal forcing has been added as the E_{inj}. All other parameters are same as in fig 5.2

the periodic frequency to obtain best response in the desired noise window and under the particular threshold criteria.

5.4 Conclusion

In this work we have demonstrated that the performance of a VCSEL based stochastic logic gate can be enhanced by addition of a periodic signal in the orthogonal LP mode. This enhancement was observed for both the optoelectronic configuration as well as the all optical configuration and both in form of increase in the optimal noise window as well as decrease in minimum bit time. By tuning the amplitude and frequency of the periodic forcing we can have better control over the stochastic logic gate and can improve its response in the desired noise window with a particular threshold criteria.

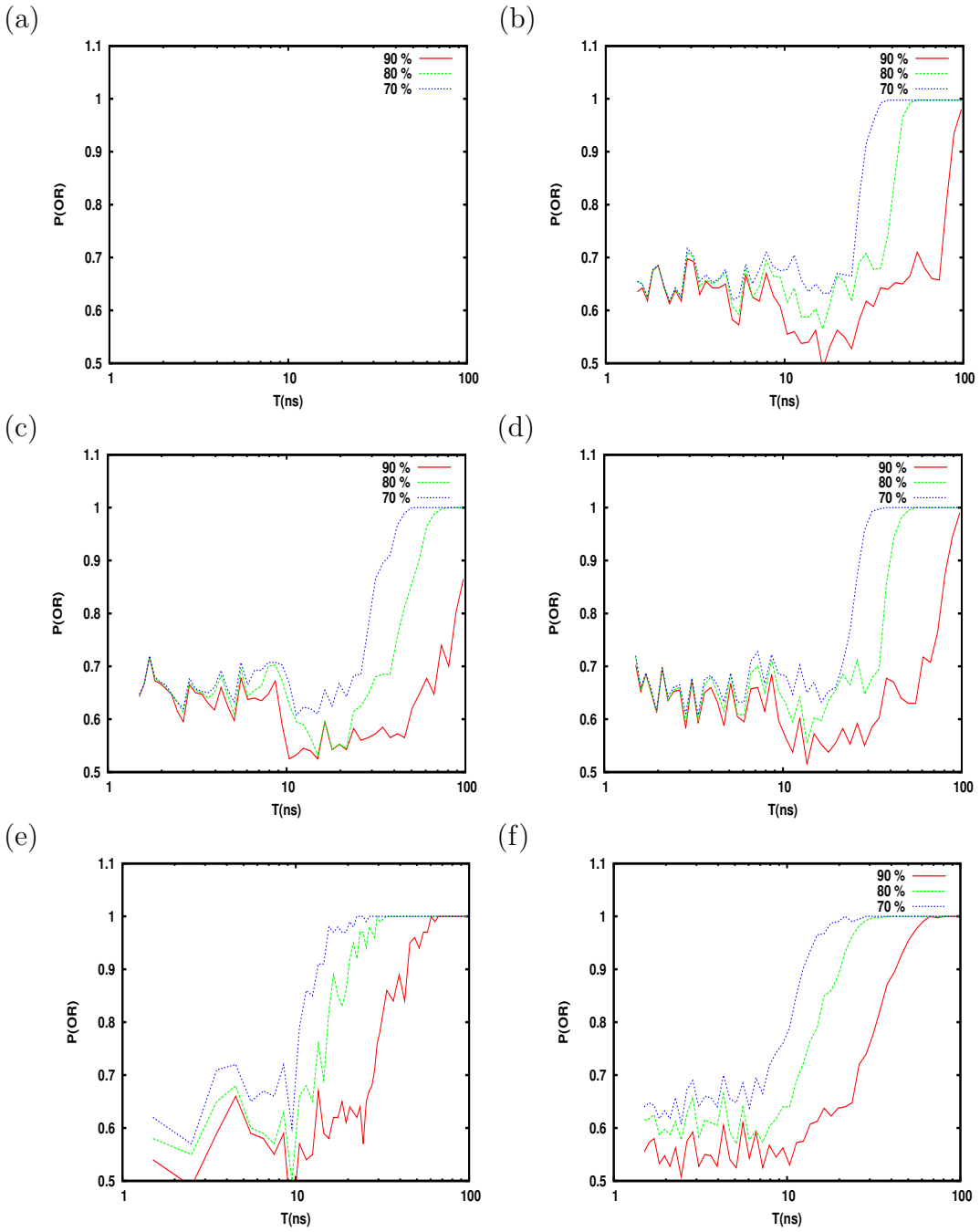

Figure 5.5: The probability of correct operation of stochastic logic gate vs bit time in the optoelectronic configuration when periodic forcing is added as E_{inj} in the orthogonal LP mode. Left figure shows the results in absence of periodic forcing. Clearly there is performance enhancement of the gate for low noise intensities. Here $D = 0.00$ for (a), (b) $D = 10^{-7}$ for (c), (d) and $D = 0.0004$ for (e), (f). In (a) the probability is zero at all points.

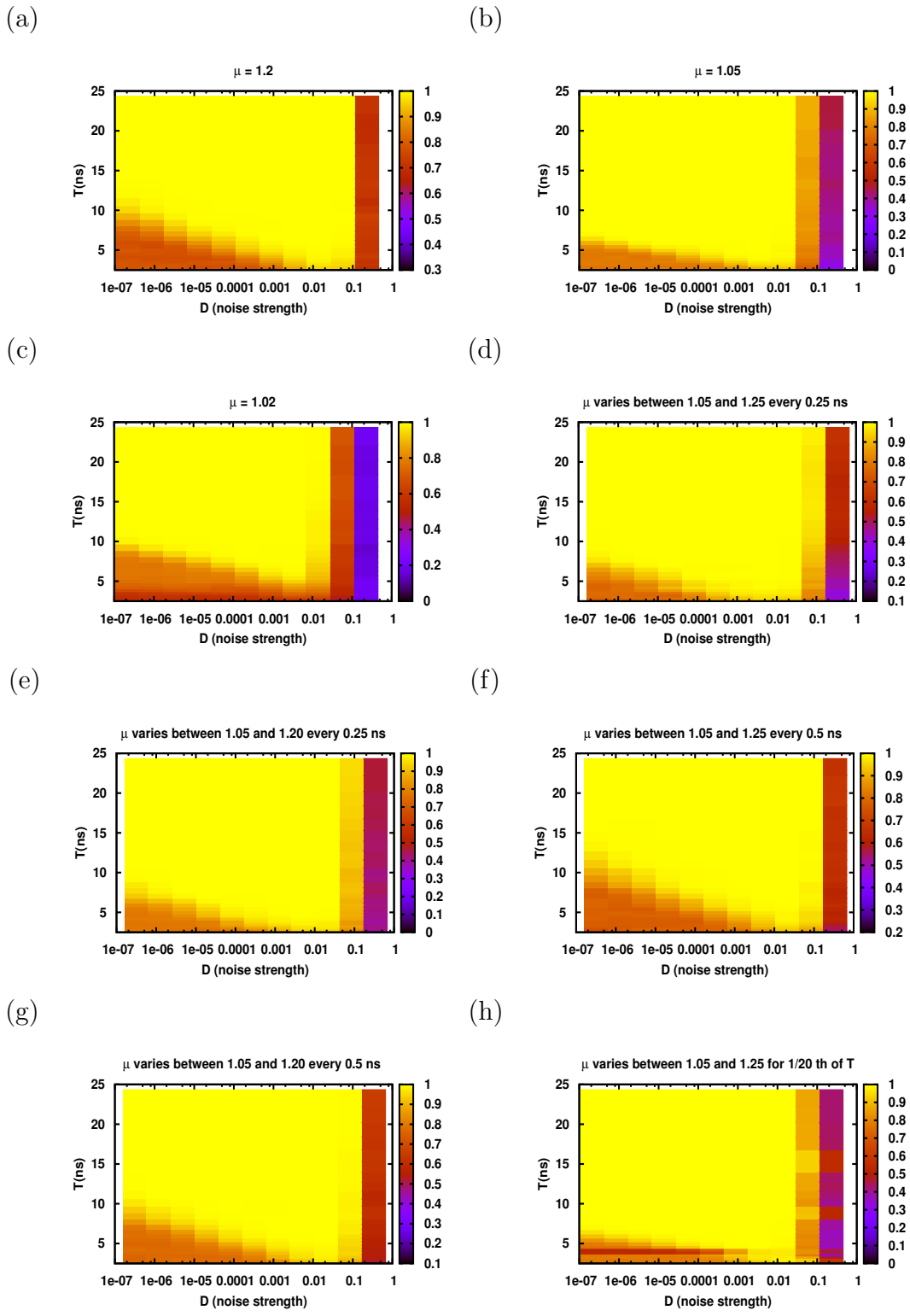

Figure 5.6: Minimum bit time required for successful operation for the all optical configuration for various noise intensities and pump currents.

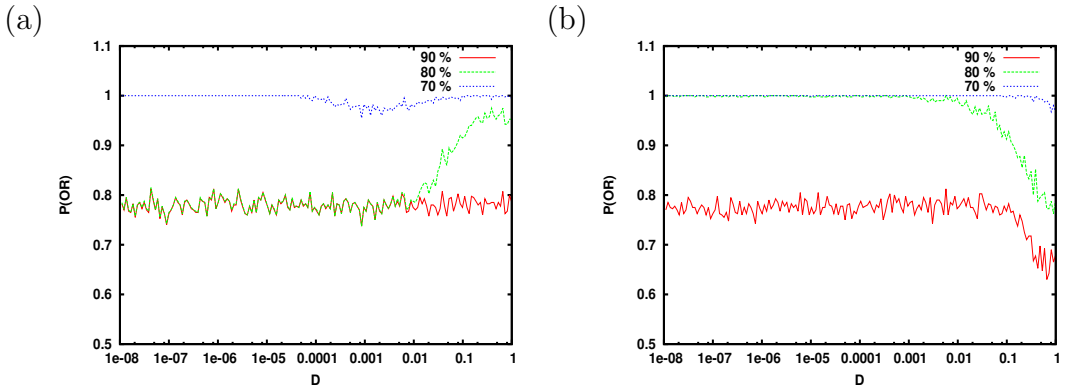

Figure 5.7: The probability of correct operation of stochastic logic gate vs noise intensity in the all optical configuration when periodic forcing is added as E_{inj} in the orthogonal LP mode. Left figure shows the results in absence of periodic forcing. The performance is enhanced for low noise intensities for the 80 percent criteria.Here $T_{bit} = 5.5ns^{-1}$

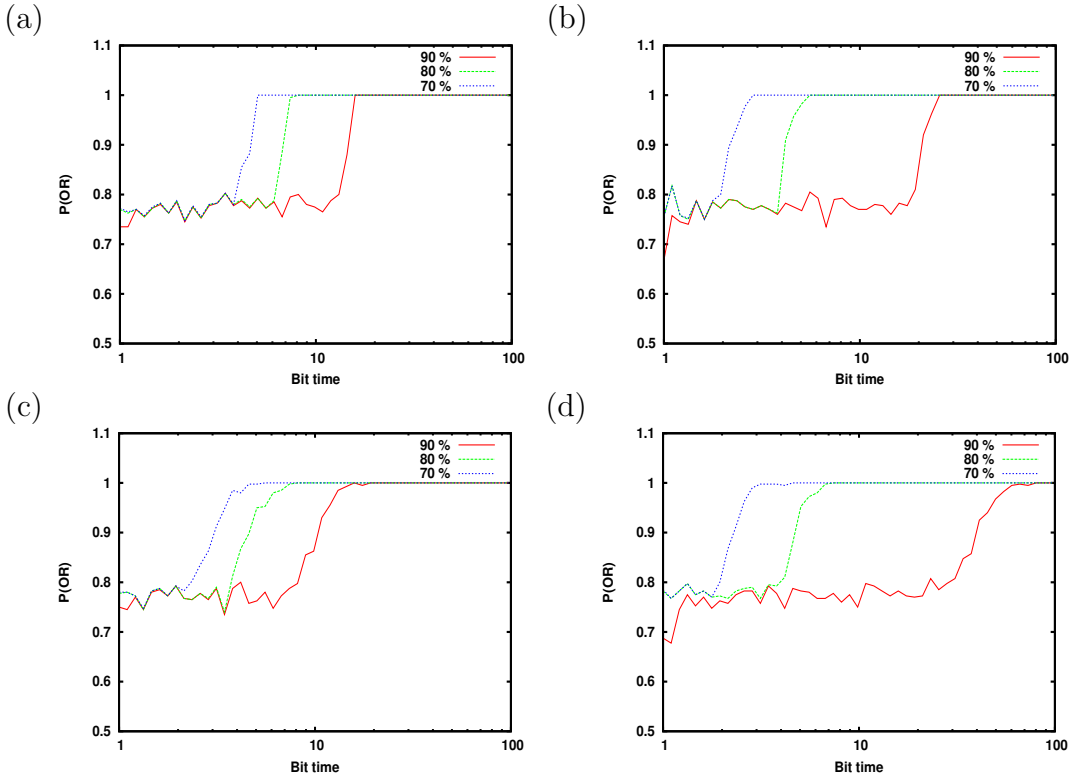

Figure 5.8: The probability of correct operation of stochastic logic gate vs bit time in the all optical configuration when periodic forcing is added as E_{inj} in the orthogonal LP mode. Left figure shows the results in absence of periodic forcing. Here $D = 10^{-5}$ for (a), (b) and $D = 0.1$ for (c), (d).

Part II

Spatiotemporal patterns in Complex Systems

Chapter 6

Verification of scalable ultra-sensitive detection of heterogeneity in an electronic circuit

6.1 Introduction

Complex interactive systems have been widely used to model spatially extended physical, chemical and biological phenomena. The effect of heterogeneity in the evolution of spatiotemporal patterns has attracted the attention of researchers in recent times. Disorder either in form of static or quenched inhomogeneities, and coherent driving forces, have yielded a host of interesting, often counter-intuitive, behaviours. For instance, stochastic resonance [3] in coupled arrays [46, 47, 48, 49, 50, 51, 52], diversity induced resonant collective behaviour in ensembles of coupled bistable or excitable systems [53],[54] demonstrated how the response to a sub-threshold input signal is optimized.

In this direction, it was recently shown that the collective response of strongly coupled bistable elements can reflect the presence of very few non-identical inputs in a large array of otherwise identical inputs [55]. Here we verify these findings in an array of globally coupled Schmitt triggers [1]. Schmitt trigger is a simple electronic system that can be easily made from commonly available electronic elements like an op-amp, and a few resistors. It has been widely used to model bistable systems and one of the earliest demonstrations of the phenomena of stochastic resonance was realized in this system [56, 6].

[1] These results have been published in [80]

6.2 Coupled bistable elements

We consider N globally coupled Schmitt triggers, where the input voltage to each element n ($n = 1, \ldots N$) is given by:

$$V_i^n = V_a^n + C\langle V_o \rangle + V_b \tag{6.1}$$

where V_i^n is the input voltage to n^{th} element, V_a^n is the encoded voltage corresponding to input signal a^n applied to the n^{th} element, V_b is the bias and $\langle V_o \rangle$ is the average output of all the elements given by

$$\langle V_o \rangle = \frac{1}{N} \sum_{n=1,N} V_o^n \tag{6.2}$$

Now, we apply V_i^n to the non-inverting terminal of an opamp through a resistance R_1. The feedback voltage is fed into the non-inverting terminal through the resistor R_2 as shown in figure 6.1. The inverting terminal is grounded. In this configuration, the threshold voltages for the Schmitt trigger are $V_T = \pm\frac{R_1}{R_2}V_s$ where V_s is the supply voltage. So, if $V_i^n < -V_T$, then $V_o^n = -V_s$ where V_o^n is the output of n^{th} Schmitt trigger. Now as we increase V_i^n, V_o^n will remain $-V_s$ till $V_i^n \leq V_T$. As V_i^n exceeds V_T, V_o^n will become V_s. Now when we decrease V_i^n, the output will remain V_s till $V_i^n \geq -V_T$, at which point it will become $-V_s$. Thus, this element has a hysteresis as shown by its transfer function given in figure 6.1.

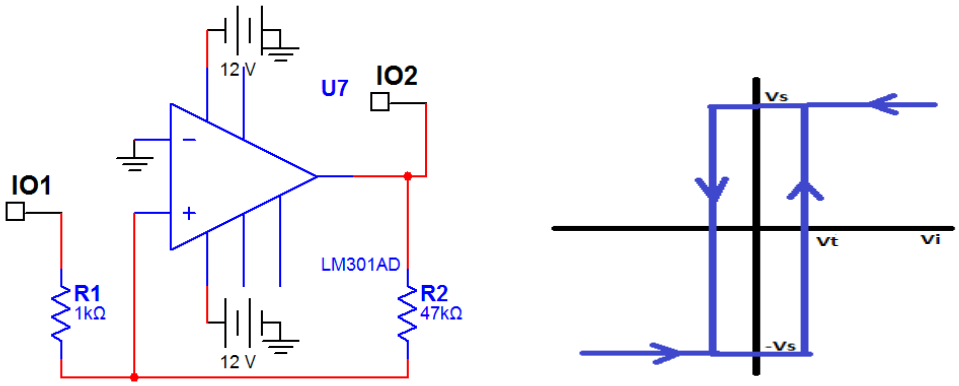

Figure 6.1: Individual Schmitt trigger and its transfer function

The heterogeneity in this collection of bistable elements occurs in the diversity of the input signal V_a^n in Eqn. 6.1. Here we consider that these inputs can have any value in between the two stable states. Without any loss of generality, we can encode one of the states as $-V_a$ and other state as V_a. Thus the inputs can be randomly distributed about

zero average, i.e. the inputs are encoded as voltages randomly distributed between $-V_a$ to V_a.

6.3 Collective response in the presence of heterogeneity

In an uncoupled system, if we take voltages encoding the inputs such that $|V_a| > |V_T|$ then the output state of the element will depend on the value of the input. If the input is in the low state the output of the element will be $-V_s$, and the output will be V_s if the input is in high state. Now when these elements are strongly coupled via average voltage i.e. average voltage of the output of all the Schmitt triggers, $\langle V_o \rangle$, the dynamics of the elements gets correlated.

Consider now the output of this coupled system as $\langle V_o \rangle$. If all inputs are identical, and such that $|V_a^n| > |V_T|$, then every element will go to the state corresponding to that input. However, if $|V_a^n| < |V_T|$ the final state of element will depend on the initial state of that particular element. Given randomly distributed initial conditions, the average voltage will stay close to zero as no element will be able to change its state in this configuration.

If the inputs are not identical, then depending on the distribution of V_a^n, and the initial state of the elements, the elements whose inputs are closer to the low state will tend to move towards $-V_s$, and vice versa. As the states of the elements will also be distributed uniformly, and so in some cases the element will go to lower state whereas in other cases it will go to the upper state. Assuming a uniform random distribution of initial states of the elements we expect that average voltage of the elements will either go to $-V_s$ or V_s. On averaging over different initial configurations the average voltage will again approach zero. If the inputs are not identical and are such that the number of inputs is not distributed uniformly about zero average, then the majority dictates the average voltage. Thus in this case it is not possible to detect the presence of small heterogeneity in the inputs, nor can one infer the number of inputs that were different.

Now consider that the inputs are not distributed over the entire range of voltages between $-V_a$ to V_a, but are two state instead i.e. they take only one of two values. Such systems are very relevant and can, for instance, represent logic 0 and 1. We will show below how to detect the number of nonidentical inputs directly in such systems. Further we will demonstrate that the average voltage of the system approaches the stable state

corresponding to the minority population, up to the limit of a single nonidentical input.

To accomplish this, in addition to $\langle V_o \rangle$ we also apply a bias V_b to all the bistable elements. The value of this bias is decided by the type of minority we wish to detect. If the minority corresponds to the low state, we apply a negative bias and vice versa. This bias essentially brings the elements to which majority input is applied, near the tipping point. As the state of a few inputs change, the elements corresponding to those inputs shift their state. This moves the average voltage away from the stable state of the majority input towards the stable state of the minority input. As the elements corresponding to the majority input were already close to the tipping point, this reduction in average voltage causes a few of them to slip over the barrier towards the stable state of the minority input. This further reduces the average voltage and creates a cascading effect so that in a few steps all the elements corresponding to the majority input are dragged to the stable state of the minority input.

Suppose we start with a state in which all inputs are in same state, let us say, in the lower state. Further the encoded voltage V_a satisfies the condition $|V_a| > |V_T|$. So when inputs are in lower state they are encoded as $-V_a$ which satisfies the condition $-V_a < -V_T$. Thus initially all the elements will go to the lower state. Now we want to find out what is the minimum fraction of elements of a different state necessary such that we can detect the heterogeneity. To do so, we first apply a bias to the system. The value of the bias is such that it alone cannot drive the system. So, in the beginning when all elements are in lower state, the average voltage is $-V_s$. Now on application of bias, the state of the system should not change in absence of heterogeneity. Or the input voltage to bistable elements should remain lower than the threshold voltage i.e. $V_b - CV_s - V_a < V_T$ or $V_b < (CV_s + V_T + V_a)$. Now let us assume that some of the inputs change their state. In this configuration let the number of inputs in the lower state be N_0, and so $N - N_0$ inputs will be in the upper state. This change in state of $N - N_0$ inputs should allow those $N - N_0$ to change their state. So we should have $V_b - CV_s + V_a > V_T$ or $V_b > (CV_s + V_T - V_a)$. From above two conditions we have

$$(CV_s + V_T - V_a) < V_b < (CV_s + V_T + V_a) \tag{6.3}$$

At this stage N_0 elements go to $-V_s$ and $N - N_0$ elements go to V_s. So the average voltage $\langle V_o \rangle$ is $\frac{(N-2N_0)}{N} V_s$. When $N_0 \sim N$, $\langle V_o \rangle$ will approach $-V_s$ and we will not be able to detect the heterogeneity. Note that the elements are coupled with the global mean field and the individual output state of the elements are not accessible. The only observable

quantity is the global mean field. If there is no bias then the majority will always drag the average voltage to its stable point.

When a bias voltage V_b is applied, then in order that the average voltage of the coupled system switches to the stable point of minority, we need that this reduction in average voltage should be sufficient to drive the other elements to the stable state of the minority. So let us consider an element on which the input signal corresponding to majority input is applied. So we require that the voltage acting on this element should exceed the threshold voltage. Namely,

$$-V_a + V_b + CV_s(1 - \frac{2N_0}{N}) > V_T \tag{6.4}$$

This is satisfied if

$$N - N_0 > \frac{N}{2}(1 - \frac{V_b - (V_T + V_a)}{CV_s}) \tag{6.5}$$

This gives the minimum number of inputs of the minority type needed for successful detection. In the limiting case when we require that a single different input should be detected, the following condition must be satisfied

$$\frac{V_b - (V_T + V_a)}{CV_s} > \frac{N-2}{N} \tag{6.6}$$

6.4 Explicit demonstration of ultra-sensitivity

In this section we will explicitly show the detection of a single heterogeneous input in an array of 20 inputs. Initially all the 20 inputs are zero. Then after sometime one input changes its state and we will show how the collective response of the whole system changes its state in response to this change.

As explained in previous sections, we use Schmitt trigger as the bistable element. The voltage applied to n^{th} Schmitt trigger is given by equation 6.1. We apply voltage V_i^n to the non inverting terminal of a comparator through a resistance $R1$. The feedback voltage is fed into the non-inverting terminal through the resistor $R2$. The inverting terminal is grounded. Thus the threshold voltages for this Schmitt trigger are $\pm\frac{R_1}{R_2}V_s$ where V_s is the supply voltage. We take $R_1 = 1k\Omega$ and $R_2 = 47k\Omega$ and thus the threshold voltages are $\pm 0.255V$. The output voltage obtained with this Schmitt trigger is $\pm 10V$.

With no loss of generality, we encode the inputs as $\pm V_a$ where $V_a = 1.5V$ i.e. if input is in low state we apply $-1.5V$ and if it is in high state we apply $1.5V$. Note that we can also encode the inputs as $0V$ and V_aV. In that case, we just have to shift V_T by applying a bias.

In this case, as we have minority of low states and a single heterogeneity of high state, so we apply a positive bias to our system. Specifically we choose $V_b = 11V$. Note that these values of the variables satisfy the criterion given by equations 6.3 and 6.6. Thus the detection of even a single heterogeneity is possible. The schematic diagram of the same is shown in figure 6.2.

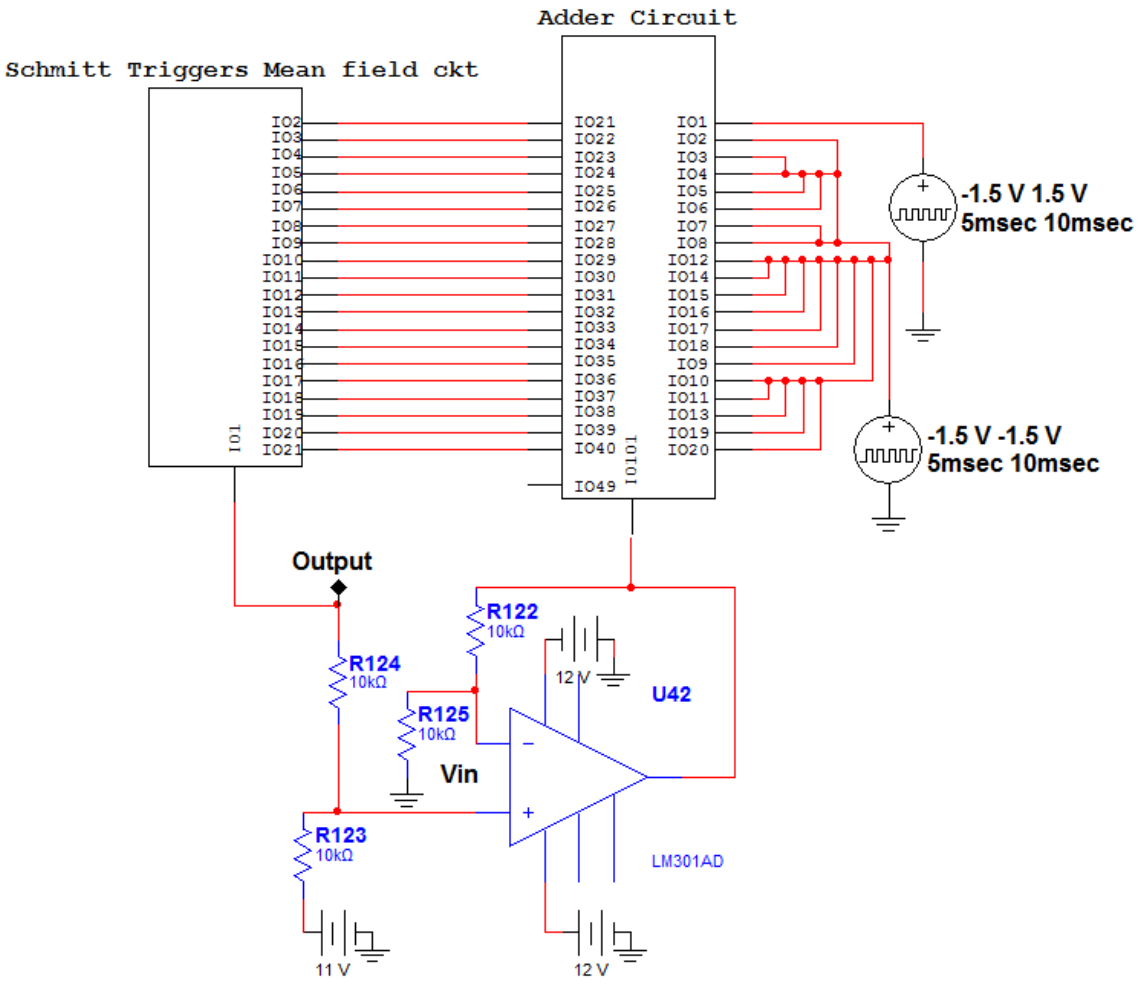

Figure 6.2: Schematic of the electronic circuit model

Here the block on left side has all the bistable elements, namely the Schmitt triggers. The internal diagram of this block is shown in figure 6.3. Each Schmitt trigger is the same as that shown in figure 6.1. This block receives V_i^n from the block on the right and

these are fed to the Schmitt triggers.

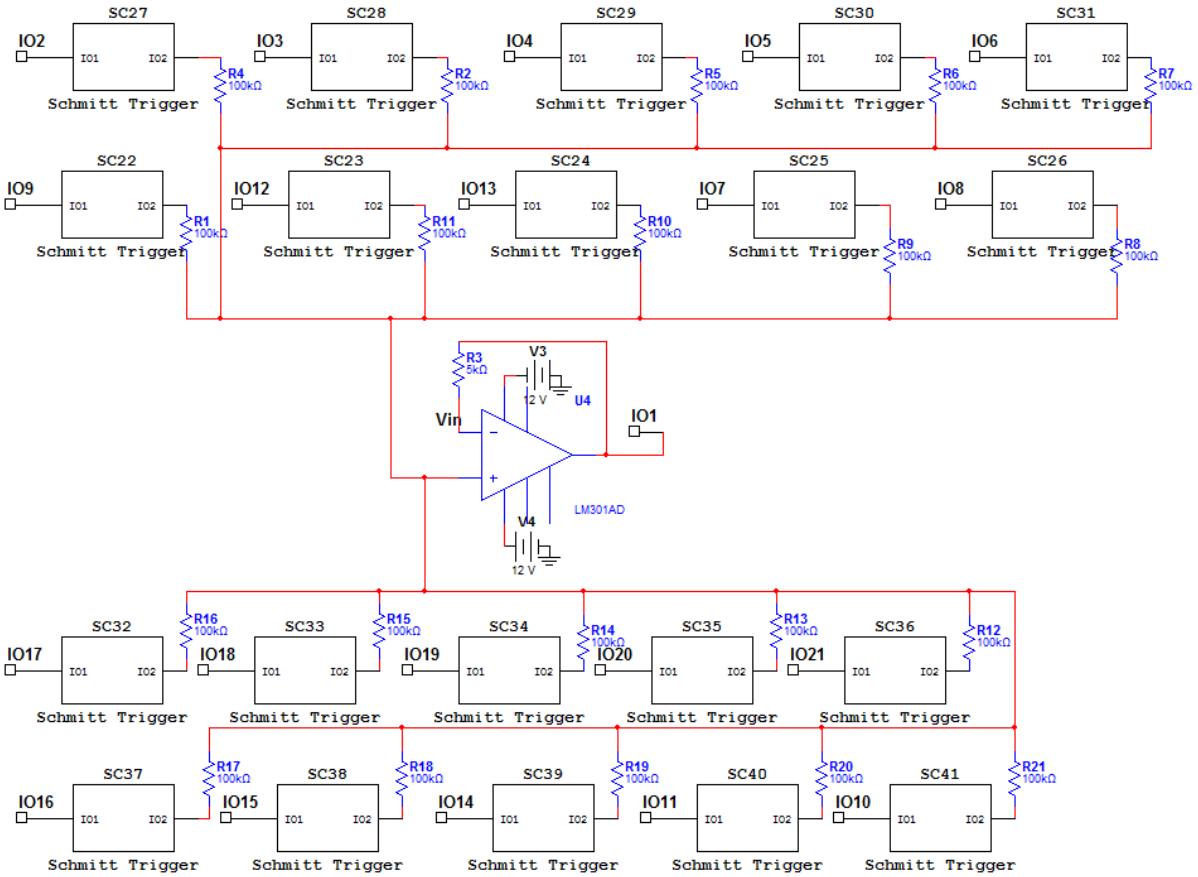

Figure 6.3: Array of Schmitt triggers and the averaging circuit represented by left block in figure 6.2

The output of all Schmitt triggers is averaged and this is fed to the opamp shown in the figure. The opamp adds the bias to this averaged value and the output is sent to the block on the right. The block on the right has 20 adder circuits which add the input received from the opamp and V_a^n and send the 20 different outputs so obtained to the block on the left. The internal block diagram of this block is shown in figure 6.4. Figure 6.5 shows the circuit diagram of an individual adder.

We display the following representative result in Fig. 6.6: initially we apply $-V_a$ voltage to all the inputs (i.e. there is no heterogeneity in the system, and all elements are identical). Then after some time, one element is changed, i.e. we have a system with 19 identical elements (with the majority having input $-V_a$) and *only one* different element with input changed to V_a. We find that the average voltage of the circuit is $-V_s$ initially, as expected, when the system has no diversity. However, after one element changes, the

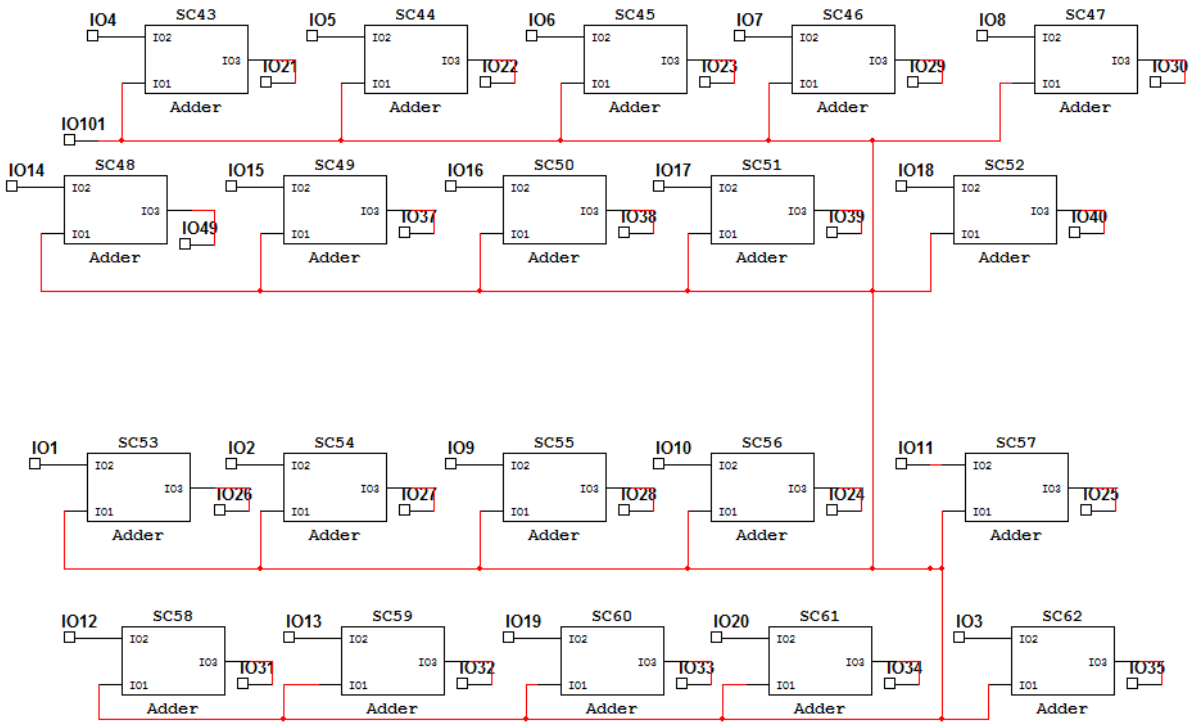

Figure 6.4: Array of adder circuits for each input represented by right block in figure 4.1

average jumps to V_s. This clearly indicates the extreme sensitivity to diversity in the coupled system.

Further note, that the circuit can be reset at any time by applying a pulse of high magnitude negative voltage. Also, importantly, by varying the bias we can infer the number of elements that differ from the majority, as evident through equation 6.5.

6.5 Conclusion

We have studied the impact of small heterogeneity in signals applied to globally coupled nonlinear bistable elements. In the absence of coupling, the output of the nonlinear elements swings towards the signal applied to that element and the collective response mirrors the state corresponding to average of all the signals. When the elements are coupled and a bias is applied, we find that even a very small number of different inputs are able to drag the collective response towards the stable state of the minority inputs. In our explicit demonstration we have taken Schmitt triggers as the basic nonlinear bistable elements, and the inputs are encoded as voltages applied to them. The average of output

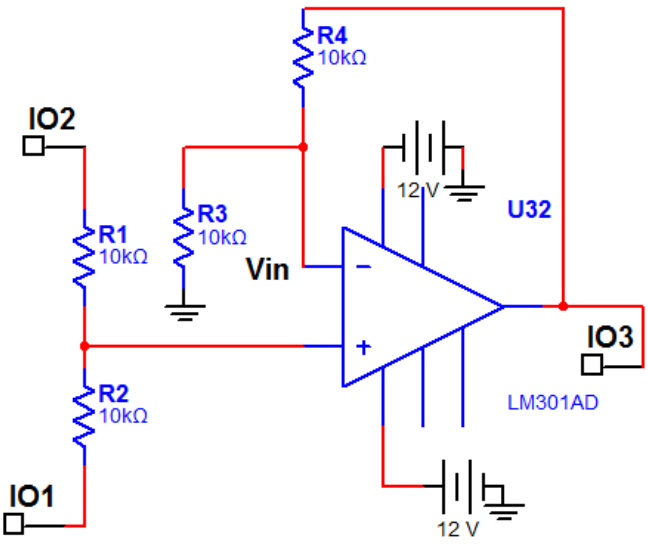

Figure 6.5: Circuit diagram of a single adder

voltages of all the Schmitt triggers corresponds to the global output of the system. We also observe that the minimum heterogeneity that can be detected scales with ratio of threshold voltage to source voltage of the Schmitt triggers, and can be be brought down to the limit of single bit detection.

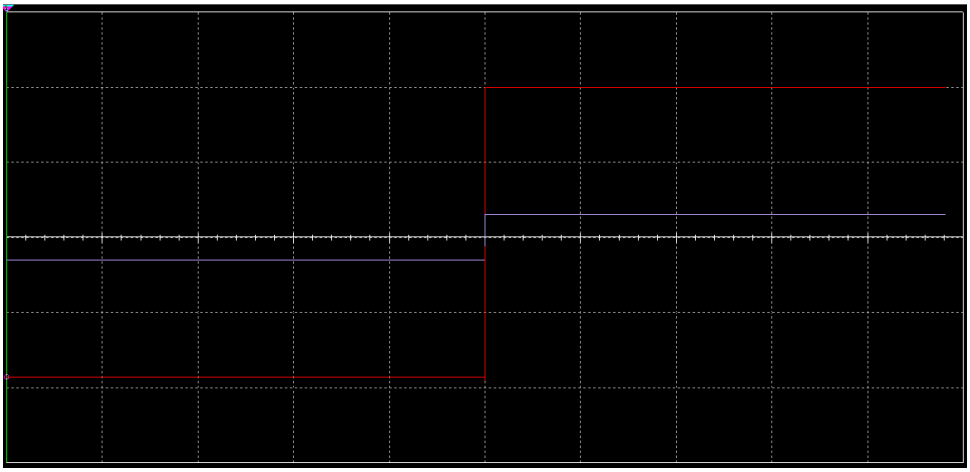

Figure 6.6: Time series of the input to one element (light blue), and the average of output voltage of 20 coupled elements (red). The input to other 19 elements is held constant at the same value as was applied to first input in first half of time series. We observe that as the input changes for just this one particular element, the average voltage, which is the collective response of the whole system, jumps to the high state. Y axis shows the voltage with each grid element representing 2V and X axis represents time with each grid element representing 1ms.

Chapter 7

Emergence of epidemics in rapidly varying networks

In this work, we shall explore how changing the underlying web of connections at different rates influences the emergent spatiotemporal patterns in an extended interactive system. Specifically, we will focus on a problem of considerable relevance, namely, the nature of infection spreading in a population of individuals connected by links that vary over a large range of time scales[1].

At the level of individuals in the population, we consider the class of communicable diseases that progress as follows: at the outset an individual is *susceptible* to infection (a stage denoted by S); on infection through contact with other infected people, the individual moves to the *infectious* stage (I). In this stage of the disease, an individual may infect susceptible members of the population it comes into contact with. The infectious period is followed by a *refractory* stage (denoted by R), where the individual is immune to the disease and also does not infect others. The immunity in this class of disease is temporary and after a while the individual is again susceptible (S). So the temporal evolution of the stages of the disease at the nodes of the network will be modeled by the well known epidemiological model of disease progression: the SIRS cycle. This model is appropriate for diseases like small pox, tetanus, influenza, typhoid fever and cholera [59].

Now, we consider such individuals linked together in a web of connections. Various approaches have been employed to analyze such disease dynamics on networks. While some studies have focused on different network topologies [82, 83, 84, 85] others have

[1]Results of this chapter have been published in [81]

analyzed using different rules for dynamics of diseases on the nodes. For example, Girvan et. al. studied how the variation in recovery times can result in different dynamical behaviours [86]. In [87], Nagy studied the impact of varying contagion scheme, time delay and infection probability on uncorrelated networks in the fast rewiring and annealed limits. Other studies have focused on adaptive networks, where the evolution of the topology of the network depends on the dynamics on the nodes. Gross *et. al.* [88] observed assortative degree correlation, oscillations, hysteresis, and first order transitions in SIS model of epidemics employing an adaptive strategy in which susceptible are able to avoid contact with the infected by rewiring their network connections. Similar strategy leads to bistability of the endemic and disease free states in the SIRS model [89]. Segbroeck *et. al* considered disease spreading as a stochastic contact process embedded in a Markov chain and found that adaptive networks in which information about health status of others is available, can be considered as well mixed population with a rescaled effective disease infectiousness [90].

In contrast to earlier studies [82, 90], we incorporate *changes in the underlying connectivity at varying time-scales*, ranging from fast to slow vis-a-vis the nodal disease dynamics. Further, at a time, not all links get rewired; rather, a fraction of the regular contacts are replaced by random interactions. This is most relevant, as some of our connections change rarely, like family and close friends, whereas others change much more rapidly, such as strangers in our work place or in public spaces. The important consequence of disease spreading on time varying networks that we will demonstrate in the subsequent sections is the following: *quick changes in the connections enhance synchronization, as compared with slow network changes.* Namely, epidemic outbreaks emerge in rapidly varying networks, while slowly changing links result in a low fluctuating state of endemic infection.

We describe our model of the disease cycle and infection spreading in the next section. Then we present the results obtained from extensive simulations of this dynamical network. We also present the phenomena arising in a probabilistic rewiring model, namely the scenario where the connections switch to random sites randomly in time. We conclude with discussions in last section.

7.1 Model of infection spreading

We consider a network of N nodes on a ring, where each node (vertex) has $2K$ directed connections (edges). Consider first a completely regular network with each site i connected to sites $i \pm 1, i \pm 2, \ldots i \pm K$ on either side. On this regular network we incorporate random rewiring, with probability p. That is, when $p > 0$, we shuffle the connections with probability p, replacing some regular connections with a few random links. With probability p, site i will then be coupled to a randomly chosen site j on the ring. So large p implies that there will be many "short-cuts" connecting neighbourhoods, with parameter p interpolating between the regular lattice at $p = 0$ and a random network at $p = 1$ [43].

Now each node in this network represents an individual whose disease progression is described by a cellular automata model of the SIRS cycle [82]. The details of this model are as follows: each node i is assigned a value $\tau_i(t)$, which evolves over time t. The variable $\tau_i(t)$ can take integer values from 0 to τ_0. If $\tau_i(t) = 0$, the site i is susceptible at time t. If $\tau_I \geq \tau_i(t) \geq 1$, it is infected and if $\tau_i(t) > \tau_I$ it is in the refractory stage at time t. So τ_I is the time during which a node remains infected after inception of infection, and τ_0 is the total length of the full disease cycle. For sites which are not susceptible, i.e. $\tau_i(t) \neq 0$, dynamics is given as:

$$\tau_i(t+1) = \tau_i(t) + 1 \quad \text{if} \quad 1 \leq \tau_i(t) \leq \tau_0 - 1 \tag{7.1}$$

and

$$\tau_i(t+1) = 0 \quad \text{if} \quad \tau_i(t) = \tau_0 \tag{7.2}$$

The dynamics does not depend on the neighbours if the site is not susceptible. Neighbours come into play only while infecting the susceptible site. The model considers that only infected sites infect their neighbours. Thus a site susceptible at time t, will be infected at time $t + 1$ with probability proportional to the fraction of infected sites in its neighborhood. In other words, if $\tau_i(t) = 0$, $\tau_i(t + 1) = 1$ with the probability $q = k_{inf}/k_i$ where k_i are total number of neighbours of site i, of which k_{inf} are infected. With probability $1 - q$, the susceptible site does not change state.

$$\tau_i(t+1) = \begin{cases} 1 & \text{with probability } q, \\ 0 & \text{with probability } 1-q \end{cases} \qquad \text{if} \quad \tau_i(t) = 0$$

It is schematically shown in Fig. 7.1

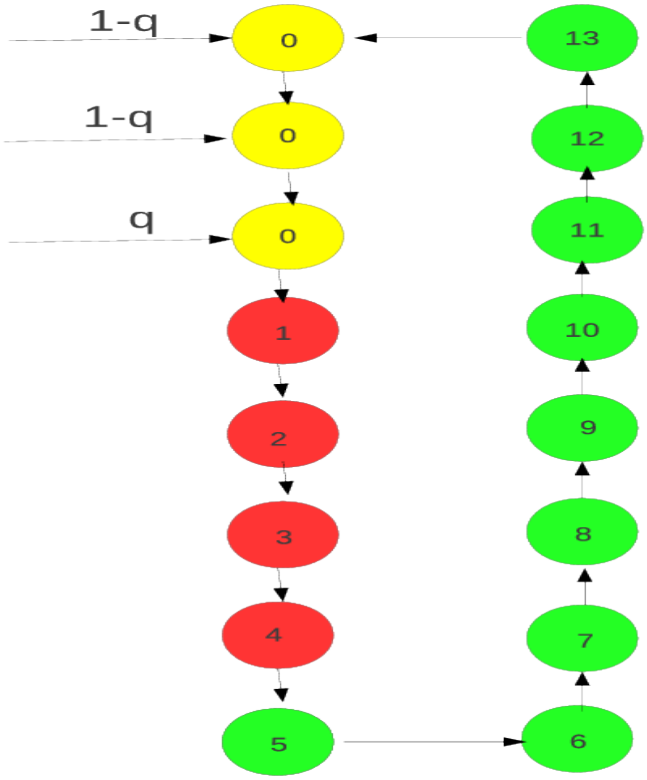

Figure 7.1: Evolution of the disease cycle.

We also introduce a small quenched disorder in the system, namely ~ 1 % of the total number of sites is always kept in the infectious state i.e. $\tau_i(t) = \tau_i(0)$ for all these sites for all times and $\tau_i(0) = 1$. This prevents the system from falling into fully synchronized state, after which there can be no further evolution. The schematic of the model is shown in Fig. 7.2.

So this system has both deterministic and probabilistic features. The disease progression for the infected site is *deterministic*, with the infected site slowly becoming refractory and then eventually becoming susceptible again, thus going through a prescribed cycle. However, the inception of the disease cycle is a random event, as the infection of susceptible nodes occur with a certain probability that depends on the state of the neighbours.

Simulations of the above model on a small world lattice [82] showed that the fraction

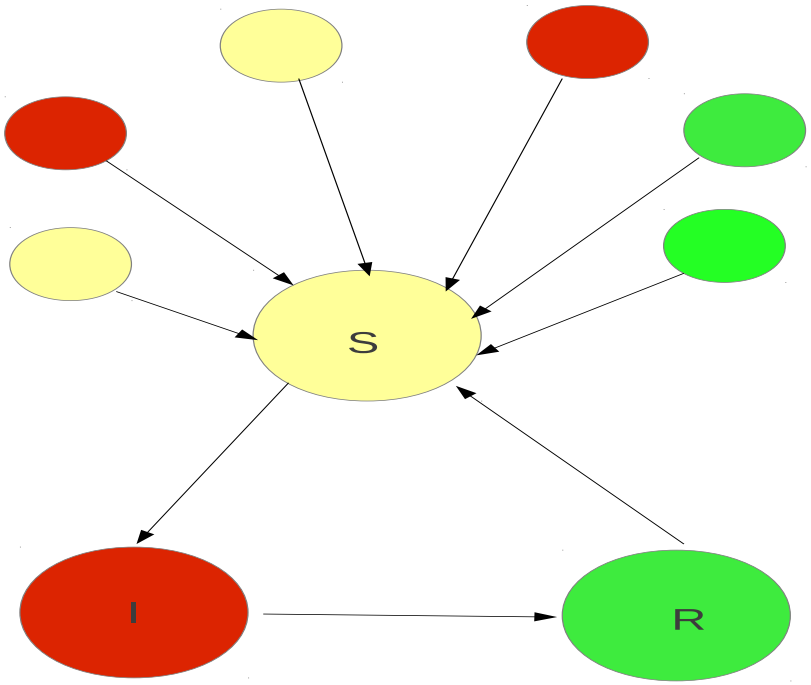

Figure 7.2: SIRS disease model. The individual at Susceptible sate can be affected by its neighbors which themselves may be in susceptible, infected or recovered state. The percentage of infected individuals gives the probability that an individual will become infected at the next step. Once it becomes infected, it passes through the infected and recovered stages deterministically.

of infected sites at a given time t shows oscillations in time for a large random rewiring probability p. One can view the system as an union of many interacting clusters. When p is large these clusters get synchronized to each other, giving rise to large amplitude collective oscillations, which can be identified as *epidemic outbreaks*.

However, it is obvious that the connectivity of the individuals will most likely vary over time, even if the average number of connections and types of links remain the same. In order to investigate this issue, we consider the underlying connection matrix to switch between different realizations, having the same fraction of random links. We consider two types of varying networks: periodically rewired networks and probabilistic link switching.

So we simulate the SIRS disease cycle on networks of sizes upto $N = 10^5$, and we looked for the effects of switching links on the emergence of synchronized infection. First the system dynamics is investigated qualitatively, through inspection of the time series of

the size of the infected set in the network. Then, we go on to characterize quantitatively the transition to large scale disease outbreak, through an order parameter reflecting the degree of synchronization of the individual disease cycles at the nodes, defined as [82]:

$$\sigma(t) = |\frac{1}{N}\Sigma_{j=1}^{N} \exp^{i\phi_j(t)}| \tag{7.3}$$

where $\phi_j = 2\pi(\tau_j - 1)/\tau_0$ is a geometrical phase corresponding to τ_j. Now, the occurrence of large oscillations corresponds to a spontaneous synchronization of a significant fraction of the elements in the system, implying that the phases $\tau_i(t)$ in the nodal disease cycles become synchronized and individuals progress through the disease together, becoming ill at the same time and recovering at the same time. Thus in this case σ will be large, with $\sigma = 1$ when all nodes are completely synchronized. On the other hand, when the system is not synchronized, the phases are widely distributed. So the value of the complex numbers $\exp^{i\phi}$ will be spread widely over the unit circle, leading to small σ.

We present in the sections below, the infection patterns emerging from our extensive simulations on different kinds of rewired networks.

7.2 Periodically Switched Links

First we consider the scenario where the network changes occur periodically, at some time period denoted by R. We study the influence of different rates of network change, ranging from links switched at every step in the disease cycle, to networks changing after several disease cycles. As we scan the full range of random rewiring probability p and time period of network change R, we look for the emergence of large oscillations in the number of infected nodes in the network, suggestive of epidemic outbreaks in the population. Our observations are presented in the subsections below.

7.2.1 Enhancement of Synchronization in rapidly varying networks

The principal observation, from our extensive simulations, is the following: for any given fraction of random links, when the network varies fast, the oscillations in the total number of infected sites have large amplitude, indicative of more synchronized disease outbreaks. This is evident in the time evolution of the fraction of infected nodes in the population,

shown for representative cases in Fig. 7.3.

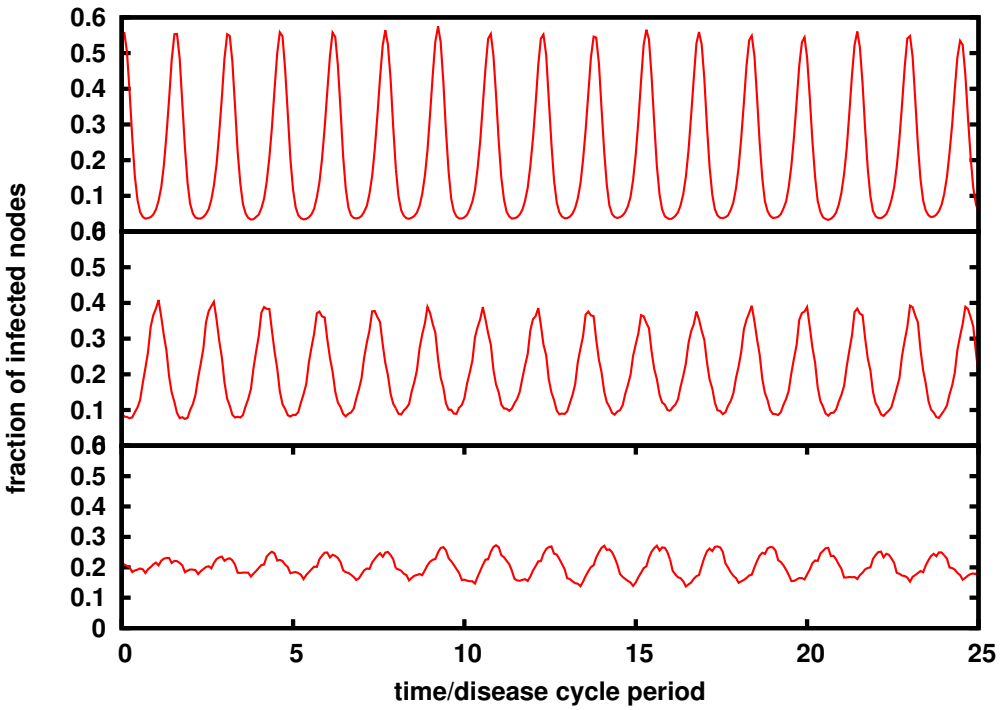

Figure 7.3: Evolution of the number of infected sites in a network of 10^4 nodes with $K = 1$, with network rewiring periods $r = 1$ (top), $r = 3$ (middle) and $r = 5$ (bottom). Here the random rewiring probability $p = 0.4$, and $\tau_I = 4$, $\tau_0 = 13$ in the SIRS disease cycle.

Further, quantitatively, it is evident from inspection of this synchronization order parameter, that when the frequency of network change is low, the rewiring probability at which transition to large oscillatory behaviour occurs, increases. For instance, in Fig. 7.4, the transition to large-scale synchronization occurs around $p = 0.2$ when the network varies with time period $r \sim 1$. In contrast, when the network changes slowly ($r \sim 10$) then the transition to synchronized disease outbreak occurs only for much larger random rewiring probabilities ($p > 0.4$). For very slow rewiring ($r \sim 50$) the transition doesn't occur at all.

For small R there is a clearly defined transition to the synchronized state as the fraction of random links increases. We obtain the transition point from the sharpest change in the slope of the curve of the synchronization order parameter as a function of rewiring probability p. The critical rewiring probability p_c thus obtained, with respect to

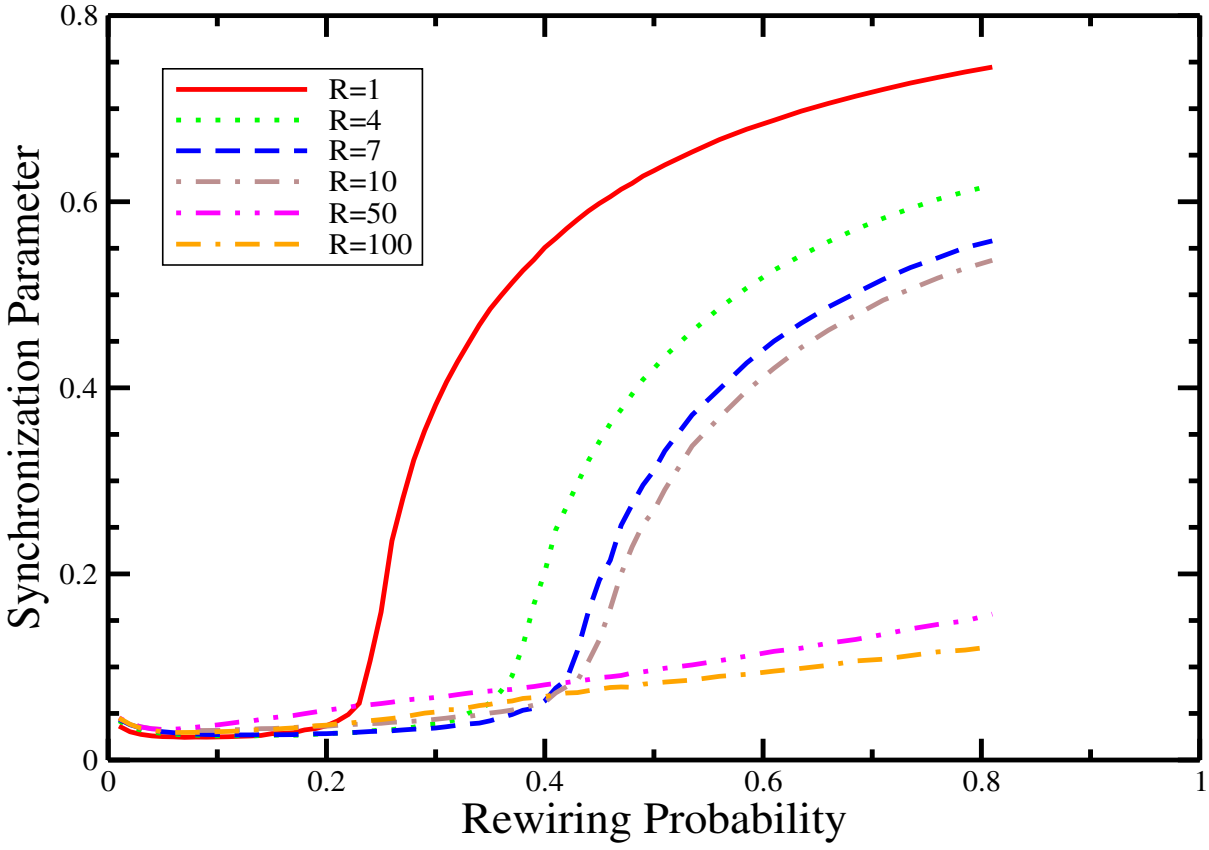

Figure 7.4: Variation of the synchronization order parameter with rewiring probability p, for a network of size $N = 10^4$, and $K = 1$, for different network rewiring periods. Here $\tau_I = 4$, $\tau_0 = 13$ in the SIRS disease cycle.

the network rewiring time period R, is displayed in Fig.7.5. It is evident that p_c increases with increasing network rewiring period R. Namely, for rapidly changing networks, i.e. with small R, we obtain synchronization at smaller values of rewiring probability p.

7.2.2 Interplay of nodal dynamics and network rewiring

The significant nodal time-scale here is τ_I, namely the time over which a node can infect others. If the network connections change rapidly compared to τ_I, it strongly aids synchronization. However, if the underlying web of links changes slower than τ_I, the effect on the emergence of synchronized cycles is much lower. So while a node is in the infective stage, if the network changes often, short-cuts are provided to many different non-local nodes in the network. Thus the infection can spread much faster, assisting the emergence of large-scale synchronization.

The above also implies that the effect of rewiring is more evident when the infective

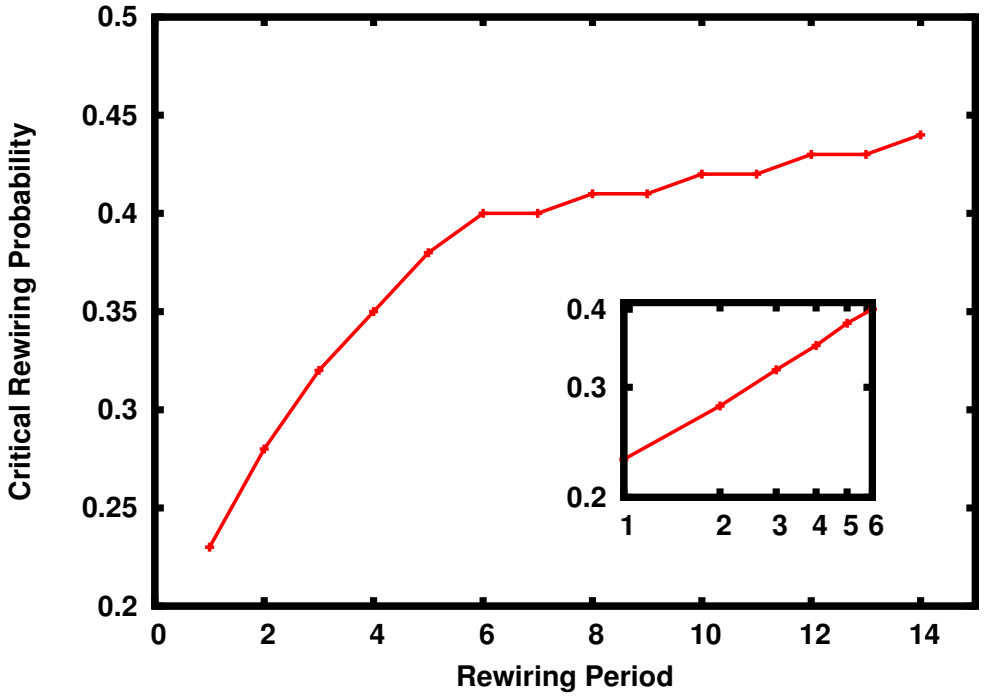

Figure 7.5: Variation of critical rewiring probability p_c, with respect to network rewiring time period R, for a network of size $N = 10^4$, and $K = 1$. Here $\tau_I = 4$, $\tau_0 = 13$ in the SIRS disease cycle. Inset shows the curve on a log-log scale, for low R values, indicating power-law scaling at small R.

stage is longer. This is demonstrated in Fig. 7.6, which displays the synchronization order parameter for networks that rewire at different frequencies, with respect to the probability of random rewiring p. It is clear that for the larger τ_I the onset of large scale synchronization is most affected by the rate of change of the underlying connections.

Interestingly, we observe that the time period of the emergent oscillations in infected nodes, $T_{epidemic}$, is larger than the length of the disease cycle τ_0. For instance, for $r = 1$, if τ_0 is 13, then the time period of the collective infection is around 18 (as evident from Fig. 7.7), and when τ_0 is 26, $T_{epidemic}$ is around 32.

Further, if the length of the infective stage τ_I increases, $T_{epidemic}$ decreases slightly and the magnitude of oscillations increases, indicating the emergence of faster and more pronounced oscillatory infection outbreaks (see Fig. 7.7). $T_{epidemic}$ also decreases slightly with increase in rewiring probability p. Lastly, the time period of the collective infection oscillations is weakly dependent on the size of the network. For instance, for a network

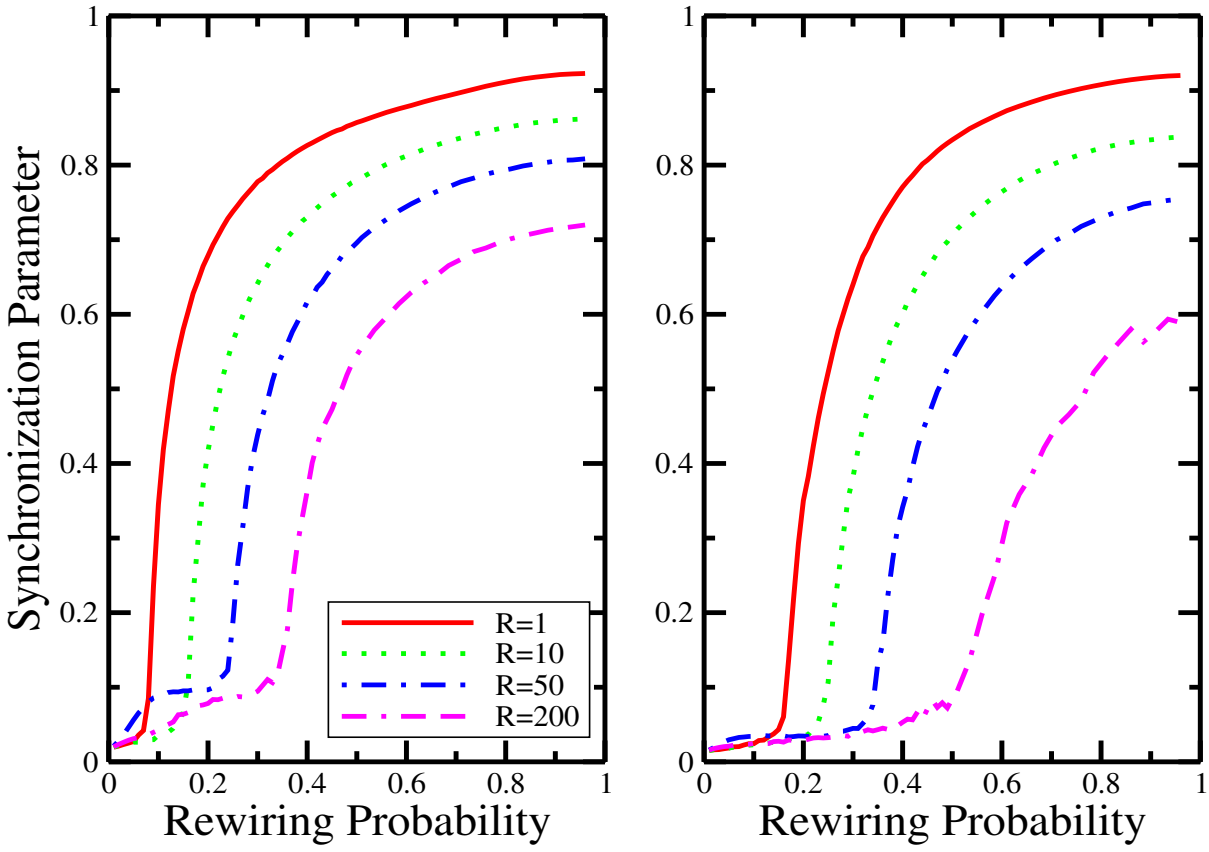

Figure 7.6: Variation of the synchronization order parameter with rewiring probability p for a network of size $N = 10^4$, $K = 1$, $\tau_0 = 26$, and infectious period $\tau_I = 8$ (left), $\tau_I = 16$ (right) for network different rewiring periods.

with 100 nodes the period is approximately 18, while for a network of 10^4 nodes $T_{epidemic} \sim$ 23.

We simulated the system for various possible combinations of τ_I and τ_0, by varying τ_I from 2 to 40, and τ_0 from 10 to 50. The results were found to be qualitatively similar over the entire spectrum.

7.2.3 Influence of neighbours

Now we investigate the effect of increasing number of neighbours on disease outbreaks. If the number of neighbours is large, namely K is large, then the effect of changing links on synchronization is less significant. This is evident in representative examples displayed in Fig. 7.8, from where it is clear that the *system with larger number of neighbours is less sensitive to network changes.*

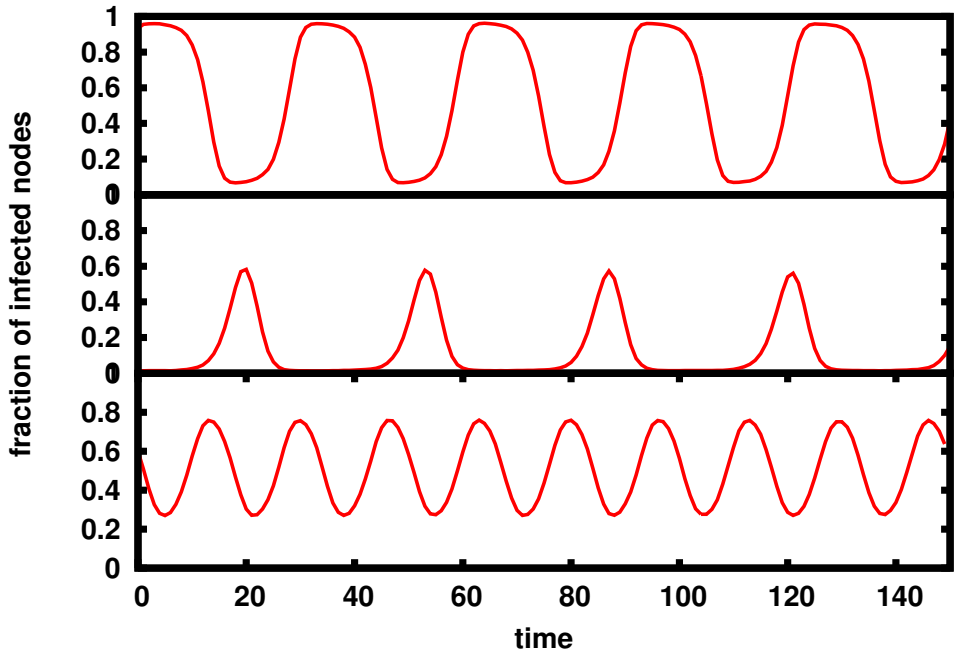

Figure 7.7: Evolution of the number of infected sites in a network of 10^4 nodes with $K = 1$, $p = 0.4$ and network rewiring period $r = 1$, for nodal SIRS cycles with: $\tau_I = 16$, $\tau_0 = 26$ (top), $\tau_I = 4$, $\tau_0 = 26$ (middle) and $\tau_I = 8$, $\tau_0 = 13$ (bottom).

One can argue that this arises from the fact that the loss in information spreading speed due to slower rewiring has been compensated by large number of links. One can also rationalize this by considering the limit of very large number of neighbours ($K \to N/2$), where the connectivity matrix has no effect on the dynamics, as the coupling is all-to-all.

At the level of nodal dynamics note that the time period decreases as the number of neighbours increases, or if the fraction of random links increases. This trend is anticipated, as more random neighbours will increase the probability of infection.

In order to demonstrate the generality of this, we show results from a very different network, namely a collection of logistic maps. We observe the same phenomena there as well (Fig. 7.9), i.e. when K is small the effects of the time variation of the network is considerable. However, for networks where nodes are connected to a large set of neighbours, this effect is not so significant.

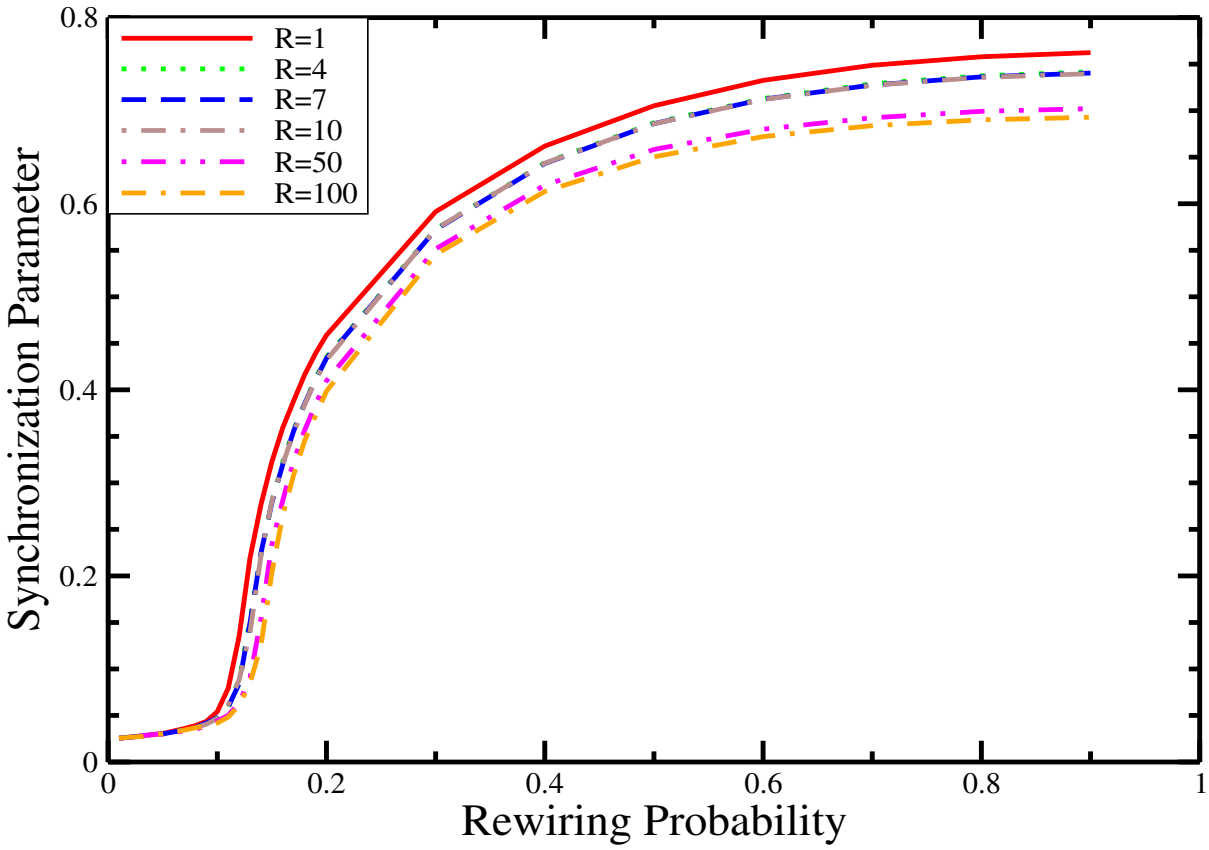

Figure 7.8: Variation of the synchronization order parameter with rewiring probability for a network of size $N = 10^4$ and $K = 5$, for various network rewiring periods. Here $\tau_I = 4$, $\tau_0 = 13$ in the nodal SIRS disease cycle.

7.2.4 Fine structure in emergent oscillations

Interestingly, over and above the broad trends mentioned above, we also observe some *fine structure in the oscillations*. These arise from the complex interplay of the changing the random links and the emergent epidemic cycles $T_{epidemic}$. The competition and cooperation between the underlying processes of infection and interaction gives rise to "resonances" in the system.

For instance, these different simultaneous periodic influences lead to *beating patterns* in the oscillations in infected population. This is clearly observable in the representative example displayed in Fig. 7.10, where the frequency of the envelope of the amplitude modulation is proportional to the difference in the emergent infection outbreak frequency and the network rewiring frequency. At specific values of p, the two periodic influences become comparable in strength, and so the beating patterns are most pronounced at these values. Such emergent beating patterns have bearing on the phenomenology of dynamically changing networks in general.

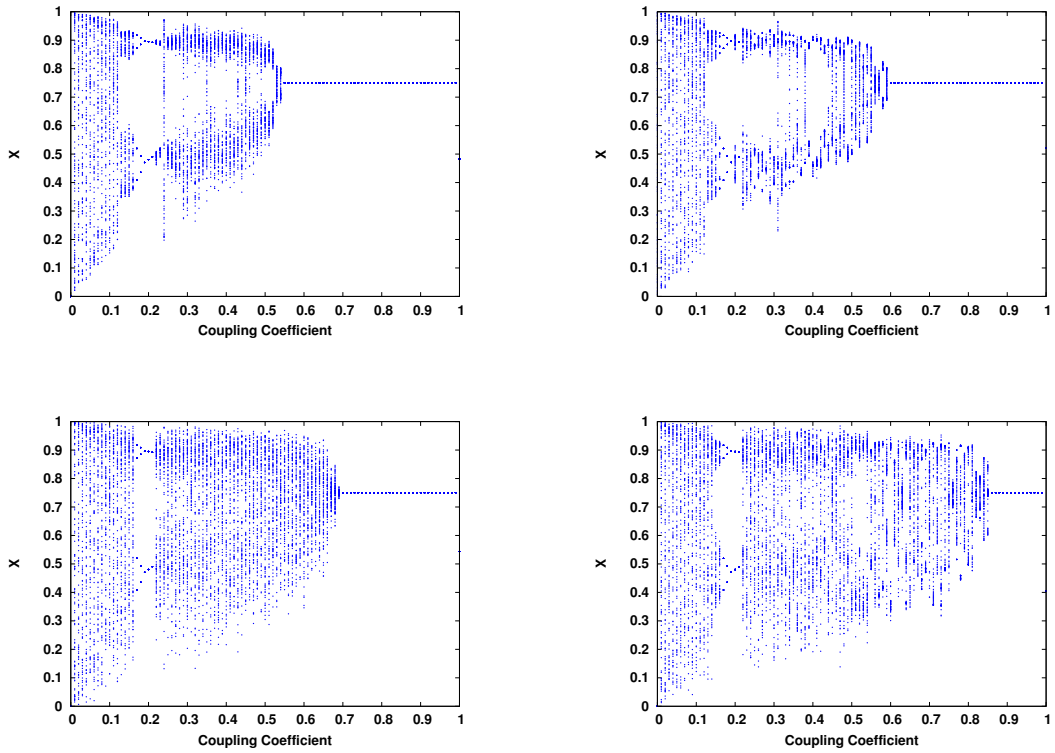

Figure 7.9: The effect of network rewiring period on the synchronization of nodes in a network of logistic maps. The figures on the top are for $K = 5$, and $r = 1$ (left), $r = 100$ (right). The figures at the bottom are for $K = 1$, and $r = 1$ (left), $r = 100$ (right).

Further we find quantitative evidence of resonant increase in synchronization occurring when the network rewiring time period is multiples of the oscillatory epidemic outbreak time period $T_{epidemic}$ (see Fig. 7.11 and 7.12). So, while we may generally expect that as we keep on decreasing the frequency of switching links, the epidemic outbreak will reduce, there may be a *sudden increase in the number of infected individuals when the network rewiring period R comes close to the frequency of emergent oscillations $T_{epidemic}$*.

To demonstrate this explicitly we took two different disease cycle lengths τ_0: 13 and 26. For the case of $\tau_0 = 13$, an increase in the amplitude of oscillations was observed around network rewiring period 17 (Fig. 7.11), which is close to the time period of the emergent epidemic oscillations $T_{epidemic}$ (~ 17). For the case of the longer disease cycle $\tau_0 = 26$ (Fig. 7.12), where $T_{epidemic}$ is larger (~ 30), increased synchronization occurred at multiples of a larger network rewiring period (namely $r \sim 30, 60, 90$). Further, we checked the generality of these qualitative features over a range of network sizes and varying lengths of the complete disease cycle and the infective stage of the disease cycle.

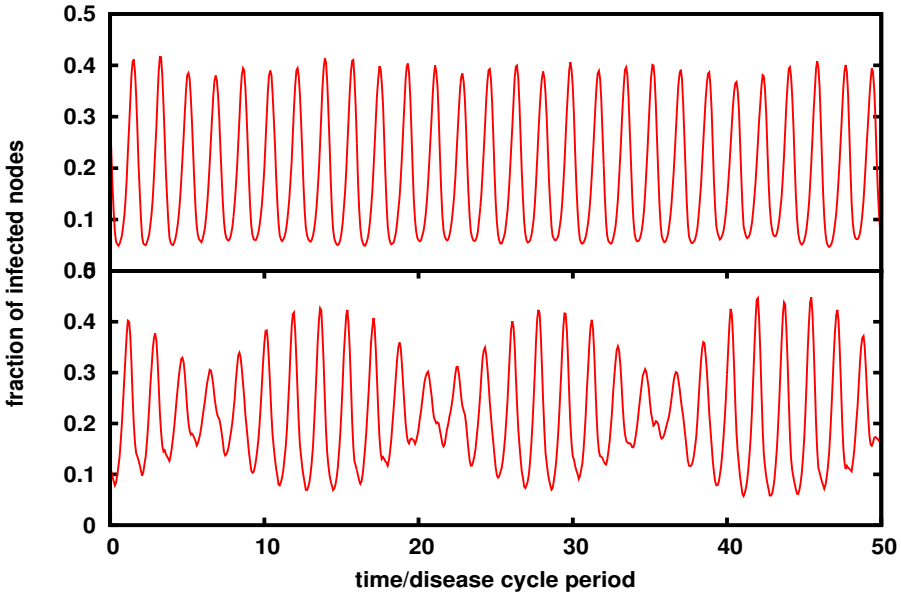

Figure 7.10: Evolution of the number of infected sites in a network of 10^4 nodes, with $K = 1$, for network rewiring period $r = 23$ and rewiring probability $p = 0.5$ (top), $p = 0.7$ (bottom). Here $\tau_I = 4$, $\tau_0 = 13$ in the SIRS disease cycle.

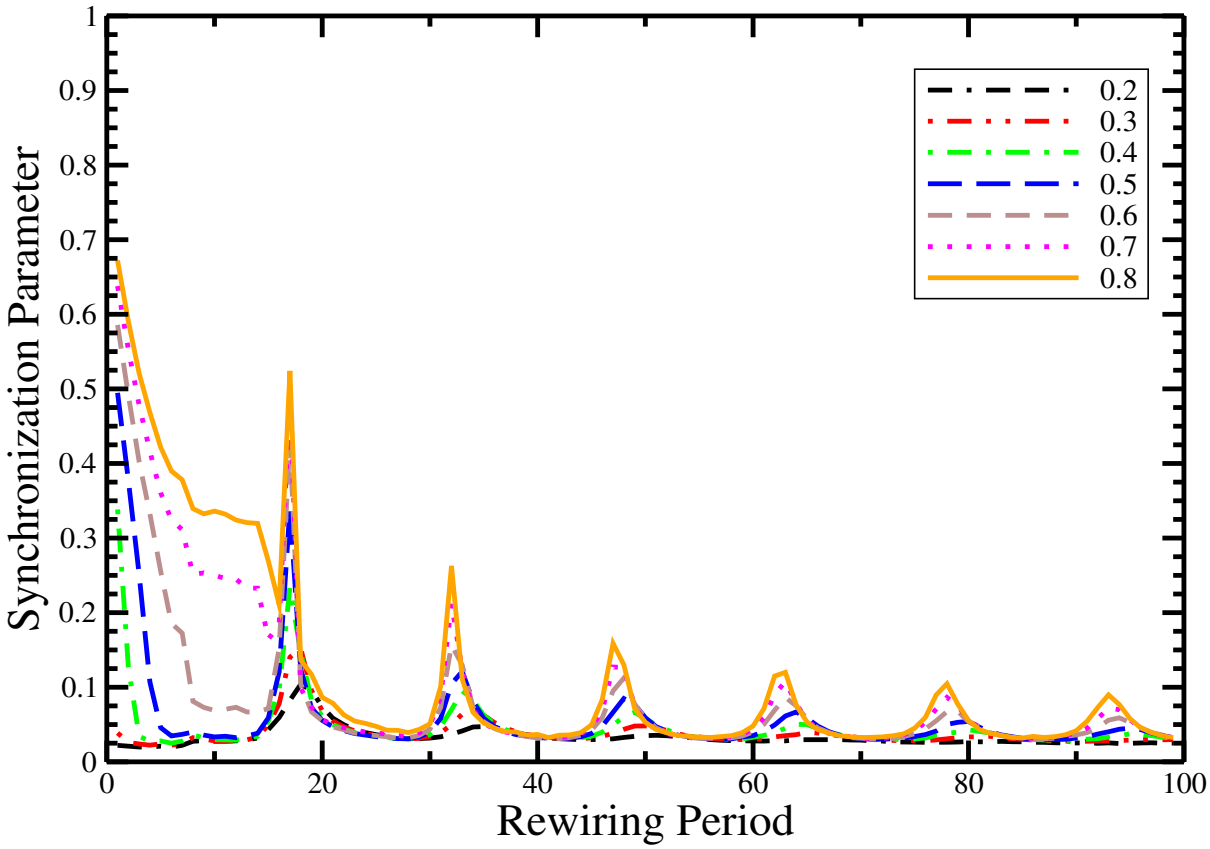

Figure 7.11: Variation of the synchronization order parameter with network rewiring period R, for a network of size $N = 10^4$, with $K = 1$, $\tau_I = 8$, $\tau_0 = 13$ and different rewiring probabilities.

7.3 Probabilistic Switching of Links

Now, we expect to see the resonance-like fine structure *only* in scenarios where the links are switched together at regular time intervals, for instance in a situation where the connections are determined by a global external periodic influence. However this is not always the most realistic scenario for disease spreading, as the interaction patterns usually don't change periodically in time. Rather we must consider a probabilistic model of link switching, such as in [91]- [92]. So in this section we study such randomly switched networks in order to determine which emergent features are robust to the manner in which links change, and which phenomena are specific to periodically switched links. Namely, we verify the generality of our observations above by investigating the SIRS dynamics on a network whose underlying links switch randomly asynchronously in time.

Specifically now, at each instant of time, a node has the probability p_r (the "link rewiring probability") of its connections being rewired. Further, as above, a node rewires

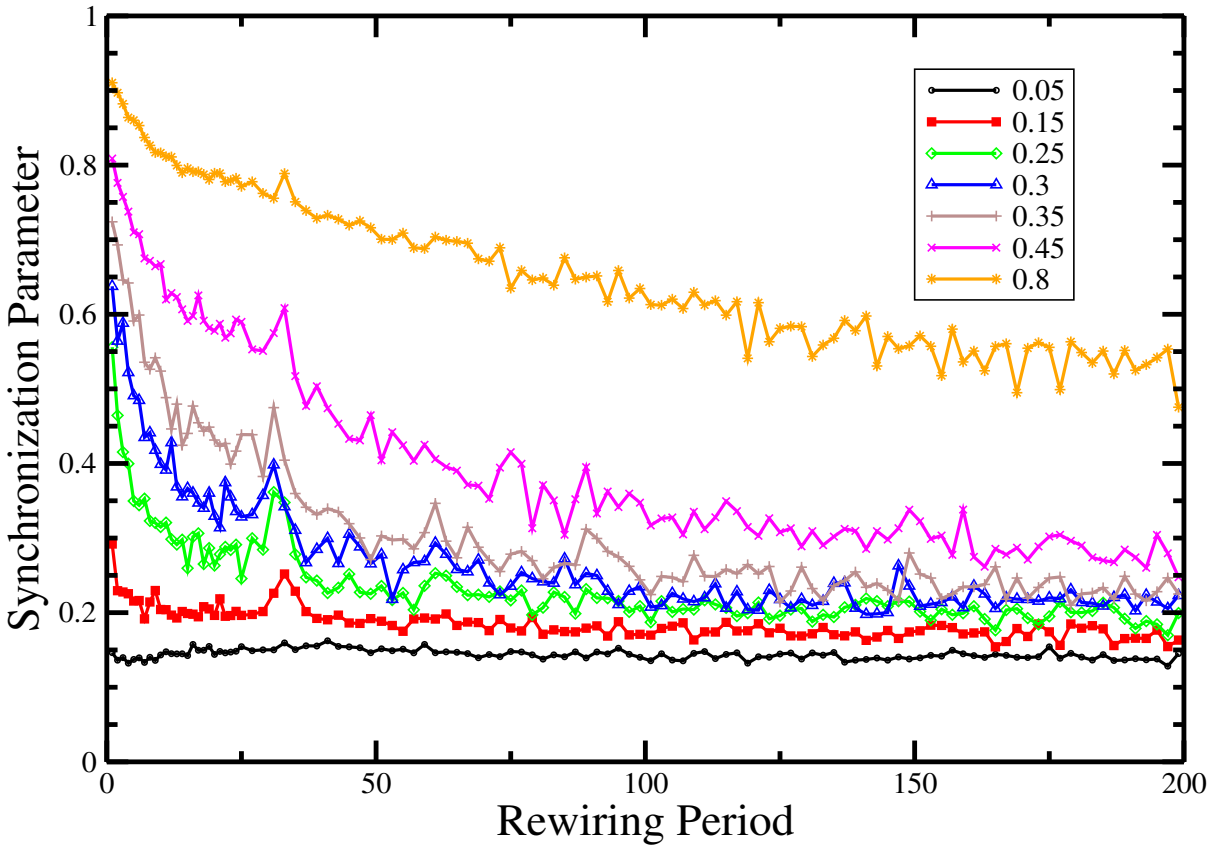

Figure 7.12: Variation of the synchronization order parameter with network rewiring period R, for a network of size $N = 10^4$, with $K = 1$, $\tau_I = 16$ and $\tau_0 = 26$ for different rewiring probabilities.

to its nearest neighbours with probability $1 - p$ and to some random neighbour with probability p (the "small world rewiring probability").

We observe transitions to synchronized epidemic cycles here as well. Further, when the link rewiring probability is increased, namely when the links change more frequently we obtain greater synchronization amongst the disease cycles in the system (Fig. 7.13). This indicates the generality of the central observation: changing links induces stronger synchronization in the SIRS disease progression, leading to the emergence of epidemics.

The only significant difference between connections varying periodically and probabilistically, is the absence of resonance-like features in the synchronization order parameter. This is expected, as there is no time scale in the random switching case that may interplay with the periodicity of the disease cycle to create "resonances".

So we conclude that the enhancement of synchronization under varying links is a robust and general phenomena. However, resonances may be observed only when there

is regularity in the link switching, perhaps driven by external periodic influences.

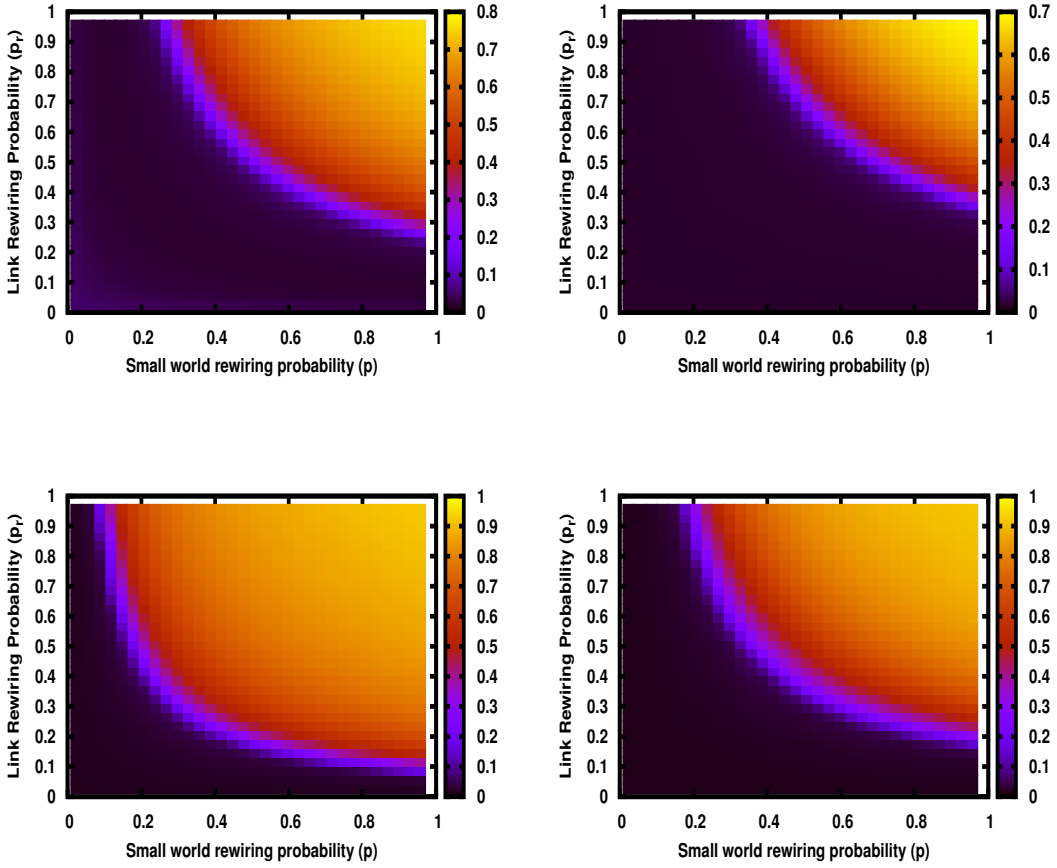

Figure 7.13: Variation of the synchronization order parameter in the parameter space of small world rewiring probablity (p) and link rewiring probablity (p_r) for a network of size $N = 10^4$, with $K = 1$ and $\tau_I = 4$, $\tau_0 = 13$ (top left), $\tau_I = 8$, $\tau_0 = 13$ (top right), $\tau_I = 8$, $\tau_0 = 26$ (bottom left) and $\tau_I = 16$, $\tau_0 = 26$ (bottom right). Again notice that the enhanced synchronization due to rewiring is more evident when the infective stage is longer.

7.4 Discussions

Here we discuss some broad, and possibly speculative, potential applications of these results. Our observations above suggest an adaptive strategy where individuals need not be quarantined for long periods, nor isolated till they fully recover. Rather, as is intuitively obvious, infected individuals just need to be quarantined during their infective phase, namely over the time during which they can infect others. More importantly, our

study suggests that large scale epidemics in the population can be prevented by simply ensuring that the infected do not swap their links for some time i.e. the infected set can retain the small set of contacts they already have, and just not be allowed to *change* their contacts.

Such a strategy is in contrast to most prevalent strategies which entail full quarantine and complete deactivation of links with the infected, which in real networks is difficult to implement and prone to failure due to inaccurate real time information on the infection status of the individuals [93]. On the other hand, if the infected can retain their set of existing contacts, it will have a positive effect on their well being, as they will be able to maintain some interactions, such as with close family, while diseased. Such a scenario will have positive implications for the psychological health of the infected, which in turn is likely to have a positive effect on their physical health, as suggested by many studies on the close interaction between the two. Also, it is easier to simply not change existing links, rather than obtain real time information of other individuals and deactivate links accordingly.

Notice that small local neighbourhoods that change rapidly, as modeled by fast switching networks with nodes of low degree, may also mimic real life scenarios better than large fixed neighbourhoods. The reason for this is that generically we come in close proximity to only few individuals at a time, though the set of individuals we interact with may change quite frequently. Further, all interactions with neighbours may not be capable of transferring an infection. It is particularly relevant in case of sexually transmitted diseases where the number of neighbours is low for vast majority of population and only contacts involving sexual partnership can be counted as edges [94]. This has analogues in other scenarios, such as spread of computer virus, as well.

Further, the analysis here can also be used to identify which groups are more vulnerable to an outbreak. For example children tend to change their connections more rapidly compared to adults [95]. Thus it may happen that an epidemic occurs only among the sub-population of children and not among adults.

In conclusion, we have described a simple model mimicking disease spreading on a network with dynamically varying connections, and we have investigated the dynamical consequences of switching links in the network. Our central observation is that the disease cycles get more synchronized, indicating the onset of epidemics, as the underlying network changes more rapidly. Further, for periodic switching of links, we observed dynamical features arising from the interplay of the time-scales of the network changes and that

of the emergent synchronized infection oscillations. Lastly, we discuss some possible implications of our results on potential epidemic management strategies.

Chapter 8

Synchronization in time varying networks

8.1 Introduction

Synchronization of dynamical units has attracted researchers from diverse fields like biology, ecology, sociology, power grids, climatology etc. [60, 61, 62, 63, 64]. Most of the earlier approaches have studied the stability of the synchronized state by linearizing the dynamical equations [65, 66]. Such approaches have enabled the analysis of stability of large class of synchronized oscillators. However, there have been studies[67] where local stability predictions do not corroborate with the actual dynamical response of the system. Jost et al.[68], have proved that linear stability provides conditions for stability of synchronized solution that are necessary but not sufficient. Detailed studies of these cases reveal that local stability results can only be valid for small perturbations and here "small" could actually be "infinitesimal" in some cases. Thus to correctly predict the dynamical response to any kind of perturbation, one should have a clear idea about complete landscape of the coupled system. By complete landscape we mean that one should know the size of basin of attraction[69, 70] for all local minimas present in the system.

To probe the stability of the synchronized state in case of large perturbations, it was proposed that the basin of attraction of the synchronized state be also estimated [69]. In this regard, Menck et al. [71] propounded the concept of Basin Stability (BS) based on the volume of basin of attraction and showed that the linear stability and BS may be quite different and both approaches should be considered to evaluate the stability of

the synchronized state. They argued that the optimization of synchronizability and the simultaneous optimization of BS act as two opposing forces and their contest results in a topological trade-off: small-worldness [43].

Furthermore, many of the initial studies assumed the interactions among the nodes to be invariant over time, though lately, there have been efforts to incorporate the time varying nature of the interactions. In one way such time variations represent the evolution of interactions over time. In another way they can be helpful in representing the discontinuities in interactions, i.e. when the nodes interact only for limited time. Such time varying interactions are commonly found in social networks, communication, biological systems, spread of epidemics, computer networks, world wide web etc and have been shown to result in significantly different emergent phenomenon [96, 97, 98, 99, 100, 101, 102, 103, 104, 105, 106, 107, 108, 109, 110, 111, 81].

Major advances have been made in the analysis of such time varying networks and it has been shown that if connections change quite rapidly, then the network can be essentially modeled as the aggregate of the interactions over time [96, 112]. It was also shown that if the Laplacian matrices at different times do not commute, the stability range is even greater [97]. When the time period of variation of links is close to time period of nodal dynamics, new stable synchronized states may appear [103]. Very recently, similar results have been found in temporal networks, i.e. where only a single edge exists at one particular instant of time [113]. Long lasting interactions slowed down diffusion in such networks and the slow eigenmodes of the effective Laplacian matrix were shown to be affected more as compared to fast eigenmodes [110].

In this work, we study the stability of the synchronized state when the underlying connection network evolves in time. The BS paradigm is particularly useful in case of time varying networks as it can be applied to large class of systems, whereas the linear stability analysis can be done exactly only in some specific cases. For this reason, most of the previous studies have considered some special switching schemes like very fast rewiring [96, 112], on-off coupling [103, 109], temporal networks [113] or a particular class of local dynamics [101]. We consider Watts-Strogatz (WS) networks and vary the fraction of random links p to cover broad range of networks varying from regular ring topology for $p = 0$ to random networks for $p = 1$. For intermediate values of p, such networks are characterized by small path length and high clustering coefficient and typically referred to as "small-world networks". The time varying character is considered by assuming that each link rewires with a rewiring frequency f. We discuss the model in the next sections and present our results and conclusions in the further sections.

8.2 Model

We begin by describing our link rewiring method. In our model each link in the network rewires stochastically and independently of the other links with an average frequency f. Specifically we consider ensembles of WS networks consisting of N Rössler oscillators, in which the dynamics at a node i is given by:

$$\begin{aligned} \dot{x_i} &= -y_i - z_i - K\sum_{j=0}^{N} L_{ij}x_j \\ \dot{y_i} &= x_i + ay_i \\ \dot{z_i} &= b + z_i(x_i - c) \end{aligned} \tag{8.1}$$

where K is a coupling constant, L the Laplacian matrix, and the parameters $a = b = 0.2$, and $c = 7.0$. For the given set of parameter values, each uncoupled Rössler oscillator has a chaotic trajectory and the synchronous state corresponds to the case when all oscillators follow the same trajectory. To construct the WS network, we start with a regular ring in which each node is connected to $2k$ nearest neighbors, k on either side. Degree distribution of such networks is shown in Fig. 8.1. Then we rewire each link with probability p by cutting it from any one side and joining to some randomly selected distant node. Then at any time t, the link is rewired with probability fdt where dt is the integration time step. If the edge is between two distant neighbors, it is rewired to a nearest neighbor of one of the nodes with a probability $1-p$. Similarly if the edge is between two nearest neighbors, then with probability p, it is broken from one of the nodes and connected to a random distant node, and not rewired otherwise. Thus on average, pkN links couple distant neighbors and $(1-p)kN$ links couple nearest neighbors and the rewiring represents the rate at which nearest neighbor links become random or vice versa. Whenever an edge is selected for rewiring, the node from which it will be cut is chosen at random. The nodes are initialized with random values, $x \in [-15:15], y \in [-15:15], z \in [-5:15]$. These values roughly correspond to the size of the chaotic attractor. We simulate the system for 10000 time units and check the final state of the system. There are three possibilities: (i) the system synchronizes, (ii) it doesn't synchronize, and (iii) it goes to infinity. We vary the rewiring frequency f from low to high and calculate the percentage of initial conditions that arrive at the synchronized state. Large f means that the edges are rewiring very quickly whereas a low value of f implies that the network is almost static.

8.3 Results

We simulate the above system for various fraction of random links p and coupling strengths K and further average out the results over different realizations of Watt Strogatz networks. Fig 8.2 shows the fraction of initial conditions arriving at the synchronous state for different f, K, p and k. It can be seen that the *range of coupling strength over which the synchronous state is stable increases considerably as the rewiring frequency increases*. Also, it is easily inferred that when the network approaches the global limit ($k \to N$) the change in connections will not affect the dynamics, while the effects of time-varying links will be most pronounced in networks with lower number of neighbors k.

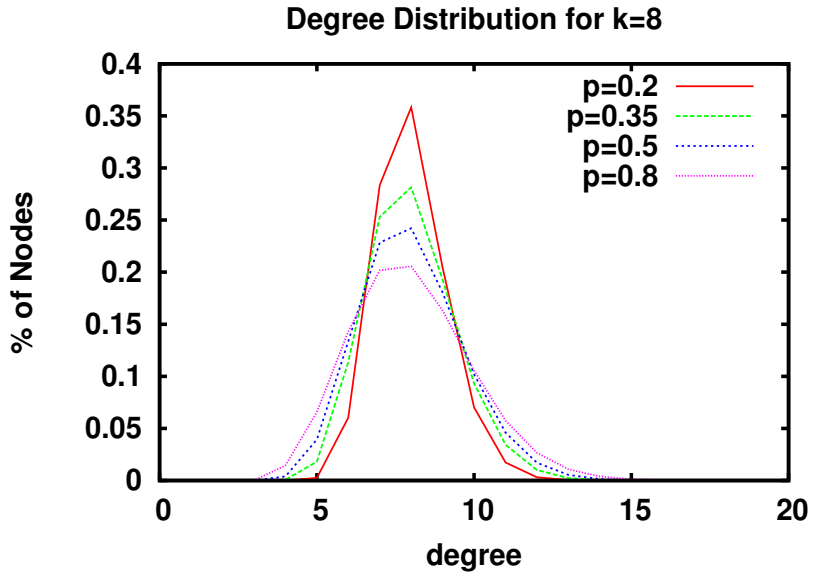

Figure 8.1: Degree distribution in WS networks.

Further notice that, while the range of synchronization is largest when the fraction of random links p is high, the *time-varying nature of the links starts to affect networks with low p at lower rewiring frequencies*. In this sense networks with low p are more sensitive to dynamic connections. To further illustrate this point, we calculate the BS of the network for fixed p and f (see Fig. 8.3). This is given as the average of the number of initial conditions arriving at the synchronized state for all possible values of coupling strengths [1] When rewiring frequency is close to 0, i.e. network is almost static, BS is higher for

[1]The values of BS obtained in this way are slightly lower than those obtained in [71], as in our case the average considers all coupling strengths whereas the upper and lower bounds for coupling strengths

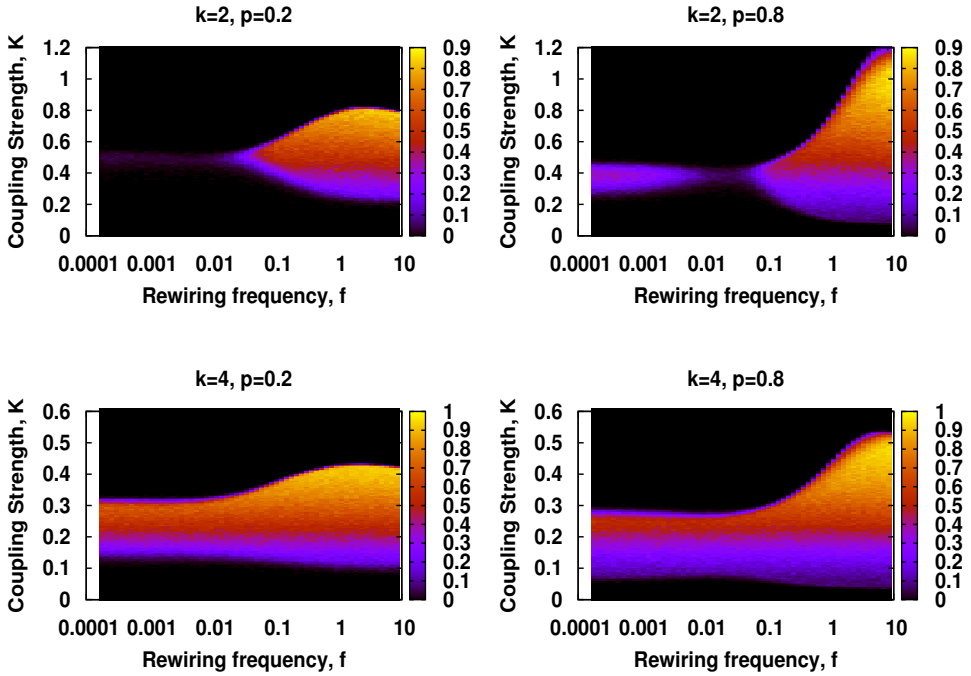

Figure 8.2: Color indicates the fraction of initial conditions arriving at the synchronized state for various rewiring frequencies f and coupling strengths K. Fraction of random links p is 0.2 (left panels) and 0.8 (right panels) and number of nearest neighbors on each side k is 2 (top panels) and 4 (bottom panels).

low values of p as reported in [71]. As rewiring frequency increases, BS for low p values rises rapidly, whereas the rise in BS for high p values is slower, indicating that BS for small world networks (low p) approaches to that of fast rewiring networks even for slowly rewiring networks, whereas a much higher rewiring frequency is needed for random (high p) networks to reach the level of fast rewiring networks. Notice also that at very fast rewiring times the basin stability is larger for networks with more spatial randomness, i.e. high p. So for networks where the connections change infrequently small-world networks are more significantly affected than completely random networks, while for networks that change rapidly random networks yield larger synchronization regions than small-world networks.

The time taken to reach the synchronized state is plotted in Fig 8.4 and it can be seen that *more randomness (i.e. higher p) and higher rewiring frequency result in lower synchronization times*. In Fig 8.2 we observe that the fraction of initial conditions arriving at the synchronized state decreases for intermediate values of rewiring frequencies in the

were obtained from the linear stability analysis based on master function approach in [71]. Results are qualitatively the same in both cases.

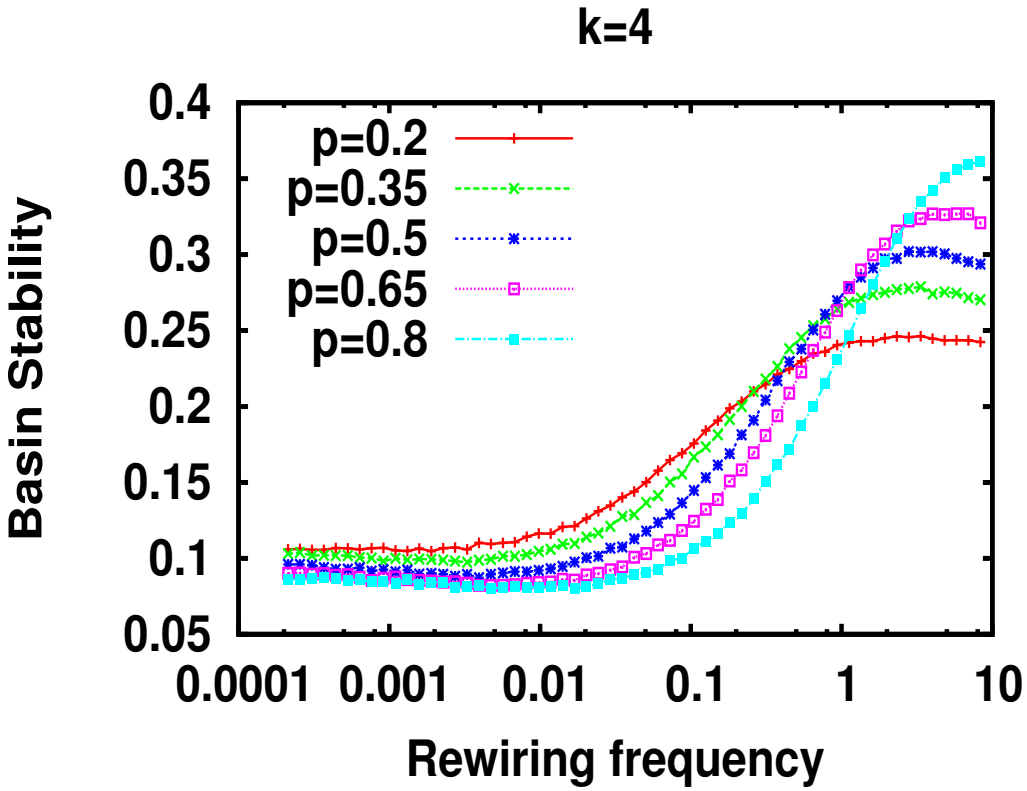

Figure 8.3: The fraction of initial conditions which arrive at the synchronized state for different rewiring frequencies averaged over different coupling strengths ($0 < K < 0.6$ for $k = 4$).

$k = 2$ case. This is so because in this range of rewiring frequencies, the time taken to arrive at the synchronized state increases (see Fig 8.5) and many initial conditions neither synchronize nor go to infinity, but continue to stay in the unsynchronized state for long times. These timescales correspond to the transition from static to dynamic behavior. For frequencies lower than these, the time varying character of the networks is lost and the dynamics is essentially that of static networks. Note that in the on-off coupling model discussed in [103], the dynamics can be determined by Lyapunov exponents for similar time scales (relating $f \sim 1/T$).

To get further insight, we plot the fraction of initial conditions that synchronize as a function of coupling strength and rewiring frequency in Fig. 8.6. We see that this fraction primarily depends on coupling strength, with randomness p or rewiring frequency having little effect on this.

It was reported in [96, 112, 103] that a time varying network can be approximated

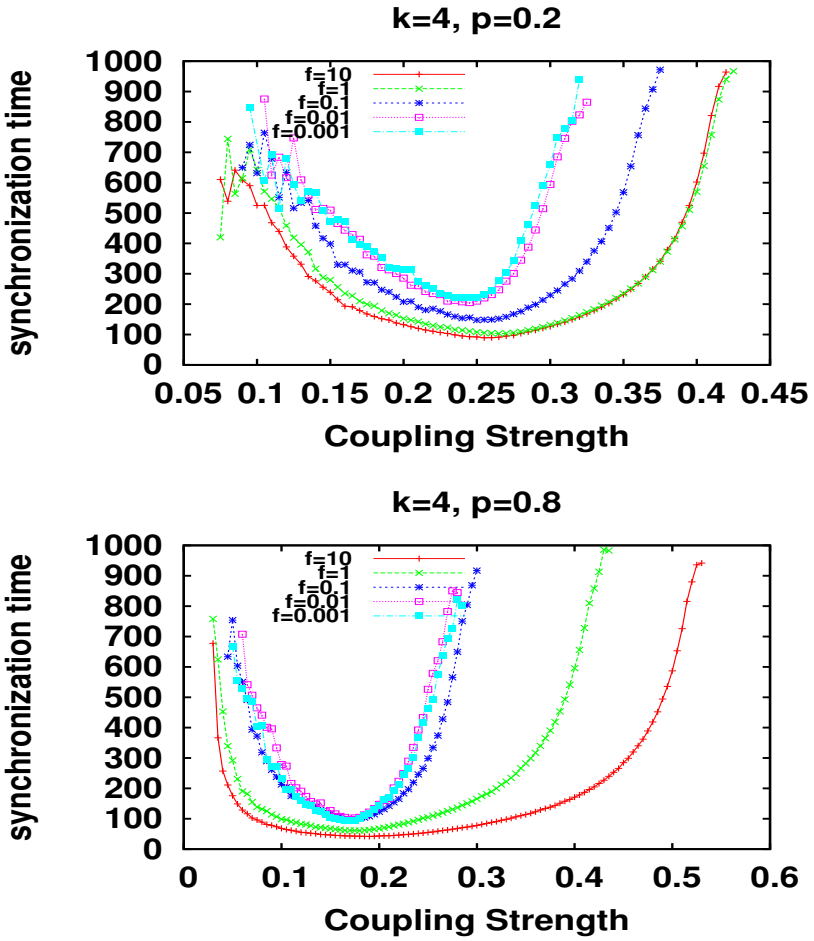

Figure 8.4: Time taken to reach the synchronized state for various coupling strengths, and rewiring frequencies at $p = 0.2$ (top) and $p = 0.8$ (bottom) for $k = 4$. It can be seen that fast rewiring networks take much lower time to reach the synchronized state.

by the time averaged network for sufficiently fast rewiring. In our case, for the time averaged network the entries in the Laplacian matrix will be $(1-p)$ for nearest neighbors and $-2kp/(N-2k-1)$ for distant nodes. Now we follow the master stability function approach [65, 66] and find the coupling range for which the synchronous state is stable. It is stable against local perturbations if the coupling strength is chosen from the interval $K \in (\alpha_1/\lambda_{min}, \alpha_2/\lambda_{max})$ where λ_{min} and λ_{max} are the minimum and maximum non-zero eigenvalues of the Laplacian matrix.

In Fig. 8.7, we plot the range of the coupling strength for which the synchronized state is stable according to master stability approach. We can see that the coupling range for which the synchronous state is stable widens considerably for the averaged network as compared to the static network. Further, the difference between static and averaged

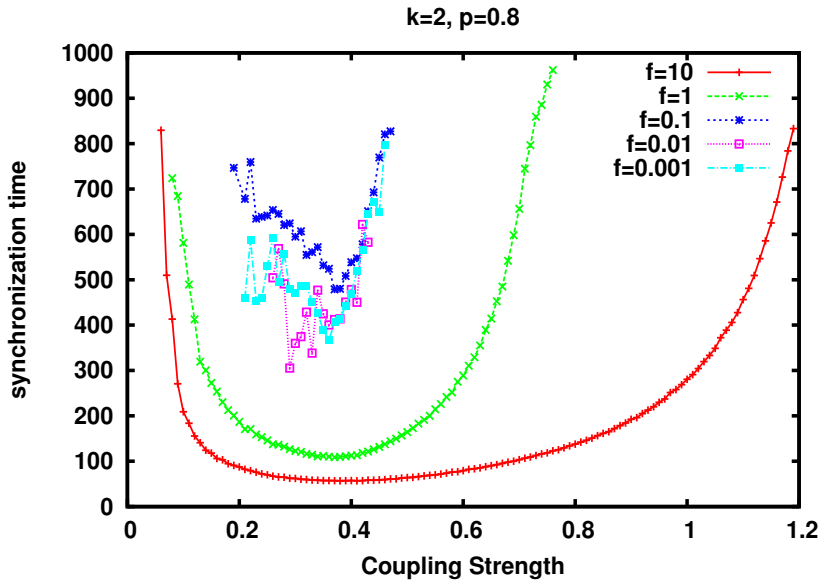

Figure 8.5: Time taken to reach the synchronized state for various coupling strengths, and rewiring frequencies at $p = 0.8$ and $k = 2$. It can be seen that synchronization time increases for intermediate values of rewiring frequencies $f \sim 0.1$.

cases is maximum when number of neighbors is smallest. All these results are consistent with those obtained using BS (see fig. 8.2).

To measure how close the effective Laplacian is to the time averaged case at various rewiring frequencies, we define an average matrix parameter as,

$$r = (K_{tv}^{max} - K_s^{max})/(K^{max} - K_s^{max}) \tag{8.2}$$

where K_{tv}^{max} is the maximum coupling strength for which even a single initial condition settles at the synchronized state for that particular value of rewiring time T and K_s^{max} is the coupling strength for which the synchronized state is stable in case of a static network. K^{max} is the maximum value of K_{tv}^{max}. The variation of this averaged matrix parameter with the rewiring frequency shows a linear increase in the averaged matrix parameter with log of the rewiring frequency (Fig. 8.8). Further, as the SW parameter p increases, the critical value of the rewiring frequency at which R starts increasing, also increases. Note that the maximum value of the coupling strength for which the synchronized state is stable is α_2/λ_{max} from the MSF approach. So the maximum coupling strength upto which the synchronous state is stable is directly related to the largest non$-$zero eigenvalue of the effective Laplacian matrix. Recently it was shown that in case of temporal networks

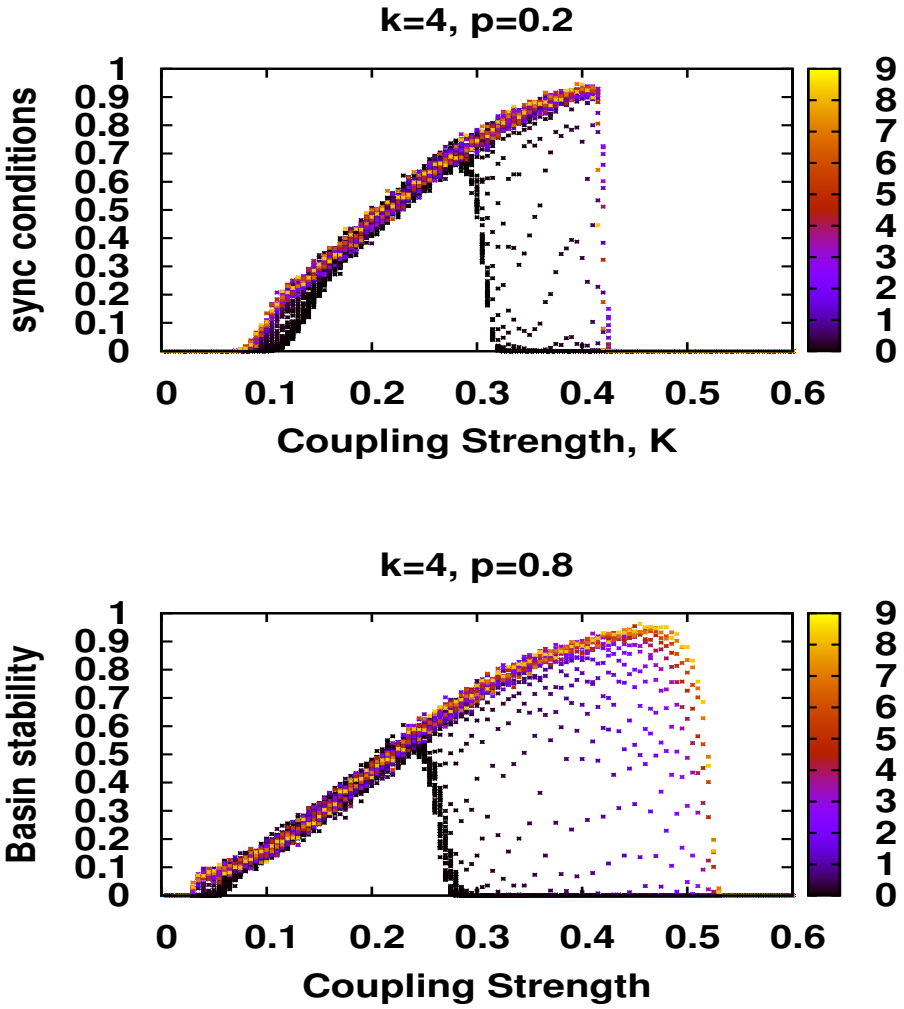

Figure 8.6: Fraction of initial conditions arriving at the synchronized state for various coupling strengths. Color indicates the frequency of rewiring.

[110], the effect of timescale of interactions is least on fast eigenmodes. In this case, as the maximum eigenvalue of the time averaged SW networks is more than the maximum eigenvalue of time averaged random networks, we can say that the eigenmodes of the time averaged SW networks are faster as compared to eigenmodes of the time averaged random networks. So the effect of rewiring is less on eigenmodes of time averaged SW networks as compared to those of random networks. Thus the time averaged character can be retained even at slower rewiring for the case of SW networks.

Stability in the on-off model We have also studied the on-off coupling model [103], in order to gain further insights into the power of the BS approach in time-varying networks. In this model, the network is switched "on" if $nT < t < (n + \theta)T$ and "off"

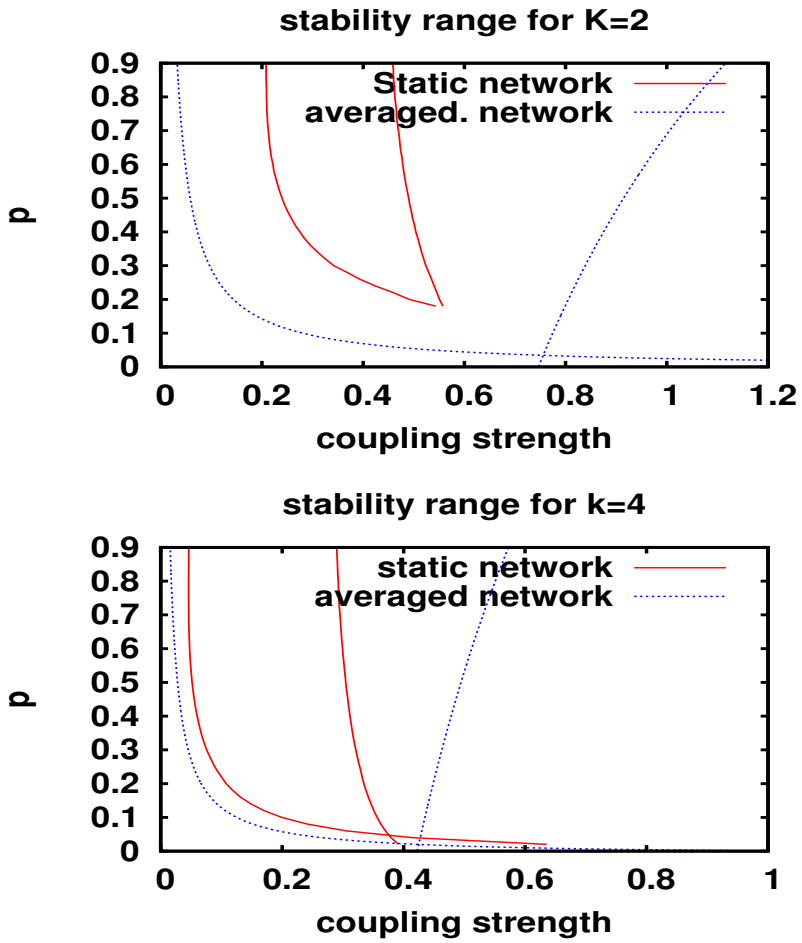

Figure 8.7: The region between solid red (dotted blue) corresponds to the range of coupling strengths for which the synchronized state is stable in the static (averaged) network for that particular value of small world rewiring probability p calculated by following the master stability function approach. For the static case, the values have been obtained by averaging over 10000 different networks.

if $(n+\theta)T < t < (n+1)T$ for $n = 0, 1, 2, ...$ and $0 \leqslant \theta \leqslant 1$. $\theta = 0$ implies that the network is always off and all nodes are isolated, whereas if $\theta = 1$, the nodes are always connected. For other values of θ the connections become on and off with time period T. It was shown in [103] that the time scale T is of critical importance for the network dynamics. If T is very small, the stability of the synchronized state can be predicted by a static time averaged coupling. For very large T, stability can be explained by Lyapunov exponents. When T is of the order of the timescale of nodal dynamics, not only the region of stability increases but the time taken to reach the synchronized state also decreases. It was shown that for intermediate values of T, the traditional bound for synchronization due to short-wavelength bifurcations ($SWBs$) disappears and more stable regions emerge.

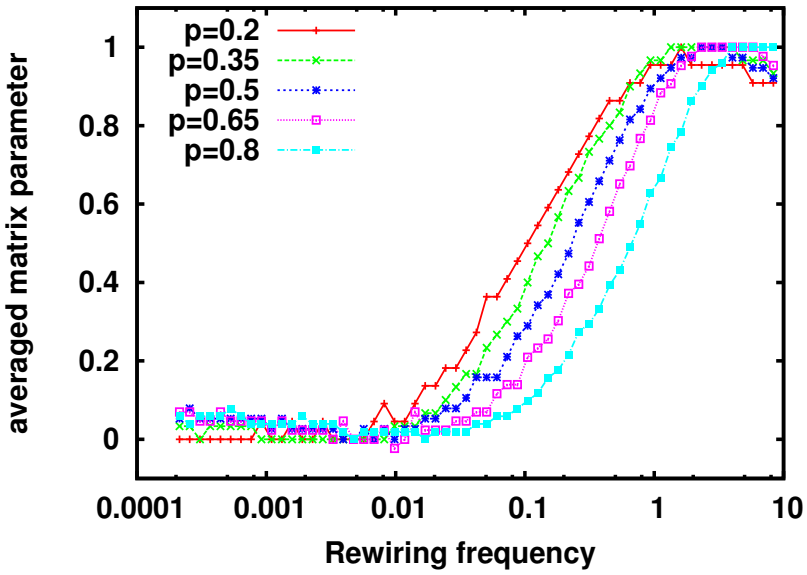

Figure 8.8: Averaged matrix parameter as a function of rewiring frequency.

This analysis, based on linear stability of the synchronous state is valid only for small perturbations. To understand whether the linear stability analysis can accurately predict the stability for large perturbations also, we calculate the BS (calculated as the number of initial conditions that arrive at the synchronous state) for an on−off coupling model by taking Rössler oscillators on WS networks. The results are shown in Fig. 8.9. As can be seen in the left panels, the linear stability rises and falls gradually with increasing coupling strength, whereas the BS (right panels) rises smoothly for low values of coupling and then drops sharply. Further, in bottom panel we see that whereas linear stability analysis predicts that the upper bound for synchronous state disappears, but from the BS we find that it disappears only for the synchronous state corresponding to low θ values. For the synchronous state corresponding to high θ values, the BS approaches zero for high coupling strengths. Furthermore, the BS is much higher for intermediate time−scales. Thus for time varying networks linear stability analysis alone is not sufficient and we need to calculate the BS also to accurately predict the stability of the synchronized state.

8.4 Conclusion

We have studied the stability of synchronous state in dynamic WS networks. In line with previous results [96, 112], we have found that for sufficiently fast rewirings, the time varying networks can be approximated by static time averaged networks. To the best of

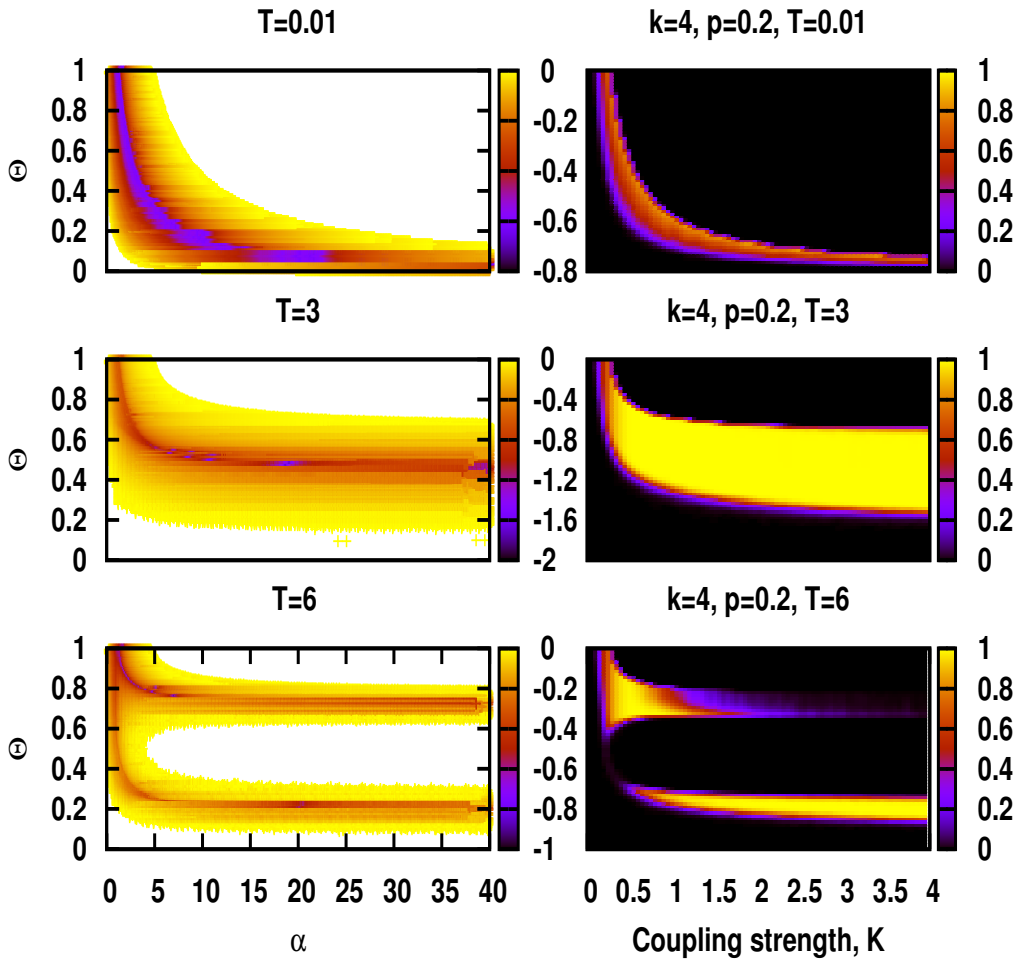

Figure 8.9: Maximum Lyapunov exponent (left panels) for the on-off coupling model obtained from linear stability analysis for $T = 0.1$ (top), $T = 3$ (middle) and $T = 6$ (bottom). Colored regions correspond to cases when maximum Lyapunov exponent is negative, i.e. the synchronized state is stable. The panels on right show the BS of WS networks for $p = 0.2$. The results are qualitatively same for other values of p also.

our knowledge, till now there is no method of finding out how fast the rewiring should be in order to consider it sufficiently fast. Using the BS framework, we have been able to estimate the rewiring frequency at which the network can be approximated by the static time average. Further we also able to get insight into how the transition from static to time averaged case takes place. We showed how the stability range changes at different rewiring timescales. Our central result from the extensive numerical simulations is that in case of small world networks the transition to time averaged case occurs at much slower link rewiring frequency compared to the random networks. We found that not only the BS of small world networks highest in static cases as reported earlier, but they approach the time averaged coupling case fastest. That is, their BS approaches that of time averaged case even for very slow rewiring time periods. It was observed that

if the links are rewiring rapidly, random networks yield larger synchronization regions than small-world networks.Further, it was found that the impact of rewring is maximum when the number of neighbors is less. Lastly, faster rewiring networks were found to synchronize quickly.

Chapter 9

Conclusions and future directions

In this thesis, we have studied the emergent patterns in nonlinear systems and the possible use of nonlinear dynamical systems in designing computing systems capable of functioning robustly in noisy environments. We have explicitly shown that a nonlinear system can produce a completely consistent logic as well as Set-Reset latch operation on two inputs, streaming in any random sequence. We have found that for very small or very large noise strengths the system does not yield a reliable output. However, in a reasonably wide band of moderate noise strength, the system produced the desired output very consistently. Furthermore, the response of the system could be easily switched from memory to logic operations by varying the bias in the system. It has been shown that noise can reduce the latency in the response of the system to switched inputs.

We have also shown through numerics and circuit experiments, that it is possible to obtain a logic response exactly similar to LSR, without the presence of noise. Using only a periodically driven bistable system, we have produced a logical combination of two inputs streaming in any random sequence. For very small or very large forcing frequencies the system did not yield any consistent logic output, but in a wide band of moderate frequencies the system produced the desired logical output very reliably. Furthermore, the logic response of the system could be easily switched from one logic gate to another by varying the bias in the system. Thus it has been shown that noise is not a necessary ingredient to facilitate changes of state that reliably mirror logical outputs.

Further, we have explicitly shown that by utilizing the constructive interplay of noise and periodic forcing it is possible to obtain a logic response similar to LSR even when the strength of noise is lower then the minimum threshold. This enables us to use the LSR elements in sub-threshold noise conditions. Moreover, by coupling the LSR element

to another LSR element with a lower potential barrier we can make the systems adapt to varying noise intensity, so that its operation is robust even in high noise conditions. The results that we have presented are quite general, and can potentially be extended to other systems which show enhanced performance in the presence of noise, such as typically observed in generalized stochastic resonance phenomena.

We have also demonstrated that the performance of a VCSEL based stochastic logic gate can be enhanced by addition of a periodic signal in the orthogonal LP mode. This enhancement has been observed for both the optoelectronic configuration as well as the all optical configuration and both in form of increase in the optimal noise window as well as decrease in minimum bit time.

So it is evident that "LSR Elements" can reliably function as logic and memory devices even for sub-threshold signals, thus consuming very low power. These "LSR Elements" can potentially act as building blocks of futuristic "Smart Computing Devices". Potentially, such devices will not only operate robustly in noisy environments, but can also be capable of optimal utilization of their resources by configuring their "LSR Elements" into latches, or any of the logic gates, depending on the requirements of the task being performed. For example, if we are performing tasks requiring more computational power like running a code, then these computing devices will morph most of the LSR elements to logic gates, whereas in case of tasks requiring memory like plotting large values of data, LSR elements will be morphed into memory enabling efficient use of resources. Furthermore, it is conceivable that devices based on such elements can potentially help in reducing boot times thus achieving what is commonly called "instant boot". This can be accomplished by morphing large number of LSR elements into memory at the time of shut down and start up. This significant increase in memory will enable us to keep most of the data required for the applications readily accessible, paving way for faster boot times.

In future, we want to demonstrate LSR in other bistable and multi-stable systems and realize some other basic operations like adder. We would try to obtain different operations in parallel by measuring the state of different state variables. LSR appears to be a fairly generic phenomenon and we plan to demonstrate it with chaotic signals also.

In the second part of the thesis, we have shown that when bistable elements are coupled and a bias is applied, even a very small number of heterogeneous inputs can drag the collective response towards the stable state of the minority inputs. In our explicit demonstration we demonstrated this phenomenon in mean−field coupled Schmitt

triggers. We have shown that the minimum heterogeneity that can be detected scales with ratio of threshold voltage to source voltage of the Schmitt triggers, and can be be brought down to the limit of single bit detection.

We also described a simple model mimicking disease spreading on a network with dynamically varying connections, and investigated the dynamical consequences of switching links in the network. We have observed that the disease cycles get more synchronized, indicating the onset of epidemics, as the underlying network changes more rapidly. Further, for periodic switching of links, we observed dynamical features arising from the interplay of the time-scales of the network changes and that of the emergent synchronized infection oscillations.

Lastly, we have studied the stability of synchronous state in dynamic WS networks. We have found that for sufficiently fast rewirings, time varying networks can be approximated by static time averaged networks. To the best of our knowledge, till now there is no method of finding out how fast the rewiring should be in order to consider it sufficiently fast. Using the BS framework, we have been able to estimate the rewiring frequency at which the network can be approximated by the static time average. Further we have got insights into how the transition from static to time averaged case takes place. We have shown how the stability range changes at different rewiring timescales. Our central result from the extensive numerical simulations is that in case of SW networks the transition to the time averaged case occurs at a much slower link rewiring frequency compared to random networks. We have found that not only the BS of SW networks is highest in static cases as reported earlier, but they approach the time averaged coupling case fastest. That is, their BS approaches that of the time averaged case even for very slow rewiring time periods. It has been observed that if the links are rewiring rapidly, random networks yield larger synchronization regions than SW networks. Further, we have found that the impact of rewiring is maximum when the number of neighbors is less. Lastly, faster rewiring networks have been uncovered to synchronize quickly.

In future, we would like to further extend our work on stability of synchronized states in complex networks which is relevant across fields like study of neurons in the brain, power grids, climate systems, social networks, communication, biological systems, spread of epidemics, computer networks, world wide web etc. Specifically, we would like to explore the stability of synchronous states in complex networks using BS framework. Our emphasis will be on comparing the linear stability and BS and then possibly study the limits of BS. Till now we have studied chaotic systems on small world networks. Next we plan to explore other systems like continuous systems, discrete systems and excitable

systems and see if there are any differences and possible reasons for those differences.

We will also check for other network configurations like scale free and random networks. We want to see the changes when we vary a single network parameter and the network varies between Erdos Renyi networks on one side to Albert Barabasi on the the other. We plan to explore the effect of delay in the dynamical equations. Another point to explore will be the changes in BS when perturbations come from different distributions like uniform, Gaussian or long tailed distributions. Our emphasis will be on estimating the size and shape of sync basins and if it is theoretically possible to predict the behavior in different cases.

Briefly, we plan to build a stronger theoretical and mathematical framework for analyzing complex networks by BS analysis along with the time tested linear stability analysis. We also want to explore other diverse complex systems and ways to control the emergent spatiotemporal dynamics thereby contributing toward the growing understanding of complex systems and their control.

Bibliography

[1] Steven H Strogatz. Exploring complex networks. *Nature*, 410(6825):268–276, 2001.

[2] Steven H Strogatz. *Nonlinear dynamics and chaos (with applications to physics, biology, chemistry a.* Perseus Publishing, 2006.

[3] Luca Gammaitoni, Peter Hänggi, Peter Jung, and Fabio Marchesoni. Stochastic resonance. *Rev. Mod. Phys.*, 70:223–287, Jan 1998.

[4] Kurt Wiesenfeld, Frank Moss, et al. Stochastic resonance and the benefits of noise: from ice ages to crayfish and squids. *Nature*, 373(6509):33–36, 1995.

[5] R Roy, PA Schulz, and A Walther. Acousto-optic modulator as an electronically selectable unidirectional device in a ring laser. *Optics letters*, 12(9):672–674, 1987.

[6] S Fauve and F Heslot. Stochastic resonance in a bistable system. *Physics Letters A*, 97(1):5–7, 1983.

[7] RN Mantegna and B Spagnolo. Stochastic resonance in a tunnel diode. *Physical Review E*, 49(3):R1792, 1994.

[8] S Arathi, S Rajasekar, and Jürgen Kurths. Characteristics of stochastic resonance in asymmetric duffing oscillator. *International Journal of Bifurcation and Chaos*, 21(09):2729–2739, 2011.

[9] W Hohmann, J Müller, and FW Schneider. Stochastic resonance in chemistry. 3. the minimal-bromate reaction. *The Journal of Physical Chemistry*, 100(13):5388–5392, 1996.

[10] Dante R Chialvo, André Longtin, and Johannes Müller-Gerking. Stochastic resonance in models of neuronal ensembles. *Physical review E*, 55(2):1798, 1997.

[11] Sylvain Barbay, Giovanni Giacomelli, and Francesco Marin. Stochastic resonance in vertical cavity surface emitting lasers. *Physical Review E*, 61(1):157, 2000.

[12] C Masoller. Noise-induced resonance in delayed feedback systems. *Physical review letters*, 88(3):034102, 2002.

[13] Giuseppe Consolini and Paola De Michelis. Stochastic resonance in geomagnetic polarity reversals. *Physical review letters*, 90(5):058501, 2003.

[14] Marcelo Kuperman and Damián Zanette. Stochastic resonance in a model of opinion formation on small-world networks. *The European Physical Journal B-Condensed Matter and Complex Systems*, 26(3):387–391, 2002.

[15] John K Douglass, Lon Wilkens, Eleni Pantazelou, and Frank Moss. Noise enhancement of information transfer in crayfish mechanoreceptors by stochastic resonance. *Nature*, 365(6444):337–340, 1993.

[16] K. Murali, Sudeshna Sinha, William L. Ditto, and Adi R. Bulsara. Reliable logic circuit elements that exploit nonlinearity in the presence of a noise floor. *Phys. Rev. Lett.*, 102:104101, Mar 2009.

[17] GA Patterson, AF Goya, PI Fierens, SA Ibánez, and DF Grosz. Experimental investigation of noise-assisted information transmission and storage via stochastic resonance. *Physica A: Statistical Mechanics and its Applications*, 389(9):1965–1970, 2010.

[18] S. A. Ibez, P. I. Fierens, R. P.J. Perazzo, G. A. Patterson, and D. F. Grosz. On the dynamics of a single-bit stochastic-resonance memory device. *The European Physical Journal B*, 76(1):49–55, 2010.

[19] Canjun Wang, Ming Yi, and Keli Yang. Time delay-accelerated transition of gene switch and-enhanced stochastic resonance in a bistable gene regulatory model. In *Systems Biology (ISB), 2011 IEEE International Conference on*, pages 101–110. IEEE, 2011.

[20] Peter Hänggi, Peter Jung, Christine Zerbe, and Frank Moss. Can colored noise improve stochastic resonance? *Journal of Statistical Physics*, 70(1-2):25–47, 1993.

[21] RN Mantegna and B Spagnolo. Stochastic resonance in a tunnel diode in the presence of white or coloured noise. *Il Nuovo Cimento D*, 17(7-8):873–881, 1995.

[22] Xiaoqin Luo and Shiqun Zhu. Stochastic resonance driven by two different kinds of colored noise in a bistable system. *Physical Review E*, 67(2):021104, 2003.

[23] Daichi Nozaki, Douglas J Mar, Peter Grigg, and James J Collins. Effects of colored noise on stochastic resonance in sensory neurons. *Physical Review Letters*, 82(11):2402, 1999.

[24] Ya Jia, Xiao-ping Zheng, Xiang-ming Hu, and Jia-rong Li. Effects of colored noise on stochastic resonance in a bistable system subject to multiplicative and additive noise. *Physical Review E*, 63(3):031107, 2001.

[25] KP Singh, G Ropars, M Brunel, and A Le Floch. Lever-assisted two-noise stochastic resonance. *Physical review letters*, 90(7):073901–073901, 2003.

[26] Yang Tang, Huijun Gao, Wei Zou, and Jürgen Kurths. Pinning noise-induced stochastic resonance. *Physical Review E*, 87(6):062920, 2013.

[27] S Saikia, AM Jayannavar, and Mangal C Mahato. Stochastic resonance in periodic potentials. *Physical Review E*, 83(6):061121, 2011.

[28] WL Reenbohn and Mangal C Mahato. Relative stability of dynamical states and stochastic resonance in a sinusoidal potential. *Physical Review E*, 88(3):032143, 2013.

[29] Markus Loecher. *Noise Sustained Patterns: Fluctuations and Nonlinearities*, volume 70. World scientific, 2003.

[30] P.I. Fierens, S.A. Ibez, R.P.J. Perazzo, G.A. Patterson, and D.F. Grosz. A memory device sustained by noise. *Physics Letters A*, 374(22):2207 – 2209, 2010.

[31] Adi R. Bulsara, Anna Dari, William L. Ditto, K. Murali, and Sudeshna Sinha. Logical stochastic resonance. *Chemical Physics*, 375(23):424 – 434, 2010. Stochastic processes in Physics and Chemistry (in honor of Peter Hanggi).

[32] Adi R Bulsara and Luca Gammaitoni. Tuning in to noise. *Physics Today*, 49(3):39–47, 1996.

[33] L Worschech, F Hartmann, TY Kim, S Höfling, M Kamp, A Forchel, J Ahopelto, I Neri, A Dari, and L Gammaitoni. Universal and reconfigurable logic gates in a compact three-terminal resonant tunneling diode. *Applied Physics Letters*, 96(4):042112, 2010.

[34] Diego N Guerra, Adi R Bulsara, William L Ditto, Sudeshna Sinha, K Murali, and P Mohanty. A noise-assisted reprogrammable nanomechanical logic gate. *Nano letters*, 10(4):1168–1171, 2010.

[35] J Zamora-Munt and C Masoller. Numerical implementation of a vcsel-based stochastic logic gate via polarization bistability. *Optics express*, 18(16):16418–16429, 2010.

[36] Kamal P. Singh and Sudeshna Sinha. Enhancement of logical responses by noise in a bistable optical system. *Phys. Rev. E*, 83:046219, Apr 2011.

[37] Sudeshna Sinha, JM Cruz, T Buhse, and P Parmananda. Exploiting the effect of noise on a chemical system to obtain logic gates. *EPL (Europhysics Letters)*, 86(6):60003, 2009.

[38] Hiroyasu Ando, Sudeshna Sinha, Remo Storni, and Kazuyuki Aihara. Synthetic gene networks as potential flexible parallel logic gates. *EPL (Europhysics Letters)*, 93(5):50001, 2011.

[39] Anna Dari, Behnam Kia, Adi R Bulsara, and William Ditto. Creating morphable logic gates using logical stochastic resonance in an engineered gene network. *EPL (Europhysics Letters)*, 93(1):18001, 2011.

[40] Morris Mano. Computer system architecture, 1993. *Prentice Hall*, 3:299.

[41] Thomas C Bartee. *The Computer Architecture and Logic Design*. McGraw-Hill, Inc., 1990.

[42] S. Boccaletti, V. Latora, Y. Moreno, M. Chavez, and D.-U. Hwang. Complex networks: Structure and dynamics. *Physics Reports*, 424(45):175 – 308, 2006.

[43] Duncan J Watts and Steven H Strogatz. Collective dynamics of small-worldnetworks. *Nature*, 393(6684):440–442, 1998.

[44] Albert-László Barabási and Réka Albert. Emergence of scaling in random networks. *science*, 286(5439):509–512, 1999.

[45] Réka Albert and Albert-László Barabási. Statistical mechanics of complex networks. *Rev. Mod. Phys.*, 74:47–97, Jan 2002.

[46] Rajarshi Roy, TW Murphy Jr, TD Maier, Z Gills, and ER Hunt. Dynamical control of a chaotic laser: Experimental stabilization of a globally coupled system. *Physical Review Letters*, 68(9):1259, 1992.

[47] Peter Jung, Ulrich Behn, Eleni Pantazelou, and Frank Moss. Collective response in globally coupled bistable systems. *Physical review. A*, 46(4):R1709–R1712, 1992.

[48] AR Bulsara and G Schmera. Stochastic resonance in globally coupled nonlinear oscillators. *Physical Review E*, 47(5):3734, 1993.

[49] Hu Gang, H Haken, and Xie Fagen. Stochastic resonance with sensitive frequency dependence in globally coupled continuous systems. *Physical review letters*, 77(10):1925, 1996.

[50] M Löcher, D Cigna, and ER Hunt. Noise sustained propagation of a signal in coupled bistable electronic elements. *Physical review letters*, 80:5212–5215, 1998.

[51] John F Lindner, Brian K Meadows, William L Ditto, Mario E Inchiosa, and Adi R Bulsara. Array enhanced stochastic resonance and spatiotemporal synchronization. *Physical Review Letters*, 75(1):3, 1995.

[52] Changsong Zhou, Jürgen Kurths, and Bambi Hu. Array-enhanced coherence resonance: nontrivial effects of heterogeneity and spatial independence of noise. *Physical review letters*, 87(9):098101, 2001.

[53] Claudio J Tessone, Claudio R Mirasso, Raúl Toral, and James D Gunton. Diversity-induced resonance. *Physical review letters*, 97(19):194101, 2006.

[54] Jierui Xie, Sameet Sreenivasan, Gyorgy Korniss, W Zhang, C Lim, and Boleslaw K Szymanski. Social consensus through the influence of committed minorities. *Physical Review E*, 84(1):011130, 2011.

[55] Kamal P Singh, Rajeev Kapri, and Sudeshna Sinha. Scalable ultra-sensitive detection of heterogeneity via coupled bistable dynamics. *EPL (Europhysics Letters)*, 98(6):60004, 2012.

[56] Otto H Schmitt. A thermionic trigger. *Journal of Scientific Instruments*, 15(1):24, 1938.

[57] Sudeshna Sinha. Random coupling of chaotic maps leads to spatiotemporal synchronization. *Physical Review E*, 66(1):016209, 2002.

[58] Arghya Mondal, Sudeshna Sinha, and Juergen Kurths. Rapidly switched random links enhance spatiotemporal regularity. *Physical Review E-Statistical, Nonlinear and Soft Matter Physics*, 78(6):066209, 2008.

[59] Herbert W Hethcote. Qualitative analyses of communicable disease models. *Mathematical Biosciences*, 28(3):335–356, 1976.

[60] Arkady Pikovsky, Michael Rosenblum, and Jürgen Kurths. *Synchronization: a universal concept in nonlinear sciences*, volume 12. Cambridge university press, 2003.

[61] Grigory V Osipov, Jürgen Kurths, and Changsong Zhou. *Synchronization in oscillatory networks*. Springer, 2007.

[62] Arthur T. Winfree. Biological rhythms and the behavior of populations of coupled oscillators. *Journal of Theoretical Biology*, 16(1):15 – 42, 1967.

[63] Alex Arenas, Albert Daz-Guilera, Jurgen Kurths, Yamir Moreno, and Changsong Zhou. Synchronization in complex networks. *Physics Reports*, 469(3):93 – 153, 2008.

[64] Takashi Nishikawa and Adilson E. Motter. Network synchronization landscape reveals compensatory structures, quantization, and the positive effect of negative interactions. *Proceedings of the National Academy of Sciences*, 107(23):10342–10347, 2010.

[65] Louis M. Pecora and Thomas L. Carroll. Master stability functions for synchronized coupled systems. *Phys. Rev. Lett.*, 80:2109–2112, Mar 1998.

[66] Mauricio Barahona and Louis M. Pecora. Synchronization in small-world systems. *Phys. Rev. Lett.*, 89:054101, Jul 2002.

[67] Bo S Goh. Global stability in many-species systems. *American Naturalist*, pages 135–143, 1977.

[68] Jürgen Jost and Maliackal Poulo Joy. Spectral properties and synchronization in coupled map lattices. *Physical Review E*, 65(1):016201, 2001.

[69] Daniel A. Wiley, Steven H. Strogatz, and Michelle Girvan. The size of the sync basin. *Chaos*, 16(1):015103, 2006.

[70] Yong Zou, Tiago Pereira, Michael Small, Zonghua Liu, and Jürgen Kurths. Basin of attraction determines hysteresis in explosive synchronization. *Phys. Rev. Lett.*, 112:114102, Mar 2014.

[71] Peter J Menck, Jobst Heitzig, Norbert Marwan, and Jürgen Kurths. How basin stability complements the linear-stability paradigm. *Nature Physics*, 9(2):89–92, 2013.

[72] Vivek Kohar and Sudeshna Sinha. Noise-assisted morphing of memory and logic function. *Physics Letters A*, 376(89):957 – 962, 2012.

[73] Sandro Perrone, Ramon Vilaseca, and Cristina Masoller. Stochastic logic gate that exploits noise and polarization bistability in an optically injected vcsel. *Optics express*, 20(20):22692–22699, 2012.

[74] Animesh Gupta, Aman Sohane, Vivek Kohar, K. Murali, and Sudeshna Sinha. Noise-free logical stochastic resonance. *Phys. Rev. E*, 84:055201, Nov 2011.

[75] Vivek Kohar, K. Murali, and Sudeshna Sinha. Enhanced logical stochastic resonance under periodic forcing. *Communications in Nonlinear Science and Numerical Simulation*, 19(8):2866 – 2873, 2014.

[76] Cristina Masoller, MS Torre, and Paul Mandel. Influence of the injection current sweep rate on the polarization switching of vertical-cavity surface-emitting lasers. *Journal of applied physics*, 99(2):026108, 2006.

[77] M. Sciamanna and K. Panajotov. Route to polarization switching induced by optical injection in vertical-cavity surface-emitting lasers. *Phys. Rev. A*, 73:023811, Feb 2006.

[78] Takeo Katayama, Tomohiro Ooi, and Hitoshi Kawaguchi. Experimental demonstration of multi-bit optical buffer memory using 1.55-polarization bistable vertical-cavity surface-emitting lasers. *Quantum Electronics, IEEE Journal of*, 45(11):1495–1504, 2009.

[79] Josep Martin-Regalado, F Prati, Maxi San Miguel, and NB Abraham. Polarization properties of vertical-cavity surface-emitting lasers. *Quantum Electronics, IEEE Journal of*, 33(5):765–783, 1997.

[80] V Kohar, A Choudhary, KP Singh, and S Sinha. Verification of scalable ultra-sensitive detection of heterogeneity in an electronic circuit. *The European Physical Journal Special Topics*, 222(3-4):721–728, 2013.

[81] Vivek Kohar and Sudeshna Sinha. Emergence of epidemics in rapidly varying networks. *Chaos, Solitons & Fractals*, 54(0):127 – 134, 2013.

[82] Marcelo Kuperman and Guillermo Abramson. Small world effect in an epidemiological model. *Physical Review Letters*, 86(13):2909, 2001.

[83] Matt J Keeling and Ken TD Eames. Networks and epidemic models. *Journal of the Royal Society Interface*, 2(4):295–307, 2005.

[84] Shweta Bansal, Bryan T Grenfell, and Lauren Ancel Meyers. When individual behaviour matters: homogeneous and network models in epidemiology. *Journal of the Royal Society Interface*, 4(16):879–891, 2007.

[85] Prashant M Gade and Sudeshna Sinha. Dynamic transitions in small world networks: Approach to equilibrium limit. *Physical Review E*, 72(5):052903, 2005.

[86] Michelle Girvan, Duncan S Callaway, Mark EJ Newman, and Steven H Strogatz. Simple model of epidemics with pathogen mutation. *Physical Review E*, 65(3):031915, 2002.

[87] Viktor Nagy. Mean-field theory of a recurrent epidemiological model. *Physical Review E*, 79(6):066105, 2009.

[88] Thilo Gross, Carlos J Dommar DLima, and Bernd Blasius. Epidemic dynamics on an adaptive network. *Physical review letters*, 96(20):208701, 2006.

[89] Leah B Shaw and Ira B Schwartz. Fluctuating epidemics on adaptive networks. *Physical Review E*, 77(6):066101, 2008.

[90] Sven Van Segbroeck, Francisco C Santos, and Jorge M Pacheco. Adaptive contact networks change effective disease infectiousness and dynamics. *PLoS computational biology*, 6(8):e1000895, 2010.

[91] Federico Vazquez and Damián H Zanette. Epidemics and chaotic synchronization in recombining monogamous populations. *Physica D: Nonlinear Phenomena*, 239(19):1922–1928, 2010.

[92] Damián H Zanette and Sebastián Risau-Gusmán. Infection spreading in a population with evolving contacts. *Journal of biological physics*, 34(1-2):135–148, 2008.

[93] Lixin Zhong, Tian Qiu, Fei Ren, Pingping Li, and Bihui Chen. Time scales of epidemic spread and risk perception on adaptive networks. *EPL (Europhysics Letters)*, 94(1):18004, 2011.

[94] Ken TD Eames and Matt J Keeling. Modeling dynamic and network heterogeneities in the spread of sexually transmitted diseases. *Proceedings of the National Academy of Sciences*, 99(20):13330–13335, 2002.

[95] Roy M Anderson, Robert M May, and B Anderson. *Infectious diseases of humans: dynamics and control*, volume 28. Wiley Online Library, 1992.

[96] Igor V. Belykh, Vladimir N. Belykh, and Martin Hasler. Blinking model and synchronization in small-world networks with a time-varying coupling. *Physica D: Nonlinear Phenomena*, 195(12):188 – 206, 2004.

[97] RE Amritkar and Chin-Kun Hu. Synchronized state of coupled dynamics on time-varying networks. *Chaos*, 16(1):015117, 2006.

[98] Jinhu Lu and Guanrong Chen. A time-varying complex dynamical network model and its controlled synchronization criteria. *Automatic Control, IEEE Transactions on*, 50(6):841–846, 2005.

[99] Daniel J Stilwell, Erik M Bollt, and D Gray Roberson. Sufficient conditions for fast switching synchronization in time-varying network topologies. *SIAM Journal on Applied Dynamical Systems*, 5(1):140–156, 2006.

[100] J. Tang, S. Scellato, M. Musolesi, C. Mascolo, and V. Latora. Small-world behavior in time-varying graphs. *Phys. Rev. E*, 81:055101, May 2010.

[101] Maoyin Chen. Synchronization in time-varying networks: A matrix measure approach. *Phys. Rev. E*, 76:016104, Jul 2007.

[102] W. L. Lu, F. M. Atay, and J. Jost. Chaos synchronization in networks of coupled maps with time-varying topologies. *The European Physical Journal B*, 63(3):399–406, 2008.

[103] L. Chen, C. Qiu, and H. B. Huang. Synchronization with on-off coupling: Role of time scales in network dynamics. *Phys. Rev. E*, 79:045101, Apr 2009.

[104] Aurelien Gautreau, Alain Barrat, and Marc Barthlemy. Microdynamics in stationary complex networks. *Proceedings of the National Academy of Sciences*, 106(22):8847–8852, 2009.

[105] Juliette Stehlé, Alain Barrat, and Ginestra Bianconi. Dynamical and bursty interactions in social networks. *Phys. Rev. E*, 81:035101, Mar 2010.

[106] F De Vico Fallani, V Latora, L Astolfi, F Cincotti, D Mattia, M G Marciani, S Salinari, A Colosimo, and F Babiloni. Persistent patterns of interconnection in time-varying cortical networks estimated from high-resolution eeg recordings in humans during a simple motor act. *Journal of Physics A: Mathematical and Theoretical*, 41(22):224014, 2008.

[107] M. Valencia, J. Martinerie, S. Dupont, and M. Chavez. Dynamic small-world behavior in functional brain networks unveiled by an event-related networks approach. *Phys. Rev. E*, 77:050905, May 2008.

[108] Amr Ahmed and Eric P. Xing. Recovering time-varying networks of dependencies in social and biological studies. *Proceedings of the National Academy of Sciences*, 106(29):11878–11883, 2009.

[109] Lei Wang and Qing guo Wang. Synchronization in complex networks with switching topology. *Physics Letters A*, 375(34):3070 – 3074, 2011.

[110] Naoki Masuda, Konstantin Klemm, and Víctor M. Eguíluz. Temporal networks: Slowing down diffusion by long lasting interactions. *Phys. Rev. Lett.*, 111:188701, Oct 2013.

[111] A. Choudhary, V. Kohar, and S. Sinha. Taming Explosive Growth through Dynamic Random Links. *ArXiv e-prints*, November 2013.

[112] Paul So, Bernard C. Cotton, and Ernest Barreto. Synchronization in interacting populations of heterogeneous oscillators with time-varying coupling. *Chaos*, 18(3):037114, 2008.

[113] Petter Holme and Jari Saramki. Temporal networks. *Physics Reports*, 519(3):97 – 125, 2012. Temporal Networks.